THE FLORIDA MANATEE SOMATOSENSORY SYSTEM

By

DIANA KAY SARKO

A DISSERTATION PRESENTED TO THE GRADUATE SCHOOL
OF THE UNIVERSITY OF FLORIDA IN PARTIAL FULFILLMENT
OF THE REQUIREMENTS FOR THE DEGREE OF
DOCTOR OF PHILOSOPHY

UNIVERSITY OF FLORIDA

2006

In loving memory of my grandfather, John Sarko, who always supported my educational pursuits and who I wish could be here on my graduation day, and every day

ACKNOWLEDGMENTS

First and foremost, I thank my parents. Their support and their own pursuit of knowledge, both of them going back to school later in life to earn master's degrees, is an inspiration. I thank my mentor Dr. Roger Reep for showing me everything that an advisor should be—available, good-humored, supportive, and able to balance work with play. I only hope that one day when I have my own lab that I can do him justice. I am grateful to my committee members for their time, wisdom and invaluable contributions to this project: Dr. Gordon Bauer, Dr. Pete McGuire, and especially Dr. Floyd Thompson, from whom I have learned a great deal about being an exceptional professor and researcher. Many, many thanks are due to Maggie Stoll, who has not only dealt with troubleshooting on every level, but has been with me through personal trials that I could not have undergone alone.

I thank my love and my fiancé JJ Kennard for his patience and devotion, and especially for helping me to turn my brain to the much-needed, often-ignored "off" position now and then. Besides Roger and Maggie, my time in this lab has also afforded me the pleasure and privilege of meeting Dr. Joe Cheatwood, who gave me guidance when I first joined the lab and who will be a lifelong friend. Many thanks to Susan Oliver, my best friend, who always knew that I could get through this, even when I had serious doubts. I also thank Dave Schoenberg, who has been a shoulder and one of my dearest friends since college; and Kevin Chadbourne, who has gone above and beyond what it has taken to maintain my sanity towards the end of this journey. Every little thing that he has done has helped me more than he will ever know.

Certain events from my graduate career have made me realize that life is too short to waste pursuing anything but what you love to do. These last four and a half years I have had the privilege to do just that. I have learned so much from so many, and yet I have only just begun.

TABLE OF CONTENTS

LIST OF TABLES

LIST OF FIGURES

Abstract of Dissertation Presented to the Graduate School
of the University of Florida in Partial Fulfillment of the
Requirements for the Degree of Doctor of Philosophy

THE FLORIDA MANATEE SOMATOSENSORY SYSTEM

By

Diana Kay Sarko

December 2006

Chair: Roger L. Reep
Major Department: Medical Sciences—Neuroscience

Florida manatees are thought to be tactile specialists, and in an effort to systematically characterize this system, the research presented here first used immunolabeling to functionally characterize sensory innervation in facial follicles with behavioral relevance in object recognition and exploration as well as in follicles from select perioral and postfacial regions. Facial vibrissae exhibited dense C- and Aδ-fiber innervation of the epidermis and rete ridge collar, novel "tangle" endings at the inner conical body level, dense Merkel cell and moderate longitudinal lanceolate ending distribution at the ring sinus, and novel endings located along the trabeculae of the cavernous sinus. Postfacial vibrissae contained Merkel endings and dense C- and Aδ-fiber distribution at the rete ridge collar. Dense Merkel ending networks and "tangle" endings were present at the inner conical body and ring sinus levels along with moderate longitudinal lanceolate ending innervation. No novel endings were present within the trabeculated cavernous sinus of any postfacial vibrissae. We conclude that the facial vibrissae are in fact more densely innervated, with more varied sensory endings, in accordance with their behavioral importance in active tactile exploration. Furthermore, it seems that manatees are heavily invested in directionality detection, an adaptation that would enhance their perception of underwater hydrodynamic stimuli.

A histochemical and cytoarchitectural analysis was also completed for the brainstem, thalamus, and neocortex of the Florida manatee in order to localize primary sensory areas. Based on the location of cytochrome oxidase (CO)-dense staining, we found that somatosensory nuclei of the brainstem (Bischoff's, trigeminal, and cuneate-gracile nuclei) and thalamus (VP) appear disproportionately large and, in the case of the trigeminal and cuneate-gracile complex, show evidence of parcellation that may be somatotopically related to discrete body areas. Flattened cortex preparations stained for CO were assigned preliminary functional divisions for S1 with the face represented laterally followed by the flipper, body and tail representations proceeding medially. Coronal cortical sections stained for CO, myelin, or Nissl bodies were also systematically analyzed in order to accurately localize the laminar and cytoarchitectural extent of CO staining. Overall, S1 appears to span seven cytoarchitectural areas for which we have proposed functional assignments.

CHAPTER 1
INTRODUCTION

The Florida Manatee

Manatees belong to the order Sirenia, of which over 35 species existed during the past 50 million years, with only 4 remaining presently (Domning, 1982). There are three extant manatee species: the West Indian, of which the Florida manatee (*Trichechus manatus latirostris*) and the Antillean manatee (*T. manatus manatus*) are subspecies; the Amazonian, *T. inunguis*; and the West African, *T. senegalensis*. As the only obligate herbivores among marine mammals, sirenians possess unique behavioral, physiological, and neuroanatomical adaptations. The US Fish and Wildlife Service currently classifies the Florida manatee as endangered, a status that is supported by their low total population which was estimated at the last aerial survey in February 2004 to be 2,568 manatees (provided by the Manatee Technical Advisory Council and the Manatee Population Status Working Group). In the year 2003 alone, the Florida Fish and Wildlife Conservation Commission Marine Mammal Pathobiology Laboratory reported a total of 380 manatee deaths—a significant percentage of the population, indicating that the opportunity to learn from this unique species is rapidly disappearing.

Sensory Specializations of the Manatee Body

Manatees appear to have reasonably well-developed hearing (Gerstein and Gerstein, 1999) but reduced vision (e.g., Bauer et al., 2003). Though little is known about the extent of their olfactory or gustatory capabilities, these appear to be senses of subordinate importance to the manatee as well (Levin and Pfeiffer, 2002; Mackay-Sim et al., 1985). However, recent evidence suggests the presence of a sophisticated tactile sense through a system of sinus-type tactile hairs, or follicle sinus complexes (FSCs), covering the entire postfacial body (Reep et al., 2002). The postfacial body is covered in approximately 3,000 hairs with hair density decreasing

dorsoventrally (Reep et al., 2002) and calves exhibit greater hair density distribution that is attributed to the fixed number of follicles in a mammal at birth. Hair density then decreases with age as the body, and especially the midsection, of the manatee expands (Reep et al., 2002). Each body hair has an external length of 2–9 mm, with most hairs separated by 20–40 mm, giving each hair an independent field of movement (Reep et al., 2002). A single body vibrissa is innervated by 20–50 axons whereas 40–200 axons supply innervation to each facial vibrissa (Reep et al., 2001; 2002). The distribution of vibrissae over the entire postfacial body is a unique arrangement among mammals, most of which have tactile hairs restricted only to certain body regions, and is proposed to be analogous to the lateral line system in fish by functioning as a "touch at a distance" sense through passive deflection of tactile hairs by hydrodynamic stimuli. Such a system is potentially capable of conveying crucial information about water currents, the approach of other animals, and other features of the underwater environment (Reep et al., 2002).

The manatee face possesses further sensory specializations that aid in adaptation to the animal's unique environmental niche. Facial hair is distributed thirty times more densely than on the rest of the body (Reep et al., 1998), an attribute that should increase spatial resolution, and can be distinguished from body hair by the greater stiffness of facial hair due to smaller length/diameter ratios (Reep et al., 1998). Body hair is located on the supradisk portion of the face posterior to the orofacial ridge and on the chin in addition to the entire postfacial extent of the body (Reep et al., 1998). Manatees have an expanded philtrum called the oral disk that contains bristle-like hairs (BLHs) that are used as tactile "feelers" in addition to perioral bristles that are essentially modified vibrissae (Reep et al., 1998). Vibrissae provide detailed textural information about objects and surfaces in an animal's immediate environment, and most mammals use vibrissae exclusively for sensory purposes such as finding prey and navigating

successfully when vision is compromised, such as in low-light situations (Brecht et al., 1997; Dehnhardt et al., 1998; Dehnhardt et al., 2001; Ling, 1977). Facial hair is crucial in manatee feeding and tactile exploration of the environment, accomplishing dual and synergistic motor and sensory roles. The hair and bristles of the manatee face are composed of 9 distinct regions, 6 of which are perioral bristle—4 upper perioral fields (U1–U4) on each side of the upper lips and oral cavity, and 2 lower perioral fields (L1–L2) on each side of the lower lip pad (Reep et al., 1998). Each of these follicles can be classified as a vibrissa according to the criteria established by Rice et al. (1986): 1) substantial innervation, 2) a dense connective tissue capsule, and 3) a prominent, circumferential blood sinus complex. The 9 regions of the manatee face are discernible by location as well as the number, range of length/diameter ratios, and behavioral role of follicles within each field (Reep et al., 2001).

Perioral Vibrissae

The BLHs of the oral disk are the vibrissae primarily involved in object recognition and tactile exploration, whereas U2 and L1 follicle fields are used in a prehensile grasping fashion during feeding and oripulation (a combined sensorimotor function that is unique among mammals) as well as in social behaviors including mouthing, nuzzling, and also pinching a conspecific's back in an attempt to gain access to food (Reep et al., 2001; Marshall et al., 1998b). The right and left U2 bristle fields specifically act in a prehensile manner during feeding by reaching out and grasping food while L1 bristles actively push vegetation farther into the oral cavity (Marshall et al., 1998b). The U1 vibrissae may also be involved in some level of tactile exploration during feeding while the U3, U4, and L2 fields may assist L1 bristles in the movement of food (Marshall et al., 1998b). Upon encountering a particularly difficult food item, manatees can use each U2 field independently, even reversing direction in order to expel undesirable food (Marshall et al., 1998b). Such evidence reveals a high level of dexterity and

perioral tactile discrimination and is supported by the manatee's relative tactile difference threshold of 14%—favorably comparable to that of an Asian elephant's trunk (Bachteler and Dehnhardt, 1999). Notably, the eyes are often closed during feeding and tactile exploration (Marshall et al., 1998b; Bachteler and Dehnhardt, 1999), further indicating an emphasis on haptic over visual input. The prehensile ability of facial tactile hairs is present in dugongs as well, but absent in pinnipeds despite their higher tactile resolving power (Bachteler and Dehnhardt, 1999; Marshall et al., 1998b; Marshall et al., 2003).

In an earlier study of manatee follicle innervation U2s were found to contain the largest FSCs composed of the longest hair shafts, the widest ring sinuses, the thickest capsules, and the highest degree of innervation at over 200 axons per follicle (Reep et al., 2001). The L1 bristles are innervated by the second largest number of axons at approximately 200 per FSC, followed by U3, U4, and L2 bristles (approximately 100) and finally U1 bristles, whose range overlaps that of the BLH vibrissae at 49–74. The body hair follicles of the chin and supradisk contain the least axonal innervation with a range of 34–48 axons per follicle. Most FSC axons terminate in the mesenchymal sheath and the outer root sheath lining the hair follicle proper along the level of the ring sinus. Reep et al. (2001) described general morphological features and axonal counts for each follicle type but the silver staining was often inconsistent with inadequately defined nerve endings. This limitation can be solved through a systematic analysis using immunolabeling, and given the co-varying behavioral and sensory tasks for which each follicle field is specialized, concurrently varying attributes in innervation patterns might be elucidated through immunofluorescence.

Upon examination of muscular supply to facial vibrissae, Reep et al. (1998) discovered that the dorsal and ventral buccal branches of the facial nerve supply the lips and perioral regions

with the dorsal branch supplying the upper lip and nasal area and the ventral branch terminating in the lower jaw and lip muscles to enable vibrissal eversion and feeding behavior. Furthermore, each facial bristle follicle in the U1–U4 fields is supplied by the infraorbital branch of the maxillary nerve (the sensory trigeminal branch), making these fields homologous to mystacial vibrissae. Sensory innervation of the lower jaw is provided by the inferior alveolar branch of the mandibular nerve while the lingual branch innervates the tongue and the mylohoid branch courses ventrally to innervate *M. mylohyoidus* and the ventral mandible skin. The inferior alveolar branch separates into 2 mental nerves, supplying L1 and L2 and making them homologues of the mental vibrissae present in other taxa.

Comparative trends in mammals indicate that vibrissae have evolved to perform complex functions in order to provide feedback about an animal's environment, but although sensory detection is often accompanied by vibrissal movement, it is not accompanied by prehensile grasping behaviors (Reep et al., 2001). Harbor seals appear to use vibrissae in touch discrimination as effectively as a monkey is able to utilize its hands (Dehnhardt and Kaminski, 1995), and pinnipeds as a whole have been found to employ their long vibrissae in tactile exploration as well as in social display behavior (Dehnhardt, 1994; Dehnhardt and Ducker, 1996; Dehnhardt and Kaminski, 1995; Peterson and Bartholomew, 1967; Miller, 1975; Kastelein and Van Gaalen, 1988). Rodents utilize a whisking behavior of their mystacial vibrissae in tactile exploration (Carvell and Simons, 1990; Welker, 1964; Wineski, 1985) and freshwater river dolphins (*Platanistidae*), which have poor vision, use vibrissae on their upper and lower jaws to locate prey (Ling, 1977). Sensory specializations of the skin and hair in mammals are accompanied by expanded cortical representations to accommodate the greater level of neural input (Johnson, 1990; Kaas and Collins, 2001). A clear example of this can be seen in the star-

nosed mole (*Condylura cristata*). The 22 fleshy nasal appendages, or rays, that it uses to explore the environment can be seen in cytochrome oxidase preparations of somatosensory cortex with a distinct band corresponding to each ray (Catania and Kaas, 1995, 1997). Catania and Kaas (1997) further discovered that the eleventh appendage, used preferentially in environmental exploration, also assumes the largest cortical representation. Therefore, it is reasonable to hypothesize that in the manatee additional neuroanatomical space would be allotted to complement tactile specializations with a particularly expanded facial representation. We examine this further by identifying and characterizing the somatosensory areas of the brainstem, thalamus and cortex in order to more completely understand any specializations that might be present and might complement the Florida manatee's adaptation to its environmental niche.

The Manatee Brain: General Attributes

The Florida manatee brain possesses a unique and intriguing set of attributes that combine more primitive traits with those considered to be quite derived. The former include a very smooth (highly lissencephalic) cortex and an extremely small brain size compared to what would be expected for an animal of its body size, a parameter known as the encephalization quotient, or EQ. The EQ of the manatee was found to be 0.27, or about 1/4 the value expected for its body size (O'Shea and Reep, 1990). The gyration index, a measure of cortical folding, of 1.06 for the Florida manatee quantifies the high level of lissencephaly observed (Reep and O'Shea, 1990). Johnson et al. (1994) also reexamined phylogenetic classifications by examining a number of brain traits that were scored as primitive or derived across 152 mammalian species. Manatees were found to be primitive in possessing the following attributes: 1) an optic tract that terminates in closely apposed nuclei of the thalamus, 2) a lack of fasciculus aberrans, 3) no visible separation of the claustrum from cortex, and 4) no clear separation between external cuneate nucleus and cuneate nucleus. Dietary features such as the low quality and abundance of

food along with a low metabolic rate are also characteristic of many mammals with EQs in the lower mammalian range, including the manatee (McNab, 1978; 1980).

Despite the above evidence, most of the life history, ecological and behavioral traits of the Florida manatee are typical of large-brained species with higher EQs (O'Shea and Reep, 1990). With a gestation period of approximately 1 year, an age range at sexual maturity spanning 5–10 years, an average interbirth interval of 2–5 or more years, and longevity in the wild estimated at 50–60 years (Hartman, 1979), manatees appear to be more typical of altricial species following principles of K-selection. Also, while the manatee brain is small relative to its body size, the telencephalon comprises 71% of the total brain volume, 90% of which consists of cerebral cortex. The cortex also possesses well-defined laminae. These qualities are comparable to taxa with large relative brain size, including primates (Reep and O'Shea, 1990). The Johnson et al. (1994) study further indicated that manatees have the following derived brain traits: 1) lack of accessory olfactory formation, involved in pheromone detection, 2) deep position of the optic tract in the collicular tectum, 3) emergence of the facial nerve ventral to the trigeminal sensory column, 4) olfactory bulb mitral cells gathered into a monolayer, 5) hemispheres connected by a corpus collosum, 6) medial position of the ventral nucleus to the principal nucleus of the inferior olive, 7) presence of Rindenkerne, cell clusters in cortical layer VI, and 8) a delaminated dorsal cochlear nucleus. Johnson et al. also proposed that the secondary loss of lamination in the auditory dorsal cochlear nucleus along with loss of the accessory olfactory formation indicate convergent evolutionary consequences of departure from a terrestrial habitat.

Cytochrome Oxidase: A Metabolic Marker for Primary Sensory Areas

Cytochrome oxidase (CO) is an effective endogenous metabolic marker for neurons due to the tight coupling between neuronal activity and oxidative metabolism (Wong-Riley, 1989 for review). This enzyme is an integral transmembrane protein found in the inner mitochondrial

membrane of all eukaryotes and generates ATP through oxidative phosphorylation (Wikstrom et al., 1981). CO accounts for over 90% of oxygen consumption by eukaryotes (Wikstrom et al., 1981) and is vital for organs like the brain that rely on oxidative metabolism—in the case of neurons, particularly in the maintenance of ionic balance (Lowry, 1975; Sokoloff, 1974). It has been suggested that dendritic metabolism makes the single largest contribution to this metabolic activity since the level of oxidative enzymes in dendrites reflects the intensity and type of synaptic input to a neuron (DiFiglia et al., 1987; Kageyama and Wong-Riley, 1982; Kageyama and Wong-Riley, 1985; Lowry, 1954; Mourdian and Scott, 1988; Wong-Riley, 1984). This is supported by the observation that CO activity levels are responsive to experimentally induced changes in functional activity (Wong-Riley, 1989 for review).

Cerebral cortex stained for CO shows a laminar pattern of activity with highly active regions representing the thalamic-recipient and other synapse-rich layers (Carroll and Wong-Riley, 1984; Jones and Friedman, 1982; Matelli et al., 1985; Price, 1985). Neurons with intense CO activity are likely to be tonically active and maintain a high enzyme capacity for energy production to be able to drive the high rate of spontaneous activity (Wong-Riley, 1989). Since primary sensory areas of the cortex are more tonically active, they are easily discernable when stained for CO, and it has been found that CO can be used to separate functionally different cortical areas (e.g., Carroll and Wong-Riley, 1984). In fact, a recent study of human cortex was successful in differentiating primary and secondary sensory areas through CO and acetylcholinesterase (AChE) staining. Primary sensory areas 3a and 3b showed dark CO staining of layer IV and a low level of AChE positive pyramids, a pattern also seen in primary visual and auditory areas. Secondary association areas 1 and 2 revealed dark CO staining in layer III with an abundance of AChE positive pyramidal cells (Eskenasy and Clarke, 2000). Physiologically

highly active nuclear groups of the basal ganglia, thalamus, brainstem and spinal cord also show strong enzymatic activity (DiFiglia et al., 1987; Jones et al., 1986; Nomura and Mizuno, 1986; Wallace, 1986; Wiener, 1986; Wong-Riley, 1976; Wong-Riley and Kageyama, 1986), making cytochrome oxidase useful in identifying the primary somatosensory components of the brainstem and thalamus in addition to the cortex.

Brainstem Somatosensory Nuclei and Barrelettes

Commitment to specific sensory modalities in restricted regions of the body creates a commensurate commitment of neurons from the periphery through the brainstem, thalamus, and cerebral cortex. Following this paradigm, if somatic sensation is prevalent for the manatee, then associated nuclei in the thalamus and brainstem are expected to be relatively larger and/or more subdivided in order to accommodate the greater amount of information being taken in and processed. The brainstem nuclei of interest for the manatee somatosensory system include trigeminal, cuneate, gracile, and Bischoff's nuclei. It has already been noted that cranial nerve V (the trigeminal nerve) is large in the manatee (Reep et al., 1989). Further studies have shown that visual thalamic and brainstem nuclei are reduced, whereas trigeminal and other somatosensory nuclei are well developed (Johnson et al., 1986; 1987; Reep et al., 1989; Welker et al., 1986). Assessments of the relative importance of these sensory systems in sirenian behavior parallel these results, particularly for the trigeminal nerve system extensively associated with the use of the facial vibrissae in tactile exploration, a crucial aspect of manatee behavior. However, these findings have never been revisited, and more remains to be discovered. Bischoff's nucleus, a distinct group of cells in the midline of the caudal medulla (Johnson et al., 1968), has not previously been analyzed in the manatee but has been shown, along with the cuneate and gracile nuclei, to project heavily to the ventrobasal thalamus in the raccoon (Ostapoff and Johnson, 1988). In the raccoon, the tail representation occupies the dorsal portion of this nucleus while the

hindlimb representation occupies the ventral portion (Johnson et al., 1968). In the manatee, Bischoff's nucleus would represent the fluke. CO studies of the rat revealed that the afferent projection pattern from individual vibrissa follicles was topographically related to CO-dense cell clusters ("barrelettes") in the trigeminal principal sensory nucleus (PSN) with a nearly one-to-one ratio between follicles and corresponding CO-dense clusters (Florence and Lakshman, 1995). These results supported earlier findings by Jacquin et al. (1993) that showed that PSN axon collaterals were concentrated within corresponding CO-dense subdivisions, and terminal branches of individual trigeminal afferents rarely crossed over into adjacent regions. In contrast, in three subdivisions of the spinal trigeminal nucleus—the pars oralis, pars interpolaris, and pars caudalis—a topographical arrangement still existed, but with less specificity and more overlapping representations (Florence and Lakshman, 1995). Goyal et al. (1992) showed that the human principal trigeminal nucleus also demonstrated a parcellated CO-dense pattern. Therefore, size and parcellation data for the trigeminal nucleus would further elucidate the sensory specializations of manatees.

The same principle of CO somatotopic parcellation is also evident in the cuneate and gracile dorsal column nuclei. Cutaneous inputs from the upper limbs and rostral trunk of the body are represented in the cuneate nucleus while lower limbs and lower trunk are represented in the gracile nucleus. Strata et al. (2003) studied the Galago monkey to look at the pattern of peripheral nerve input. Through cell clusters that were identified as CO-dense blotches in both nuclei, they discovered a greater segregation of inputs within the cuneate (fingers and hand representation) than in the gracile (foot representation), which is consistent with the Galago's extensive and highly differentiated use of its hands and fingers relative to its feet. In macaques, inputs from specific parts of the hand relate to CO-dense rostrocaudal clusters of cells (Florence

et al., 1991). While the manatee lacks the manual dexterity of a primate, CO analysis of the cuneate and gracile nuclei would complete the evidence for manatee somatosensory processing and any concurrent specializations.

Thalamus and Barreloids

In the thalamus, AChE staining reveals robust patterns that allow for the discrimination of different nuclei and that are consistent in rodents, cats and primates (Jones, 1985). Densest staining occurs in the ventral lateral geniculate nucleus (LGN), intralaminar, anteroventral, anterodorsal, rhomboid, paraventricular, habenular, and medioventral nuclei. Lighter staining distinguishes the dorsal LGN, medial geniculate nucleus (MGN), reticular nucleus, anterior of the lateral posterior nucleus, and parts of lateral and ventral complexes. The principal somatic sensory nucleus in the thalamus consists of an area referred to as the ventrobasal (VB) or ventroposterior (VP) nucleus. A lateral subnucleus, the ventral posterior lateral (VPL) nucleus, represents the body while a medial subnucleus, the ventral posterior medial (VPM) subnucleus, represents the face and most of the head (e.g., Jones, 1985). In rodents and marsupials, the medial division of the VB nucleus (VBm) was discovered to contain "barreloids", or neuronal clusters related to individual vibrissae, that are highly reactive for CO (Jones, 1983; Land and Simons, 1985b; Van der Loos, 1976). Chronic trimming of the vibrissae results in reduced staining for CO in both the somatosensory cortical barrels (Land and Simons, 1985a; Wong-Riley and Welt, 1980) and the thalamic barreloids (Land and Akhtar, 1987) associated with the trimmed vibrissae. These findings were similar to those in *Macaca fascicularis* monkeys where peripheral nerves were cut, resulting in reduced staining of "rods" within the VPM (Jones et al., 1986). Using horseradish peroxidase axonal tracing, Jones et al. also discovered that CO staining was primarily due to terminations of trigeminal afferent fibers that formed somatotopically organized inputs to the rods. They postulated that each rod of the thalamus formed the basis of

columnarity of afferent input to the somatosensory cortex by providing bundles of thalamocortical axons terminating in focal domains of the cortex. Given the manatee's reliance on haptic input, the VPM would be expected to be relatively large and may possess barreloid parcellation related to input from the facial vibrissae.

Rindenkerne

Rindenkerne are cortical cell clusters that stain darkly for cytochrome oxidase and appear to be unique to sirenia, having been found absent in over 150 other mammalian species examined (Reep et al., 1989; Johnson et al., 1994). While these cell clusters are reminiscent of "barrels" found in the vibrissae subfield of somatosensory cortex in rats, mice, and other rodents (Johnson, 1980; Kaas and Collins, 2001), as well as in shrews (Catania et al., 1999), opossums (Catania et al., 2000; Frost et al., 2000; Huffman et al., 1999), and hedgehogs (Catania et al., 2000), barrels are hollow aggregates of neurons in layer IV, a major afferent zone. In contrast, Rindenkerne are dense aggregates located in layer VI, an efferent zone, although they do share histochemical attributes with barrels (Reep et al., 1989). Furthermore, Rindenkerne distribution in the cortex is restricted to 5 cytoarchitectural areas termed cluster cortex (CL) 1–5 by Reep et al. (1989) and Marshall and Reep (1995). The limited distribution of Rindenkerne and the fact that they are found exclusively in sirenian cortex implies a functional significance. Species possessing barrels show a one-to-one correspondence between barrels and vibrissae. However, there appear to be many more clusters than facial bristles in the manatee and it may be that only the larger clusters (approximately 1 mm in diameter) found in CL1 represent individual bristles while smaller Rindenkerne such as those found in CL2 may correspond to postfacial hairs (Loerzel and Reep, 1991). However, this hypothesis remains untested until the somatosensory cortex, and particularly the presumed facial region, can be more precisely delineated.

The Cerebral Cortex: Relating Cytoarchitecture to Electrophysiology

Due to the manatee's status as an endangered species, traditional electrophysiological methods of ascertaining the location of primary somatosensory cortex (SI) are not possible. Fortunately, the literature provides a wide range of species for which both electrophysiology and histochemical processing have been possible. For example, in the marmoset monkey (Huffman and Krubitzer, 2001), and megachiropteran bats (Krubitzer et al., 1993; Krubitzer and Calford, 1992), microelectrode maps of somatosensory fields were found to be highly correlated with cytoarchitectural boundaries (specifically flattened cortex cut tangentially and stained for myelin). A flattened cortex preparation creates a plane of section that includes most of layer IV, the densest zone of CO staining, while also facilitating the comparative interpretation of areal patterns and allowing more direct assessment of the extent and relative position of architectonic fields (Krubitzer et al., 1995). The flying fox, a megachiropteran, was found to have myelin-dense zones in hand and face representations in area 3b (or SI) that involved non-habituating cutaneous receptors responding consistently to repetitive stimulation, whereas sparse zones rapidly habituated. In marmoset monkeys electrophysiology was also related to myeloarchitecture and revealed that the body map representation in area 3a is coextensive with a strip of lightly to moderately myelinated cortex rostral to the darkly myelinated area 3b. Overall, non-habituating neurons corresponded with myelin-dense zones considered homologous to area 3b (Krubitzer et al., 1993). Myeloarchitecture has also been compared with CO staining, tracing methods, and microelectrode recording in the dorsomedial visual area of owl monkeys (Krubitzer and Kaas, 1993) to reveal functional areas and connectivity. In monotremes, which share with the manatee the status of being an evolutionary outlier and having a unique environment to which they have had to adapt, Krubitzer et al. (1995) showed CO staining patterns that reveal somatosensory specializations and suborganization. Microelectrode mapping

was combined with CO and myelin staining revealed subdivisions and topography of somatosensory cortex. The neocortices of both the platypus and the short-billed echidna revealed 4 representations of the body surface with SI occupying a large area and containing neurons mainly responsive to cutaneous stimulation of the contralateral body. The platypus bill had a disproportionately large representation with CO-dense regions corresponding only to mechanosensory stimulation and CO-light regions responding to both electrosensory and mechanosensory stimulation. In a compilation of cortical sensory maps of additional species, including the squirrel, macaque, and quoll, Krubitzer (1995) depicts homologies that are present in neocortical organization. Therefore, in lieu of performing electrophysiological studies on the manatee, a thorough histochemical assessment can still reveal a great deal about sensory specializations of the brain.

Overall this analysis of the manatee somatosensory system, from an immunofluorescence analysis of innervation at the periphery to a systematic histochemical examination of the central nervous system, aims to elucidate in what ways the manatee is a somatosensory specialist and how it has adapted to evolutionary pressures inherent in the environment that it occupies.

CHAPTER 2
INNERVATION OF FOLLICLE-SINUS COMPLEXES IN THE FLORIDA MANATEE

Introduction

Follicle-sinus complexes (FSCs, or vibrissae) form highly innervated tactile arrays generally found on a restricted region of the mammalian body—principally the mystacial region. However, recent evidence suggests that the Florida manatee (*Trichechus manatus latirostris*) possesses a sophisticated tactile sense through a system of FSCs distributed over the entire body (Reep et al., 2002). Manatees are large-bodied, obligate aquatic herbivores (a trait unique among marine mammals) that lack predators, do not pursue active prey, usually reside in a shallow, turbid water environment and have greatly reduced visual systems. They appear to have reasonably developed hearing capabilities (Gerstein and Gerstein, 1999; Mann et al., 2005) but reduced sight (Bauer et al., 2003), and though little is known about the extent of their olfactory or taste capabilities these senses also appear to be subordinate based on anatomical assessments (Levin and Pfeiffer, 2002; Mackay-Sim et al., 1985). The haptic sense may therefore be crucial in the manatee's detection of environmental cues, and this hypothesis is supported by the distribution of sinus-type tactile hairs over the entire body with specialized and more densely packed vibrissae on the face in addition to the elaboration of somatosensory areas at the neuroanatomical level (Dexler, 1912; Welker et al., 1986; Johnson et al., 1986, 1987, 1994; Reep et al., 1989, 2001, 2002; Marshall and Reep, 1995; Sarko and Reep, 2007). The postfacial body is supplied with approximately 3,000 hairs, each having an independent field of movement, forming an arrangement unique to sirenia that is proposed to be analogous to the lateral line system in fish (Reep et al., 2002). Such a system is potentially capable of conveying crucial information about water currents, the approach of other animals, and other features of the

underwater environment through hydrodynamic stimulation of mechanoreceptors (Reep et al., 2002).

Facial vibrissae are packed thirty times more densely than on the rest of the body, an attribute that should increase spatial resolution, and they can be distinguished from postfacial vibrisse by their greater rigidity due to smaller length/diameter ratios (Reep et al., 1998). The hair and bristles of the manatee face are composed of 9 distinct regions, 6 of which are perioral bristles (Fig. 2-1B): 4 upper perioral (U1–U4) fields on each side of the upper lips and oral cavity, and 2 lower perioral (L1–L2) fields on each side of the lower lip pad (Reep et al., 1998). The 9 follicle regions are distinguishable by location, number, range of length/diameter ratios, and behavioral role (Reep et al., 2001). Each of these follicles can be classified as a follicle-sinus complex (FSC) because the follicle and its affiliated dense innervation are surrounded by a blood sinus encased within a thick connective tissue capsule (Rice et al., 1986). Manatees have an expanded philtrum called the oral disk that contains bristle-like hairs (BLHs) that are the main tactile exploration component involved in object recognition (Reep et al., 1998). Postfacial vibrissae are located on the supradisk portion of the face posterior to the orofacial ridge and on the chin in addition to the entire postfacial extent of the body (Bachteler and Dehnhardt, 1999; Reep et al., 1998). Perioral fields U2 and L1 are used in a prehensile grasping fashion ("oripulation," a behavior unique among mammals) during feeding as well as in social behaviors (Reep et al., 2001; Marshall et al., 1998b). The eyes are often closed during feeding and tactile exploration (Marshall et al., 1998b; Bachteler and Dehnhardt, 1999), further emphasizing haptic over visual input. Vibrissae are known to provide detailed textural information about objects and surfaces in an animal's immediate environment, and most mammals use vibrissae exclusively for sensory purposes such as finding prey and navigating successfully when vision is compromised,

such as in low light situations (Brecht et al., 1997; Dehnhardt et al., 1998; Dehnhardt et al., 2001; Ling, 1977). In the manatee, facial vibrissae serve dual and synergistic motor and sensory roles in manatee feeding and direct tactile exploration of the environment (Marshall et al., 1998a, 1998b) with a high level of dexterity and perioral tactile discrimination that is also reflected in the manatee's relative tactile difference threshold of 14%—comparable to that of an Asian elephant's trunk (Bachteler and Dehnhardt, 1999). The prehensile function of facial vibrissae is present in dugongs as well but is absent in pinnipeds despite their higher tactile resolving power (Bachteler and Dehnhardt, 1999; Marshall et al., 1998b; 2003).

In an earlier study of manatee follicle innervation the U2 fields were found to contain the largest FSCs having the longest hair shafts, the widest ring sinuses, the thickest capsules, and the highest degree of innervation at over 200 axons per follicle (Reep et al., 2001). L1 follicles are innervated by the second largest number of axons at about 200 per FSC, followed by U3, U4 and L2 follicles (about 100) and finally U1 follicles, whose range overlaps that of the BLHs at 49–74. The chin and supradisk follicles exhibit the least innervation, with a range of 34–48 (Reep et al., 2001; 2002). Although the manatee's status as an endangered species precludes it from more invasive analysis, Reep et al. (2001) provided data describing general morphological features and axonal counts for each follicle type. However, silver staining did not consistently reveal the morphology of nerve endings, a limitation solved here through systematic immunolabeling analysis using anti-PGP (protein gene product 9.5) as a standard pan-neuronal marker in combination with several other antigens in order to functionally characterize the innervation of manatee vibrissal FSCs. Given the varying behavioral and sensory tasks for which each manatee bristle field is specialized, we would expect to reveal similarly varying attributes in patterns of innervation, with facial vibrissae engaged in tactile behavior (the U2 and BLH follicles)

exhibiting more densely distributed and varied types of nerve endings. Also, while the anatomical structure of FSCs remains relatively consistent across a wide range of species, patterns of innervation often vary considerably, presumably due to evolutionary pressures and concurrent behavioral demands (Dehnhardt et al., 1999; Ebara et al., 2002). As an evolutionary outlier, the Florida manatee offers a unique opportunity to better understand mammalian sensory systems in general by examining a system of vibrissae that has assumed an expanded functional role. A systematic analysis of manatee FSCs may also elucidate their potential relationship to cortical cellular aggregates called Rindenkerne (Dexler, 1912; Reep et al., 1989; Marshall and Reep, 1995; Johnson et al., 1990; 1994) that appear to be similar to barrels found in the somatosensory cortex of other species (Woolsey et al., 1975; Rice, 1995).

Materials and Methods

Manatees in Florida are endangered and protected under federal law. Postmortem manatee follicle samples were acquired through the statewide manatee salvage program under Federal Fish and Wildlife Permit PRT-684532 and IACUC protocol #C233. For each specimen, necropsy sheets summarizing body morphometrics, body weight, gender, likely cause of death, and condition upon recovery were obtained. Specimens are outlined in Table 2-1 and included TM0406 (adult male, euthanized after watercraft impact; 3 BLH and 3 U2 follicles sampled), TM9728 (adult male, death due to watercraft; 3 rostrodorsal, 1 dorsocentral, and 1 dorsocaudal follicles sampled), TM0506 (male neonate, suffered multisystemic failure due to immune suppression secondary to cold stress; 2 U2, 2 BLH, 2 L1, and 1 dorsocaudal body sampled), and MNW0614 (subadult female, death due to watercraft; 3 follicles from each of 10 body regions of interest sampled). Hair follicles samples were acquired as available from 6 body regions (Fig. 2-1A; supradisk, dorsocentral midline, rostrodorsal midline, caudodorsal midline, ventrocentral midline, dorsal tail, and tail edge) as well as from perioral fields L1, U2, and BLH (Fig. 2-1B) as

described by Reep et al. (1998) using a #11 scalpel blade to extract a block of tissue (roughly 5x5x15 mm) surrounding the follicle of interest. Follicles were cut mediolongitudinally to facilitate fixation and placed in 4% paraformaldehyde overnight. After 24 hours of fixation follicles were removed and placed in 0.1M phosphate buffered saline (PBS) and 30% sucrose. Sections were cut using a cryostat. Sections for conventional epifluorescence evaluation were cut at 14 μm parallel to the long axis of the follicles. These sections were directly thawed onto slides subbed with chrome-alum gelatin, allowed to air dry, and immunolabeled on the slides. Follicles for confocal analysis were cut at 75 μm and the sections were immunolabeled free-floating before being mounted onto slides. After labeling, the slides were coverslipped using either 90% glycerin in PBS or Vectashield (Vector Laboratories).

The sections were processed for single and double immunolabeling with the following primary antibodies:

1. Anti-protein gene product 9.5 (PGP, rabbit polyclonal, 1:800; UltraClone, Isle of Wright, UK; catalog number RA95101). The antigen was human PGP9.5 protein purified from pathogen-free human brain. The antibody shows one band at 26-28 kD on Western blot and is a universal neuronal cytoplasmic protein (Thompson et al., 1983; Wilkinson et al., 1989).

2. Anti-neurofilament 200 kD subunit (NF, rabbit polyclonal, 1:800; Chemicon International, Temecula, CA; catalog number AB1982, lot number 24080051). The antigen was a highly purified bovine neurofilament polypeptide. The antibody labels phosphorylated and nonphosphorylated 200kD NF and shows a band at 200kD and bands around 170-180 kD on Western blot. The NF200 antibody identifies myelinated innervation including Merkel endings, Aβ and Aδ fibers (Rice et al., 1997).

3. Anti-calcitonin gene related peptide (CGRP, guinea pig polyclonal, 1:400; Peninsula Laboratories, Inc., San Carlos, CA; catalog number T-5027, lot number 061121). The antigen is human α-CGRP with the following sequence: H-Ala-Cys-Asp-Thr-Ala-Thr-Cys-Val-Thr-His-Arg-Leu-Ala-Gly-Leu-Leu-Ser-Arg-Ser-Gly-Gly-Val-Val-Lys-Asn-Asn-Phe-Val-Pro-Thr-Asn-Val-Gly-Ser-Lys-Al a-Phe-NH2. The antibody has 100% reactivity with human and rat α-CGRP, human CGRP (8-37); chicken CGRP, human β-CGRP. It has 0.04% cross reactivity with human amylin and 0% cross reactivity with rat amylin and with human and rat calcitonin. The CGRP antibody identifies peptidergic C-fiber innervation and Merkel cells (Rice et al., 1997) and is an endogenous sensory neuropeptide and a G-protein coupled receptor.

4. Anti-S-100 (anti-Schwann cell protein S100, rabbit polyclonal, used neat; Biogenesis Inc., Brentwood, NH, catalog number 8200-0184, lot number A2255). The antigen was purified bovine S100 protein. Anti-S100 has been found to be coextensive with axons, terminal arbors, and mechanoreceptor endings (Rice et al., 1997).

5. Anti-BNaC1α (mammalian brain sodium channel BNaC; rabbit polyclonal; 1:500; gift from Dr. Jaime García-Añoveros). The antigen was N-terminus peptide MDLKESPSEGSLQPSSC (corresponding to residues 1-16 of mouse, rat, and human BNaC1α). The BNaC antibody has been shown to identify low-threshold mechanoreceptors (Garcia-Anoveros et al., 2001).

Primary antibodies against MBP (myelin basic protein), VR1 or TrpV1 (vanilloid receptor 1; capsacin binder), NPY (neuropeptide Y, labeling sympathetic innervation), TH (tyrosine hydroxylase), and GAP43 (growth-associated protein 43, marker for neural growth), used successfully in previous rat, monkey and human studies (Albrecht et al., 2006; Fundin et al., 1997; Paré et al., 2001) did not produce detectable labeling on manatee tissue.

All 14μm thick sections were first preincubated with 1% bovine serum albumin (BSA) and 0.3% Triton X-100 in 0.1M PBS for 1 hour, then incubated with a solution of primary antibody (diluted in PBS with 4% calf serum or 1% BSA and 0.3% Triton X-100) overnight at 4°C at high humidity. Slides were then rinsed in PBS for 30 minutes and subsequently incubated in the dark at room temperature for 2 hours with either Cy3 or Alexa488 for red fluorescence (1:500) or Cy2 for green fluorescence (1:250) conjugated secondary antibodies (Molecular Probes, Inc., Eugene, OR; Jackson Immunoresearch Laboratories, Inc., West Grove, PA) diluted in PBS or BSA with 0.3% Triton X-100. Slides were then rinsed in PBS and either temporarily coverslipped under PBS (in the case of future double labeling) or permanently coverslipped. Double labeling was usually accomplished by repeating the immunofluorescence procedure described above. In some cases double labeling was achieved through a single cycle of incubations beginning with a 1:1 mix of the monoclonal and polyclonal primary antibodies. To control for non-specific labeling, incubation with primary antibody was omitted or the primary

antibody was preincubated with a specific blocking peptide. The 75µm thick sections were processed free floating in the same dilutions of antibodies as the thinner sections. Incubations were for 4 days in primary antibodies and overnight in secondary antibodies at 4°C. Rinses were for at least 4 hours.

Sections were analyzed with an Olympus Provis AX70 microscope equipped with conventional fluorescence: 1) Cy3 filters (528-553 nm excitation, 590-650 nm emission) and 2) Cy2 filters (460-500 nm excitation, 510-560 nm emission). Fluorescence images were captured with a high resolution (1280 x 1024 pixels) three chip color CCD camera (Sony, DKC-ST5) interfaced with Northern Eclipse software (Empix Imaging, Inc., Mississauga, ON). Images were deblurred using a deconvolution program based on a 1µm 2-dimensional nearest neighbor paradigm (Empix Imaging, Inc., Mississauga, ON). Samples were imaged on a Zeiss LSM 510Meta confocal microscope (Carl Zeiss MicoImaging, Inc., Thornwood, NY) equipped with an Argon (488 nm exc.) and a green HeNe (543 nm exc.) laser. Emissions were collected using a Band Pass 500-530 nm emission filter for Alexa Fluor 488. For CY3 either a Long Pass 560 nm emission filter or a Band Pass 5650-615 nm emission filter was used, depending on whether the sample was singly or doubly labeled. Images were collected with a Plan-Neofluor 25x/0.8 Imm corr DIC lens with the pinhole set for 1 Airy Unit. Confocal image Z-stacks were collected at 512 x 512 pixel x-y resolution and 1µm steps in Z. The 3-D red-green stereo anaglyph (Fig. 2-9B) and the 3-D stereo pairs (Fig. 2-9, A, D, E) were generated using the Zeiss LM510 software. The 3-D surface rendered images (Fig. 2-8, A-H) were produced using the VolumeJ plugin in the ImageJ software software (http://rsb.info.nih.gov/ij/). Figures were assembled using Adobe Photoshop CS, Adobe Illustrator CS, and Microsoft PowerPoint software.

Since the intensity of immunolabeling for the numerous antibodies used in the present study is attributed to many variables that cannot be individually quantified, this study does not attempt to quantify the relative amounts of labeled antigens. These variables include: 1) true differences in the presence and quantity of the antigen, 2) whether the antibody is monoclonal or polyclonal, 3) background labeling, 4) antibody concentration, 5) efficacy of the antibody, and 6) location of the antigen (i.e. membrane or cytosol). Because the labeling intensities differed between the various types of antibodies, the photomicrographs compiled for illustrative purposes were adjusted using Northern Eclipse, Adobe Photoshop CS (San Jose, CA), and Microsoft Powerpoint (Redmond, WA) software so that the maximum labeling contrast and intensity were similar for each antibody.

Results

Facial Vibrissae

The basic structure of the U2 follicle was examined first due to its size, behavioral significance, and substantial innervation (Reep et al., 2001; 2002). The U2 displayed a pronounced epidermal invagination at the mouth of the FSC before the beginning of the capsule and the follicle proper (Fig. 2-2; Fig. 2-3A). Dermal papillae projecting into the epidermal surface were laden with fine-caliber presumptive C fibers (Fig. 2-3B) that co-labeled for anti-PGP and anti-CGRP (Fig. 2-7A), as well as small-caliber presumptive Aδ fibers that co-labeled for anti-PGP and anti-NF200 (Fig. 2-7B) at the level of the rete ridge collar (RRC), but no Merkel cells were observed in the RRC or adjacent epidermis. A small distribution of presumptive Pacinian corpuscles was also observed just below the epidermis (Fig. 2-7M). A narrow, short outer conical body (OCB) was also present and a circumferential array of fine caliber fibers with presumptive free nerve endings (FNEs) was evident at the inner conical body (ICB) level (Fig. 2-3C) and was PGP-positive and with minimal NF-positive innervation (Fig. 2-

7C). No transverse lanceolate endings were observed. Also present at the lower extent of the ICB region and the upper extent of the ring sinus was a high distribution of "tangle" nerve endings (Fig. 2-3D), novel endings observed in this study that appear morphologically similar to reticular endings generally seen in other taxa along the mesenchymal sheath at the upper extent of the trabeculated cavernous sinus (CS). These large nerve endings were supplied by large caliber presumptive Aαβ or Aβ fibers and were positive for PGP, S100 and NF200 as well as for BNaC (Fig. 2-7H, I) which classifies them as low threshold mechanoreceptors responsive to mechanical pressure. A subregion of each ending was also CGRP-positive (Fig. 2-7J). Confocal imaging revealed an intricate mesh of NF-positive fibers interspersed among DAPI (4',6-diamidino-2-phenylindole)-positive nuclei all within a PGP-positive cytoplasmic ending (Fig. 2-8D, F; Fig. 2-9A, B). Proceeding to the ring sinus (RS) level, a dense distribution of Merkel cells (MCs) was present in the outer root sheath (Fig. 2-3E). The MCs formed a circumferential array with some branching, but individual MCs without visible innervation from branches of the deep vibrissal nerve (DVN) predominated. When present, innervation was supplied by large caliber, presumably Aαβ or Aβ fibers. Widely spaced longitudinal lanceolate endings (LLEs) were present but did not form a dense palisade as in other species. Each LLE appeared to have a single associated terminal glia, although this was not examined in detail. The majority of LLEs appeared unbranched (Fig. 2-8C) and in several morphologies: a studded blade form; a smooth blade; and a curved hook ending (Fig. 2-3E). The lanceolate endings were supplied by the DVN to the mesenchymal sheath of the RS by larger caliber afferents presumably of Aαβ or Aβ classification. Clublike endings were also found at the RS level in close proximity to the rudimentary ringwulst along the mesenchymal sheath. In the region of the cavernous sinus FNEs were observed in addition to another type of novel nerve ending discovered along the trabeculae

(Fig. 2-4A, E; Fig. 2-8A). The latter stained positively for PGP, S100 and NF200 as well as for BNaC, identifying it too as a low threshold mechanoreceptor (Fig. 2-7E, F; Fig. 2-9C, E). Low CGRP activity was also detected (Fig. 2-7G). Representative endings from each of the two novel ending groups were reconstructed using confocal imaging to confirm the three dimensional structural morphology and to ensure that the unusual structure was not simply a result of an aberrant plane of section through the FSC. No Ruffini or reticular endings were observed. Within the medulla of the hair shaft, an extensive network of fine caliber fibers labeled intensely for anti-PGP and with minimal NF-positive innervation present (Fig. 2-4B; Fig. 2-7K). The L1 vibrissae were also examined and found to be structurally similar to U2 vibrissae. Deep epidermal papillae filled with fine caliber fibers were present at the RRC level along with "tangle" endings at the lower ICB/upper RS level. Single-blade termination LLEs and predominantly uninnervated MCs were also present at the RS level. Peptidergic and non-peptidergic C fibers sparsely innervated the trabeculae and interior capsule of the CS. Novel trabecular endings and extensive FNEs were visible within the CS and notably extensive peptidergic C-fiber innervation was present within the hair shaft medulla as seen in U2 vibrissae (Fig. 2-4C).

Bristle-like hairs (BLHs; Fig. 2-2) from the oral disk region were examined next due to their involvement in tactile exploration and object recognition. Merkel endings and fine caliber fibers were present at the RRC and epidermal level but the prominent epidermal invagination leading to the follicle proper in U2 and L1 vibrissae was absent in BLHs (Fig. 2-5A). A sparse distribution of presumptive Meissner's corpuscles was also observed at this level (Fig. 2-7L). A short OCB proceeded to a highly vascularized ICB region (Fig. 2-5E) with a dense distribution of "tangle" endings at the lower ICB/upper RS level along the mesenchymal sheath (Fig. 2-5C,

D; Fig. 2-8G). Densely distributed Merkel cells, mainly without visible innervation, were present at the RS level along with widely spaced single-blade LLEs and both were innervated by large caliber fibers branching from the DVN (Fig. 2-5A, D; Fig. 2-8E). Clublike endings were present in the ringwulst region (Fig. 2-5B). Novel trabecular endings were present along the connective tissue of the CS (Fig. 2-4F) along with FNEs but the medulla of the hair shaft lacked the substantial small caliber fiber innervation seen in the U2 and L1 vibrissae (Fig. 2-5F). Supradisk follicles thought to be morphologically similar to postfacial FSCs (Reep et al., 2001) possessed attributes corresponding to those of the BLH vibrissae including the presence of "tangle" endings within the upper RS, the presence of novel trabecular endings (Fig. 2-4D), and the absence of extensive innervation of the hair shaft medulla, but with the exception of having a well-innervated Merkel network at the RS level (Fig. 2-9D) that was not seen in the BLH follicles.

Postfacial Vibrissae

Postfacial follicle innervation was characterized in 6 body regions (Fig. 2-1A; Fig. 2-2): along the dorsal midline (including rostral, central, and caudal samples), at the ventral midline, and on the tail (dorsocentral and lateral edge). Fine caliber presumptive C fibers (PGP+/CGRP+) as well as small caliber presumptive Aδ fibers (PGP+/NF200+) were found to form extensive arrays projecting into the epidermis of the RRC (Fig. 2-6B, C). Merkel endings were present within the RRC at the base of the epidermis (Fig. 2-6B). At the RS level a small distribution of "tangle" endings (Fig. 2-6D-I; Fig. 2-8H) and single-blade termination LLEs (Fig. 2-6F) were observed along with an extensive network of MEs that was particularly pronounced in the dorsocentral FSCs (Fig. 2-6F; Fig. 2-8B). In contrast to the perioral vibrissae examined, the majority of MCs at the RS level of postfacial vibrissae appeared to be innervated (Fig. 2-6A, F-I). In accordance with the facial vibrissae, no Ruffini or reticular endings were observed in the postfacial vibrissae. The novel endings present in the trabeculae of the facial follicles were also

notably absent in the postfacial vibrissae examined and though presumptive FNEs were visible within the CS, no pronounced innervation was present within the medulla of the hair papilla.

Discussion

Manatee Vibrissae: Overall Comparative Structure

The facial and postfacial vibrissae of manatees emanate from encapsulated blood-filled sinus complexes (Reep et al., 2002) making them true vibrissae (Rice et al., 1986). The FSCs are relatively short compared to the length and caliber of the hairs (Reep et al., 1998). The facial hairs are keratinized and unusually rigid, including the region close to the hair papilla. In contrast, rat and cat vibrissae are soft near the hair papilla and the deep half of the CS and gradually become more rigid near the upper end of the lower CS (Ebara et al., 2002). Vibrissae FSCs in smaller mammalian species also generally exhibit blood-filled spaces along the upper extent of the ring sinus but lack well-defined trabeculae, whereas the manatee exhibits well-developed trabeculae at the upper RS level where the mesenchymal sheath expands to form the ICB. The neck of the manatee FSC at the level of the OCB and ICB regions is very long and may contribute to the facial vibrissae being rigidly maintained within the FSC. In smaller species it is likely that the deep end of the vibrissa is more flexible, with the smaller neck of the FSC acting as a fulcrum against which the hair shaft can lever within the FSC. As such, the trabeculae of the CS in smaller species are likely to function more in lateral stabilization than in the manatee, where the hair shaft is rigidly anchored at the base and neck of the FSC. The attenuated ringwulst of manatee vibrissae extends rigidly from the mesenchymal sheath rather than hanging down from its point of attachment as seen in other species. Dense peptidergic and non-peptidergic C-fiber innervation was also intimately wrapped around the outer surface of the FSC capsule, particularly along the upper half of the capsule. This may be present in other species as well, but to a lesser extent, and has not been fully investigated.

Facial Musculature Involved in Exploratory and Prehensile Vibrissal Behaviors

Previous experiments have shown that infraorbital branches of the maxillary nerve insert into the upper bristle pad whereas the inferior alveolar branch of the mandibular nerve supplies the vibrissae of the lower pad of the manatee face. The dorsal and ventral buccal branches of the facial nerve supply the superficial facial musculature and are likely to contribute to bristle eversion and feeding behavior movements (Reep et al., 1998). The U2 follicles are specifically associated with the *M. levator nasolabialis* muscles (Marshall et al., 1998b), making them homologous to mystacial vibrissae, and although individual follicles within a U2 field are not moved independently, the left and right U2 fields can act independently from each other (Marshall et al., 1998a). The L1 follicles are supplied by mental branches of the inferior alveolar nerve (Reep et al., 1998) and are protruded by mentalis muscle contraction (Marshall et al., 1998b), making them homologous to mental vibrissae. At rest the U2 vibrissae are retracted within skin folds and are everted by volume displacement through contraction of the *M. levator nasolabialis* and the circular *M. buccinatorius* muscles during manipulative behaviors (Marshall et al., 1998a; b). When presented with a novel object, manatees generally touch the object with the oral disk (involving the BLH follicles) first in a side-to-side sweeping motion and then grasp with the U2 follicles, but the BLH follicles are not actively moved (Marshall et at., 1998a).

Sensory Innervation of the Rete Ridge Collar and Epidermis

A high density of thin, tapering dermal papillae curve toward the vibrissae at the mouth of the FSC and penetrate throughout an extremely thick epidermis (Fig. 2-2). Other species generally lack papillae in non-glabrous skin and exhibit a relatively thin epidermis. Numerous peptidergic and non-peptidergic C fibers enter the papillae and extend in a straight, unbranched manner far into the overlying epidermis and perpendicular to its surface. Little innervation was present between the papillae, but the papillae were very closely spaced, resulting in a high

density of innervation to the epidermis. Thin-caliber NF-positive fibers also penetrate into most papillae and appear to branch, indicating that these fibers may serve as mechanoreceptors of the papillae, but NF labeling was rarely seen on endings penetrating the epidermis. Occasional clusters of Merkel cells and innervation are located at the base of the epidermis between papillae, and these appear to be widely spaced over the epidermis. Throughout the upper dermis and particularly at the RRC extends a dense vascular network that is well-innervated with dense sympathetic innervation and, to a somewhat lesser extent, CGRP-positive sensory innervation. Thin NF-positive innervation was also present. Thick-walled, especially well-innervated locations appeared to be arteriovenous shunts. While we did not fully characterize innervation associated with the vascular supply in the manatee, there appears to be an extensive network for regulating blood flow to the epidermis, potentially representing a thermal regulatory mechanism (Fig. 2-7N). Occasional Pacinian-like corpuscles were also seen and appeared similar to those present among arterial networks in the glabrous skin of monkeys (Fig. 2-7M; Paré et al., 2002). However, these were at a surprisingly superficial location at the base of the epidermis in the manatee, which may be related to the manatees' extensive superficial vascular network.

Sensory Nerve Endings of the Inner Conical Body and Ring Sinus

Merkel endings are thought to be low threshold, slowly adapting mechanoreceptors capable of detecting compression stimuli and directionality (Iggo, 1963, 1966; Iggo and Muir, 1969; Johansson et al., 1982a,b; Johansson and Vallbo, 1983; Munger et al., 1971; Gottschaldt et al., 1973; Rice et al., 1986; Lichtenstein et al., 1990). Given the dense distribution of MEs in the outer root sheath of both facial and postfacial vibrissae it seems that manatee FSCs are heavily invested in detecting directionality of hair deflection (Burgess and Perl, 1973; Rice et al., 1986), and a commitment of nerve endings to this task would support our proposal that manatees use tactile hairs to detect hydrodynamic stimuli in a manner analogous to the lateral line system

present in fish (Reep et al., 2002). In microchiropteran bats, “touch domes” along the wings are heavily invested with Merkel cells and FNEs that appear to detect air flow and aid in navigation and maneuvering (Zook, in press; Zook, 2005; Zook and Fowler, 1986) in much the same way that manatee postfacial vibrissae might perceive water flow. Merkel endings in the manatee were found along the RS and ICB regions (facial and postfacial vibrissae) as well as in the RRC (postfacial vibrissae and BLHs only). The presence of the same receptor at different locations along the follicle axis may indicate that the MEs are involved in extracting different features of a stimulus at these positions. At the RS level, MEs are situated in the external root sheath between the inner root sheath and the glassy membrane, a location that makes them susceptible to small-angle deflections of the follicle (Gottschaldt et al., 1973; Rice et al., 1986) whereas MEs of the RRC are in a location that presumably lends itself to detection of large-angle deflections of a vibrissa (Rice et al., 1986). By extension, the postfacial vibrissae and BLHs of the Florida manatee appear to be specialized for the complete range of deflection intensities, due to the presence of MEs at both the RRC and RS levels, whereas perioral facial vibrissae may be more receptive to small-angle hair deflections, due to having MEs at the RS level only. While the significance of most MCs at the RS level of facial vibrissae lacking visible innervation remains uncertain, it is possible that these MCs experience a high turnover rate. The presence of clublike endings at the attachment site of the ringwulst indicates that this region is sensitive to mechanical perturbations as well.

Lanceolate endings are thought to be low threshold, rapidly adapting stretch receptors that encode dynamic properties of vibrissal deflection such as acceleration and deceleration (Burgess and Perl, 1973; Gottschaldt et al., 1973; Tuckett, 1978; Tuckett et al., 1978; Rice et al., 1986, 1997; Lichtenstein et al., 1990). Whereas the majority of the longitudinal lanceolate

afferents gave rise to a single blade-like termination at the RS level in the U2 facial vibrissae, a subset of LLEs exhibited a forked termination or a morphological variant including the studded and hook endings observed. A curved "shepard's crook" morphology was also observed in LLEs along the mesenchymal sheath at the RS level of the cat and guinea pig (Rice et al., 1986). It is possible that the morphological variants of the LLEs have common inherent physiological properties but may transduce slightly different aspects of mechanosensory perception. The relatively wide spacing and low density of distribution of the LLEs in the mesenchymal sheath of all follicles examined suggest that velocity detection is of lesser importance in both the facial and postfacial vibrissae. Circumferentially oriented peptidergic and non-peptidergic FNEs were found in the ICB and OCB regions. The density of distribution was far less than the well-organized, dense circumferential bundles seen in the ICB of rats and mice, and to a lesser degree in cats. These fibers are thought unlikely to confer linear or spatial directionality given their circumferential orientation, and the absence of transverse lanceolate endings (TLEs) supports the hypothesis that TLEs are related to whisking behavior and generally seen only in species such as hamsters, mice, rats and gerbils that utilize this behavior to explore the environment (Rice et al., 1986).

Merkel cell-neurite complexes and lanceolate endings appear to be responsive to a wide frequency range and may be used to detect sounds when a vibrissa is deflected at the proper frequency (Gottschaldt and Vahle-Hinz, 1981; Hyvärinen 1989, 1995; Stephens et al., 1973), a capability that would support the hypothesis of extensive overlap between auditory and somatosensory areas of manatee cerebral cortex (Sarko and Reep, 2007). In fact, primary auditory cortex appears to be occupied exclusively by cluster cortex areas that feature Rindenkerne, or "cortical nuclei" located in layer VI and thought to be analogous to barrels seen

in a variety of species and potentially representative of individual vibrissae (Dexler 1912; Johnson et al., 1994; Marshall and Reep, 1995; Reep et al., 1989; Rice, 1995). Furthermore, a behavioral study that assessed the underwater audiogram of the West Indian manatee found that one manatee adjusted its responses to low-frequency (<0.4 kHz) sounds by pivoting its body roughly 45 degrees and lowering its head (a response not exhibited for higher frequencies), which potentially indicates adjustment of perceptual focus from sound to vibrotactile stimuli (Gerstein and Gerstein, 1999).

The "tangle" endings observed at the lower inner conical body/upper ring sinus level, and present in all manatee vibrissae examined here, appear to be novel because we are unaware of sensory endings of this morphology and immunological characterization observed at this level in the vibrissae of any other species. "Tangle" endings consisted of two or more exceptionally large endings abutting the basement membrane and supplied by a large Aβ fiber. Each ending consisted of thick tangles of NF+ processes embedded in a matrix of PGP-positive cytoplasm and S100-positive terminal glia. The endings are concentrated in the mesenchymal sheath at the level of the upper ring sinus trabeculae and may be involved in directionality detection associated with deflection of the hair shaft against the upper trabeculae. These endings are also BNaC-positive and therefore are likely low-threshold mechanoreceptors.

Cavernous Sinus Innervation

The medulla of the hair papilla extends to an extremely superficial location, well into the neck of the FSC, in U2 and L1 facial vibrissae. Cats also exhibit a superficially extending medulla, but the interface between the medulla and the cortex is smooth whereas in manatees it has a jagged appearance (Ebara et al., 2002). Manatee U2 and L1 vibrissae also have extensive peptidergic and non-peptidergic C-fiber innervation within the medulla. The FNEs present within the hair shaft medulla and spanning the trabeculae of the CS have been implicated in pain and

temperature sensation (Rice et al., 1986). Alternatively, the FNEs found within the medulla of the hair papillae of U2 and L1 vibrissae may be analogous to dentinal tubule innervation. Given the rigidity of manatee facial follicles (particularly the perioral fields) compared to the flexible and easily displaced hair follicles of most mammals, it is possible that sensory innervation is committed to stress detection and load application in order to assess force transmission without actual material displacement as seen in the dental sensory receptors of tooth pulp (Byers, 1984; Byers and Näri, 1999). This innervation may also be a sensory adaptation to oripulative behaviors. In another marine mammal sensory specialist, the narwhal, dentinal tubules within the unusual tusk are thought to function as a hydrodynamic sensor detecting fluid flow, salinity gradients, temperature and pressure (Nweeia et al., 2005).

The absence of reticular and Ruffini endings along the basement membrane in manatee vibrissae is unusual, as is the presence of novel endings within the trabeculae of facial vibrissae. Ruffini endings are affiliated with collagen bundles and appear to function as tension receptors residing along the mesenchymal sheath (Rice et al., 1986; Zelena, 1994) whereas reticular endings terminate in the upper third of the CS against the glassy membrane and may be directionally sensitive (Ebara et al., 2002). Spiny and encapsulated endings (previously thought to be Ruffini endings; Rice et al., 1997) were also found at the lower CS level of the rat and cat, and Ebara et al. (2002) speculated that the cumulative CS innervation is responsive to tension generated by the trabeculae during follicle deflection.

The nerve endings observed within the trabeculae of the lower cavernous sinus and present only in the facial vibrissae examined here (U2, L1, BLH and supradisk follicles) appear to be novel in that they are embedded within the trabecular matrix rather than against the basement membrane. These endings were supplied by a relatively small-caliber Aβ fiber with

one axon innervating single or multiple endings. Individual endings consisted of fine-caliber tangles embedded within a terminal glial matrix and were BNaC-positive, indicating that they too are low threshold mechanoreceptors. It is possible that these trabecular endings are responsive to tension induced by deflection of exceptionally rigid vibrissae (Reep et al., 1998) which might involve modified sensory endings in order to optimally detect deflection. Alternatively, it has been proposed that the trabeculae of the CS may function in attenuating vascular pulsations in the arterial supply entering the base of the FSC, thereby creating more uniform blood flow at the RS level (Melaragno and Montagna, 1953; Rice et al., 1986). Novel endings within the trabeculae may have evolved to provide additional sensitivity in monitoring vascular supply at this level.

Marine Mammal Vibrissae

Vibrissal sensory nerve endings of a limited number of other marine mammals have also been studied. Hyvärinen (1995) examined the exceptionally well-innervated mystacial vibrissae of the ringed seal (*Phoca hispida*) using histology and electron microscopy. The length of the upper cavernous sinus (UCS) accounts for 60% of the vibrissa, situating the ring sinus at a low level compared to most mammals. At the RS level, LLEs were found abutting the glassy membrane while MEs were found below the glassy membrane and a prominent ringwulst was present (Hyvärinen and Katajisto, 1984; Hyvärinen, 1989). All MCs appeared innervated and formed a well-developed network (Hyvärinen, 1995). Hyvärinen (1995) also described numerous encapsulated end-organs in the lower CS situated within the trabeculae and morphologically similar to “Ruffin’s corpuscles.” These may be similar to the nerve endings reported here for the manatee, but documentation that would allow for a direct comparison was absent. Dykes (1975) classified and compared the afferent fibers serving cat and harbor seal vibrissae. He found that a the majority of harbor seal vibrissae respond to vibrations and that the majority of afferent fibers

from the infraorbital nerve (85% versus 66%) serve harbor seal vibrissae. Approximately two-thirds of these fibers were rapidly adapting and the remainder were slowly adapting, and most fibers (71% in harbor seals and 75% in cats) were directionally sensitive. Bearded seal (*Erignathus barbatus*) FSCs have also been characterized and are thought to be extensively innervated active-touch systems adapted to benthic foraging (Marshall et al., 2006). The mystacial vibrissae have an extensive UCS comparable to that of the ringed seal but unlike the facial follicles of the manatee where the UCS is minimal. A prominent ringwulst is present at the RS level along with an extensive ME network and LLEs. Merkel innervation predominates but was not observed at the RRC level as was observed for the manatee BLHs and postfacial vibrissae.

Comparative Considerations

Through studying a range of species (including opossums, rodents and pinnipeds) for functional variation and unifying principles of vibrissae, Brecht et al. (1997) found that mystacial macrovibrissae tend to form rows in which effective whisker length increases exponentially in the caudal direction, with each row operating as a functional unit by sampling highly overlapping spatial information perpendicular to the rostrocaudal axis. At the cortical level there also appears to be preferential connectivity between barrels within a row (Simons, 1978; Simons and Woolsey, 1979). Macrovibrissae were proposed to function in spatial orientation associated with distance detection and object location while microvibrissae appeared optimized for object recognition (Brecht et al., 1997). By extension, the postfacial vibrissae of the manatee appear to have adopted a function analogous to that of macrovibrissae through optimization for spatial and directional sensitivity while the oral disk and the BLHs in particular serve the microvibrissal role of direct tactile object recognition. Instead of the direct surface contact stimulation that macrovibrissae generally receive, manatee postfacial follicles are exposed to perturbations of the

water and consequently undergo passive deflection. It has been suggested that mammalian vibrissae may serve a complementary auditory function at low frequencies (Gerstein and Gerstein, 1999; Griffin, 1958; Mahler and Hamilton, 1966; Reep et al., 2002; Yohro, 1977). The perioral vibrissae appear to be more adapted to locating and recognizing food, an important task for a strict herbivore that spends 6-8 hours per day looking for food and that must eat the equivalent of approximately 10% of its body weight per day to compensate for a low metabolic rate (McNab, 1978; 1980).

Table 2-1. Specimen categorization.

Specimen	Sex	Length (in cm)	Weight (in kg)	Classification	Cause of Death
TM0406	M	290	393	Adult	Watercraft
TM9728	M	295	500	Adult	Watercraft
TM0506	M	172	134	Calf	Cold stress
MNW0614	F	238	326	Subadult	Watercraft

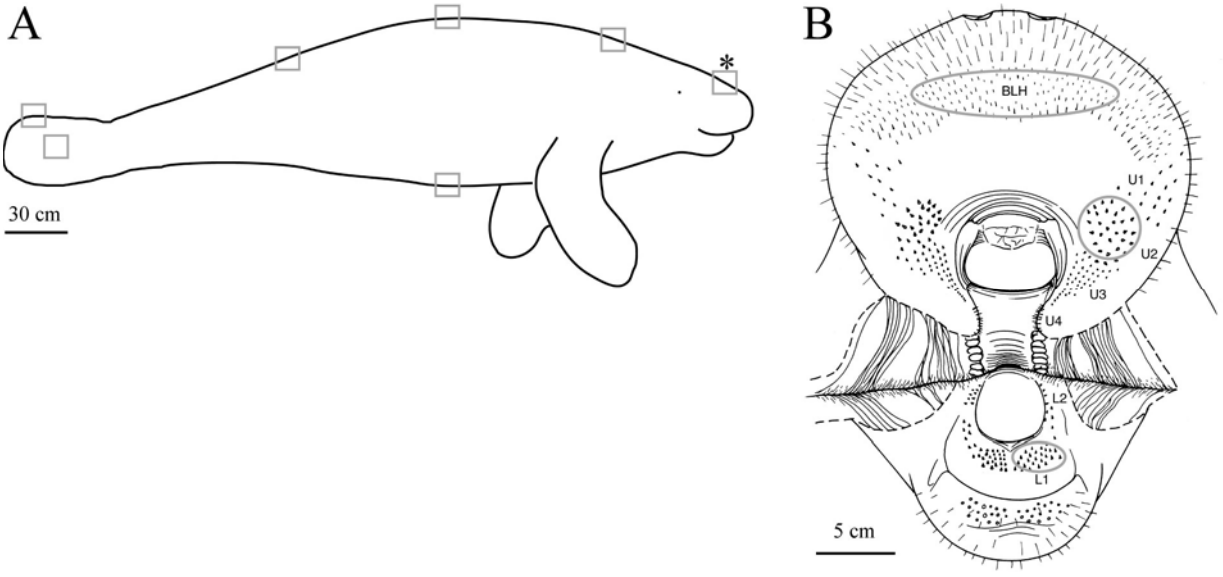

Figure 2-1. Vibrissae sampling regions of the body and face. A) Postfacial body regions of interest include the tail (lateral edge and dorsomedial areas), ventromedial area, and rostral, central, and caudal areas of the dorsal midline. The supradisk region (asterisk) is caudal to the orofacial ridge and also thought to consist of body vibrissae. B) Frontal view of the manatee face with cheek muscles cut to reveal perioral follicle fields. Facial follicles of interest include the bristle-like hairs (BLHs), U2 and L1 follicle fields due to their behavioral significance.

Figure 2-2. Schematic drawing of the structure and innervation of the U2, BLH, and postfacial vibrissal follicle-sinus complexes (FSCs) with innervation types and sensory nerve endings illustrated (RRC=rete ridge collar, OCB=outer conical body, ICB=inner conical body, BM=basement membrane, RS=ring sinus, DVN=deep vibrissal nerve, HP=hair papilla). The relative scales of each FSC are accurate, but innervation is presented for illustrative purposes only (see Fig. 3-9 for accurate scale representations). Overall morphology: The thickness of the capsule and the diameter of the vibrissa decreases progressively from the U2 to the postfacial FSC. The facial vibrissae also exhibited dual innervation from the DVN at the base of the follicle whereas the DVN entered as a single bundle of axons in postfacial vibrissae. Presumptive sympathetic fiber innervation is also depicted based on general characteristics in other mammals. Epidermis and RRC: The epidermis of the U2, BLH and postfacial vibrissae contains superficially projecting dermal papillae within which are fine-caliber Aδ and C fibers. The base of the epidermis of BLH and postfacial FSCs includes Merkel endings. The U2 FSC has a particularly pronounced invagination of the RRC. OCB and ICB: The U2 FSC exhibits a dense network of circumferential free nerve endings while the BLH and postfacial FSCs exhibit only fine-caliber and sympathetic innervation. Novel "tangle" endings are located in the facial and postfacial vibrissae. RS: Dense Merkel networks were present in vibrissae from each body region, but Merkel cells lacking visible innervation predominated in facial vibrissae. Less densely distributed longitudinal lanceolate endings were also observed at this level for each vibrissal type and clublike endings were observed in close association with the rudimentary ringwulst in facial vibrissae. CS: The trabeculae in FSCs from each body region contained fine-caliber innervation with presumptive free nerve endings. The facial vibrissae only included novel endings that spanned the trabeculae. Ruffini and reticular endings were notably absent. HP: Dense fine-caliber innervation was present in the rigid U2 follicle along a medulla that extended to an extremely superficial extent. This innervation was very sparse in the BLH and postfacial vibrissae, and the medulla of each extended less superficially.

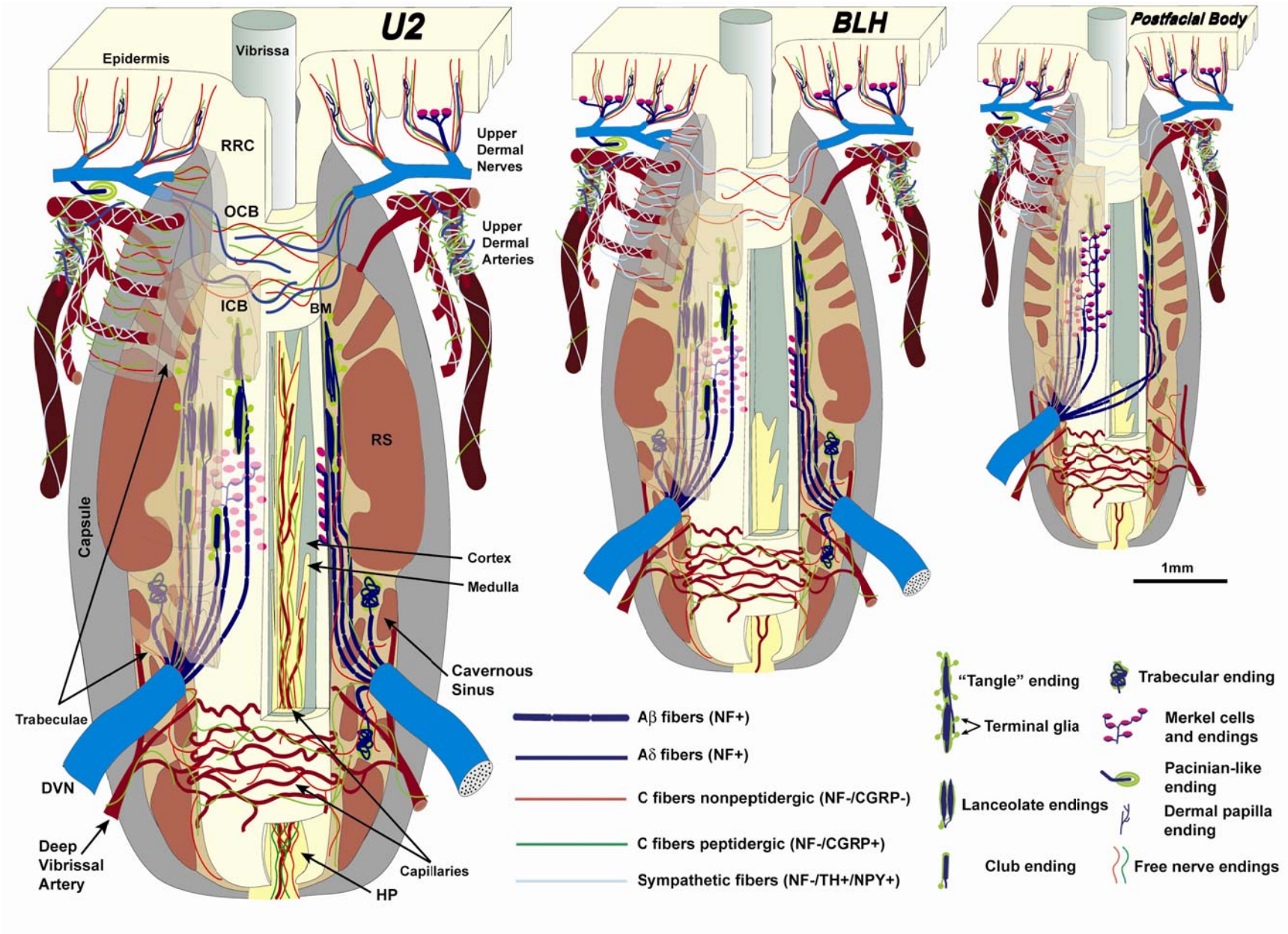
U2
BLH
Postfacial Body
Epidermis
Vibrissa
RRC
Upper Dermal Nerves
OCB
Upper Dermal Arteries
ICB
BM
RS
Capsule
Cortex
Medulla
Cavernous Sinus
Trabeculae
DVN
Deep Vibrissal Artery
Capillaries
HP
1mm
Aβ fibers (NF+)
Aδ fibers (NF+)
C fibers nonpeptidergic (NF-/CGRP-)
C fibers peptidergic (NF-/CGRP+)
Sympathetic fibers (NF-/TH+/NPY+)
"Tangle" ending
Terminal glia
Lanceolate endings
Club ending
Trabecular ending
Merkel cells and endings
Pacinian-like ending
Dermal papilla ending
Free nerve endings

Figure 2-3. Characterization of upper perioral field 2 (U2) follicle innervation. A) A longitudinal U2 section stained for PGP is shown just off the medial axis to reveal various innervation characteristics as well as the deep invagination of the RRC (specimen TM0406). B) Magnified RRC and epidermal region further off the medial axis showing a dense distribution of C- and Aδ- fiber projections (arrow) within dermal evaginations (medial is right). C) Magnification of circumferential FNEs at the ICB level (same plane of section as A). D) Close-up of a representative "tangle" ending including 3 branched mechanoreceptors and a Schwaan cell (arrows and arrowhead, respectively) within the lower ICB region along the mesenchymal sheath (plane of section along the medial axis). E) A dense distribution of Merkel cells (arrow) and representative types of LLEs (arrowheads) including a bifurcated ending, hooked formation, and studded blade-like termination (same plane of section as A). RRC, rete ridge collar; OCB, outer conical body; ICB, inner conical body; RS, ring sinus; CS, cavernous sinus; HS, hair shaft. Scale bar = 1mm for A-B, 250μm for C-E.

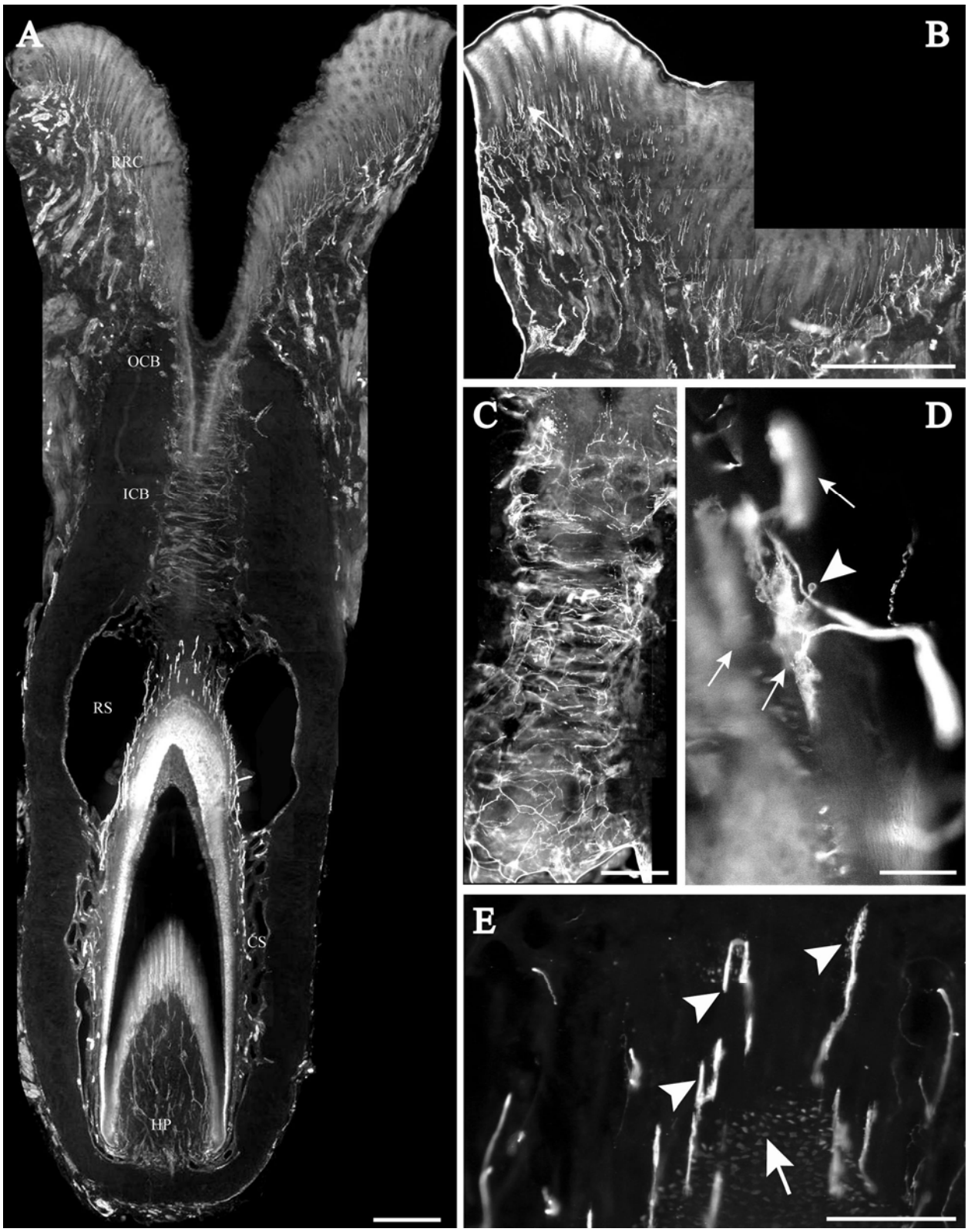
A
RRC
OCB
ICB
RS
CS
HP
B
C
D
E

Figure 2-4. Innervation of the cavernous sinus and hair shaft medulla in facial follicles. A) Extensive innervation of the trabeculated cavernous sinus of a U2 follicle (specimen TM0406) includes novel endings (arrows) and fine-caliber fibers along with the DVN continuing to the ring sinus. B-C) A dense network of small caliber axons and presumptive FNEs proceeding to a remarkably superficial extent in the medulla of a U2 follicle (B; specimen TM0406) and an L1 follicle (C; specimen MNW0614). Magnified views show details of novel trabecular endings seen in a supradisk follicle (D; specimen MNW0614, arrow) a U2 follicle (E; specimen TM0406, arrow) and a BLH follicle (F; specimen TM0406, arrow). Scale bar = 600µm (A), 1mm (B-C), 300µm (D-F).

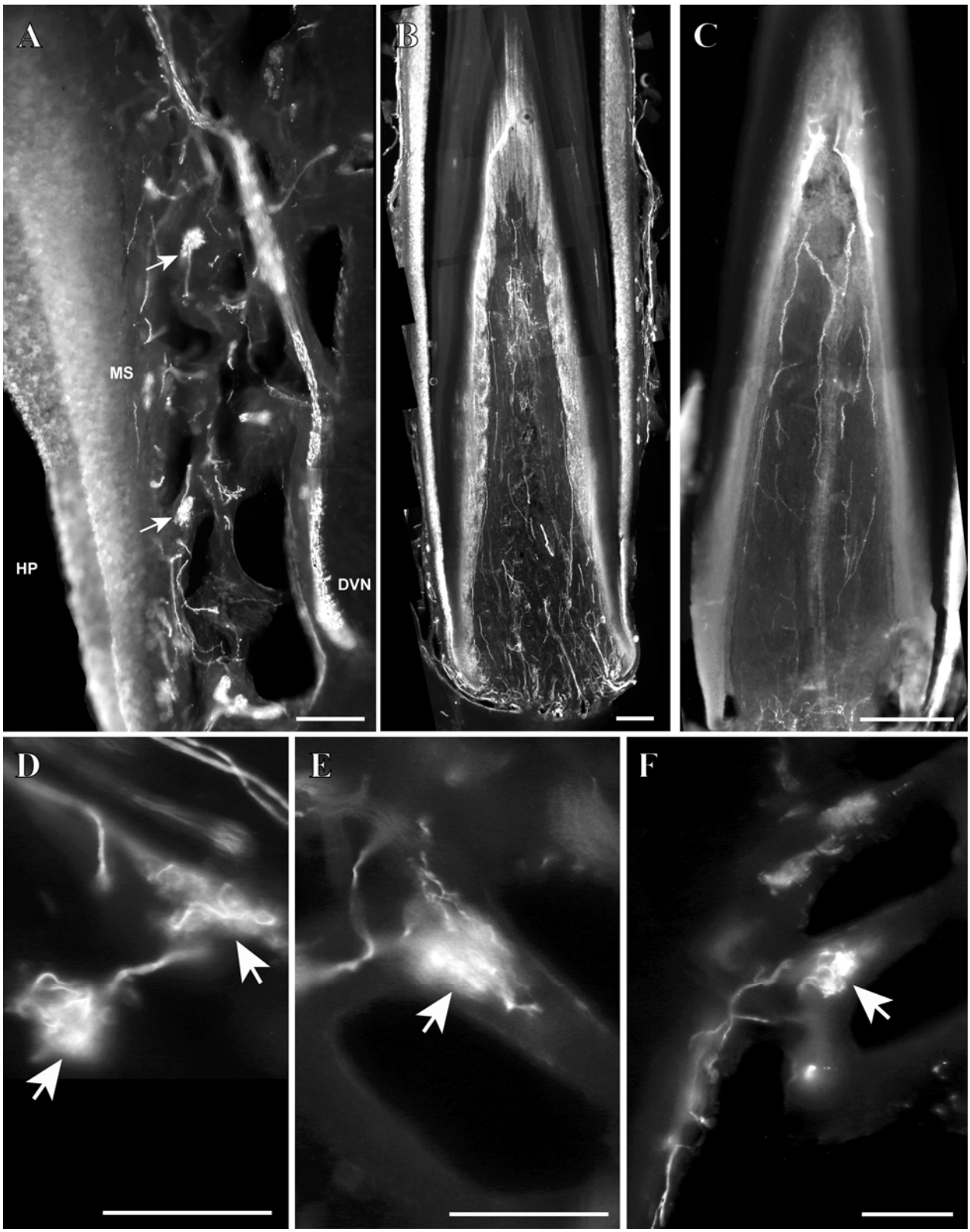
A
B
C
MS
HP
DVN
D
E
F

Figure 2-5. Innervation present in bristle-like hairs (BLHs). A) A longitudinal section of a BLH just off the medial axis stained for protein gene product 9.5 reveals characteristic innervation, including “tangle endings” at the lower ICB/upper RS level (arrowhead), in addition to LLEs (arrow) and MCs (magnified in D) at the RS level. B) “Tangle” endings parallel to a clublike ending (arrow) against the basement membrane at the ringwulst level are shown further from the medial axis. C) “Tangle” endings (arrowheads) with associated Schwaan cells at the superficial extent of the RS (plane of section along medial axis). D) Merkel cells lacking visible innervation (arrow) in addition to “tangle” endings (arrowhead) at the upper RS level (plane of section well past the medial axis). E) Sympathetic innervation of the vascularized inner conical body (plane of section well past the medial axis), and F) a dermal hair shaft medulla lacking the extensive FNE innervation seen in U2 follicles (plane of section along the medial axis). RRC, rete ridge collar; OCB, outer conical body; ICB, inner conical body; RS, ring sinus; RW, ringwulst; CS, cavernous sinus; DVN, deep vibrissal nerve. Scale bar = 1mm (A), 300µm (B-C), 600µm (D-F).

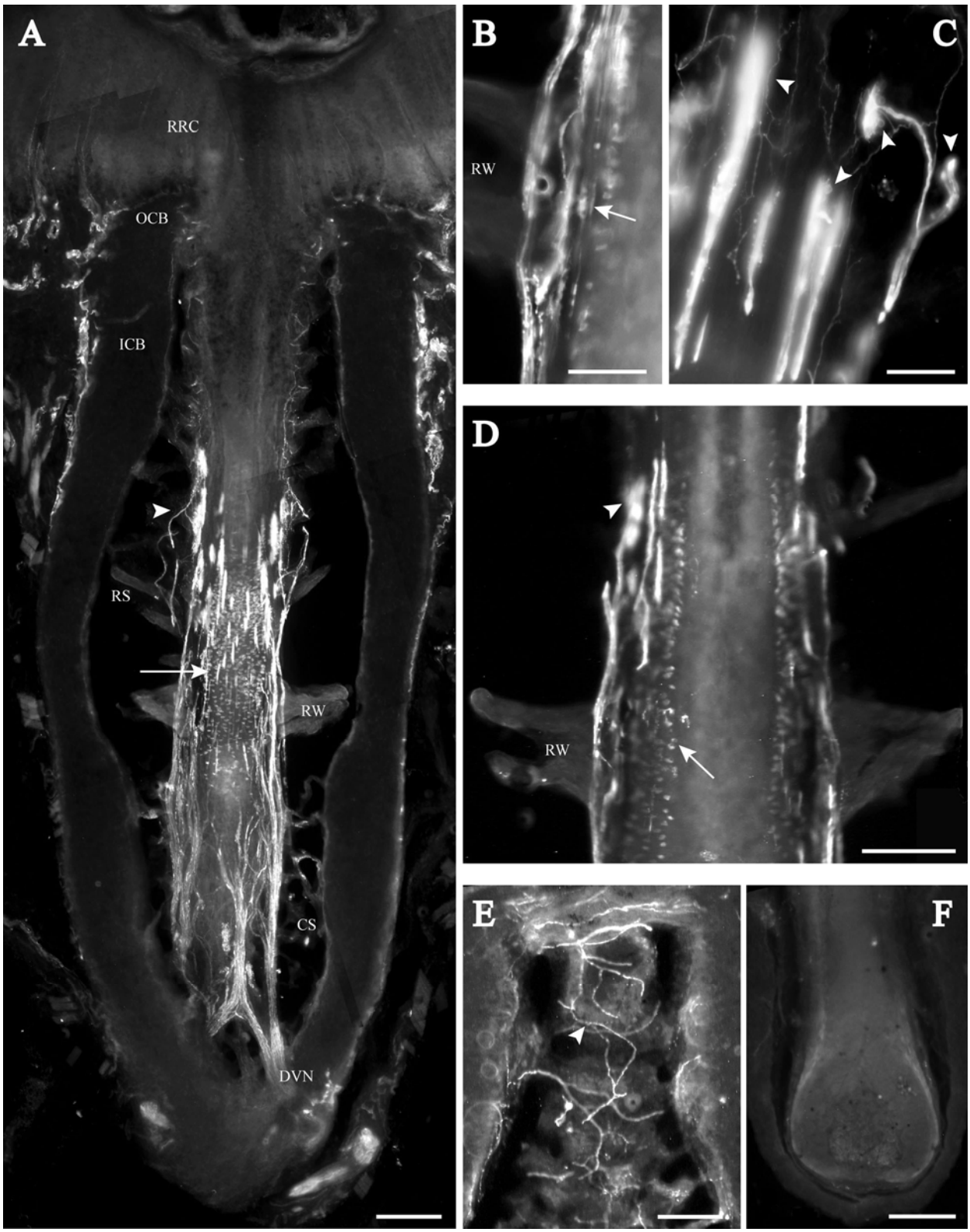
A
RRC
OCB
ICB
RS
RW
CS
DVN
B
RW
C
D
RW
E
F

Figure 2-6. Representative postfacial vibrissae innervation includes dense networks of MEs along with LLEs and "tangle" endings. A) A dorsorostral postfacial hair (TM9728) shows characteristic Merkel innervation (arrowheads) at the RS level. F) A dorsocentral postfacial hair (TM9728) exhibits the presence of LLEs (small arrow), "tangle" endings (large arrow), and a particularly extensive network of MEs (between arrowheads) at the RS and ICB levels. G-I) Follicles from the tail edge (G; MNW0614), ventral body (H; MNW0614), and dorsocaudal body (I; TM9728) reveal "tangle" endings and Merkel innervation (arrows and arrowheads, respectively) at the RS and ICB levels. B-C) Details shown for epidermal innervation (MEs shown with arrowhead; superficial is up) and "tangle" endings (D-E; dorsocentral postfacial hair, specimen TM9728 for B-E) at the upper RS/lower ICB level. All planes of section shown well past the medial axis. NF, 200 kDa neurofilament subunit; PGP, protein gene product 9.5; CGRP, calcitonin gene-related peptide. Scale bar = 1mm (A), 600µm (B-C), 150µm (D-E), 750µm (F, I), 500µm (G-H).

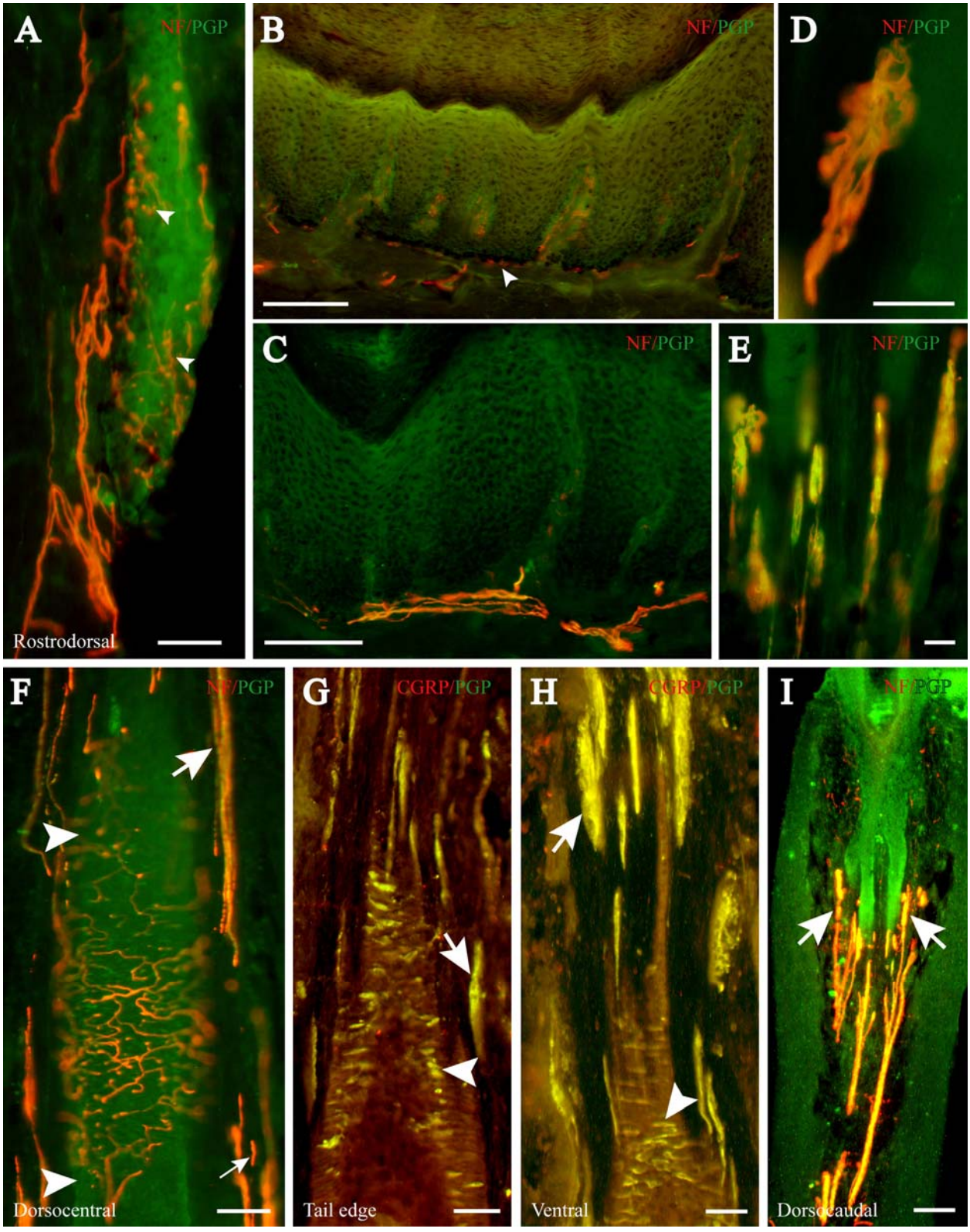
A
NF/PGP
Rostrodorsal
B
NF/PGP
C
NF/PGP
D
NF/PGP
E
NF/PGP
F
NF/PGP
Dorsocentral
G
CGRP/PGP
Tail edge
H
CGRP/PGP
Ventral
I
NF/PGP
Dorsocaudal

Figure 2-7. Immunolabeling attributes of innervation. A-B) Dermal papillae projecting into the epidermis at the RRC level contain C- and Aδ-fiber innervation (CGRP-positive and NF-positive fibers, respectively). C) Circumferential FNEs at the ICB of a U2 follicle reveal mostly fine caliber fibers interspersed among Aδ (NF+) fibers. D) Largely uninnervated MCs (CGRP+) interspersed among MEs (NF+) at the RS level. E-G) Novel endings along the trabeculae of the CS stain positively for BNaC, PGP, S100, NF, and lightly for CGRP (arrows). H-J) "Tangle" endings also stain positively for BNaC, PGP, S100, NF, and lightly for CGRP. K) Presumptive FNEs within the medulla of a U2 follicle hair shaft include mostly fine caliber fibers (PGP+/NF-) interspersed among Aδ (NF+) fibers. L) Meissner's corpuscles were sparsely distributed at the level of the epidermis. M) Pacinian ending found at the base of the epidermis. N) An example of vascular supply associated with NF-positive innervation. Scale bars = 300µm (A-D), 150µm (E-K, N), 75µm (L-M).

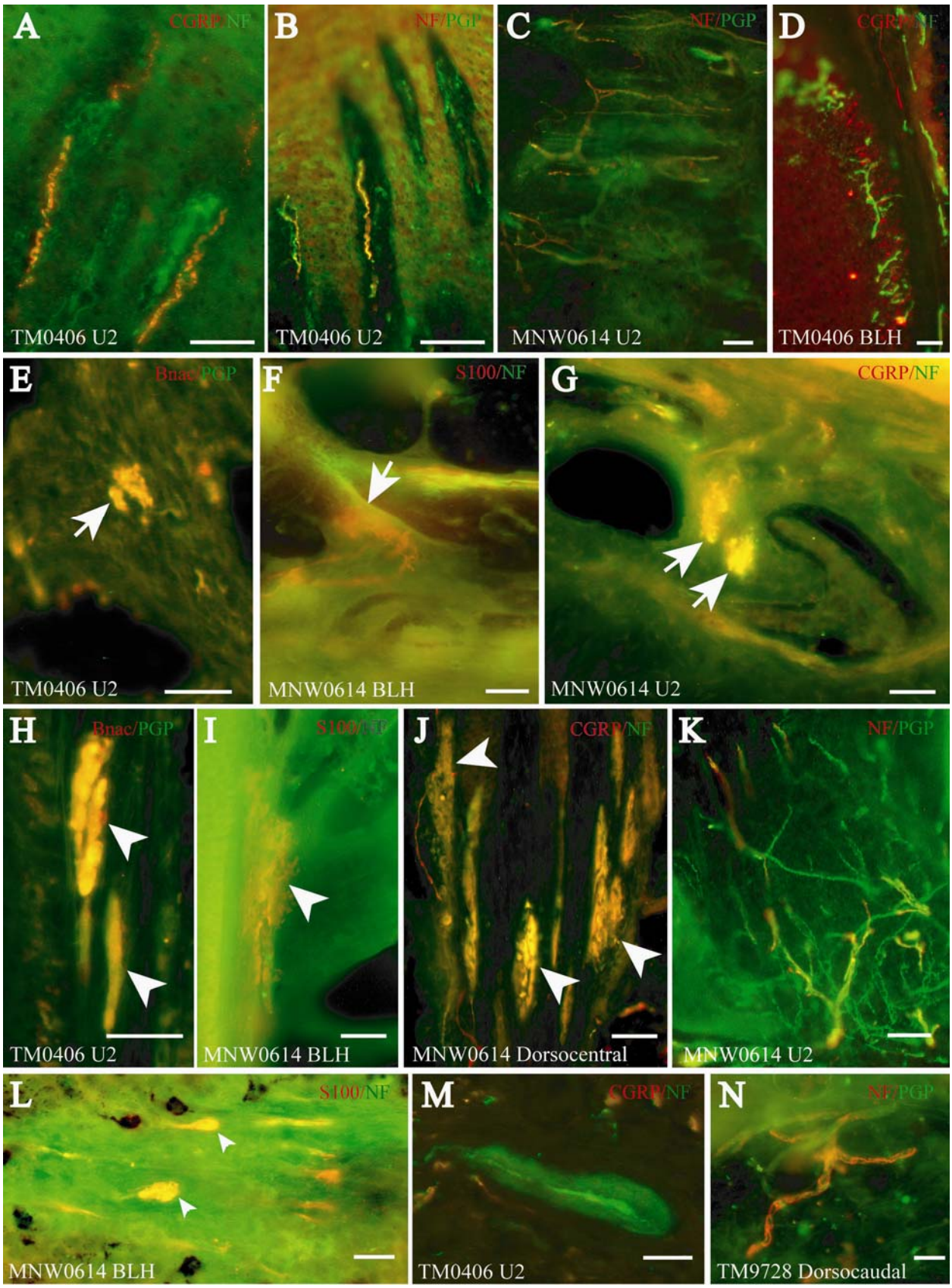
A
CGRP/NF
TM0406 U2
B
NF/PGP
TM0406 U2
C
NF/PGP
MNW0614 U2
D
CGRP/NF
TM0406 BLH
E
Bnac/PGP
TM0406 U2
F
S100/NF
MNW0614 BLH
G
CGRP/NF
MNW0614 U2
H
Bnac/PGP
TM0406 U2
I
S100/NF
MNW0614 BLH
J
CGRP/NF
MNW0614 Dorsocentral
K
NF/PGP
MNW0614 U2
L
S100/NF
MNW0614 BLH
M
CGRP/NF
TM0406 U2
N
NF/PGP
TM9728 Dorsocaudal

Figure 2-8. Confocal surface reconstructions showing the three-dimensional structure of representative follicle innervation and novel mechanoreceptors present in the ICB, RS and CS regions. A) A trabecular ending within the CS (same ending shown in Fig. 2-4E). B) Extensive Merkel ending network in a dorsocentral postfacial vibrissa shows the completeness of innervation (shown in Fig. 2-6F). C) The morphology of a lanceolate ending near Merkel cells at the RS level can be compared to the larger, more intricate "tangle" ending in the lower ICB/upper RS of a U2 follicle (D; also seen in Fig. 2-3D). E) Reconstruction of a DVN penetrating the cavernous sinus illustrating size and associated axons. F-H) Examples of "tangle" endings found in the upper RS/lower ICB level of U2 (F), BLH (G), and dorsocentral postfacial vibrissae (H; also shown in Fig. 2-6E). Scale bars=250μm (A-H).

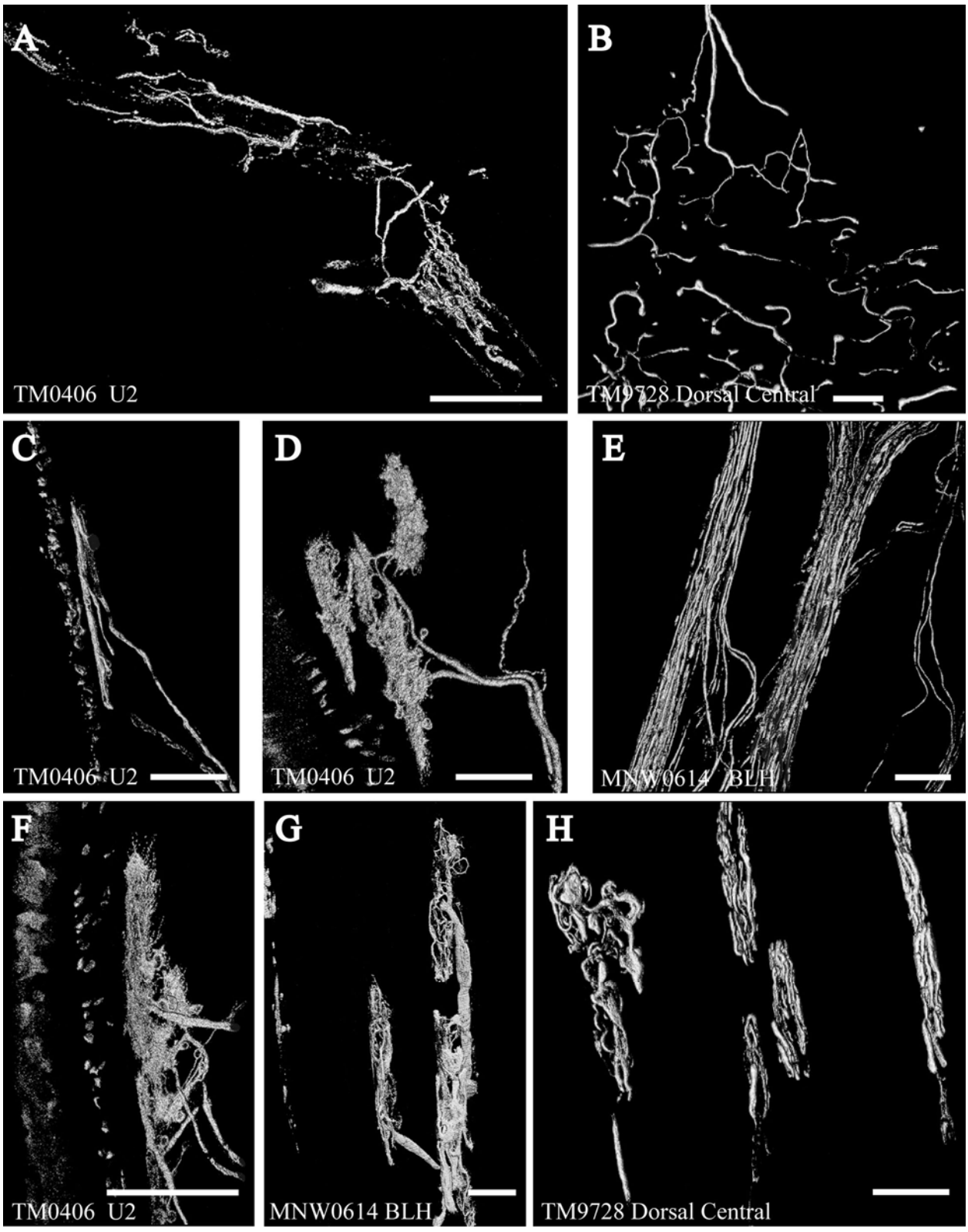
A
TM0406 U2
B
TM9728 Dorsal Central
C
TM0406 U2
D
TM0406 U2
E
MNW0614 BLH
F
TM0406 U2
G
MNW0614 BLH
H
TM9728 Dorsal Central

Figure 2-9. Confocal three-dimensional images of novel endings stained for neurofilament (NF200) and protein gene product 9.5 (PGP). A) Stereo pair depicting a group of "tangle" endings. B) A three-dimensional image (red/green anaglyph) of two "tangle" endings with shared innervation. C) A single-optical section shows a trabecular ending in detail. Red depicts NF-positive endings within a green PGP-positive cytoplasmic meshwork. D) A stereo pair showing Merkel innervation (left-hand pair) and closely associated clublike endings and "tangle" endings (right-hand pair).

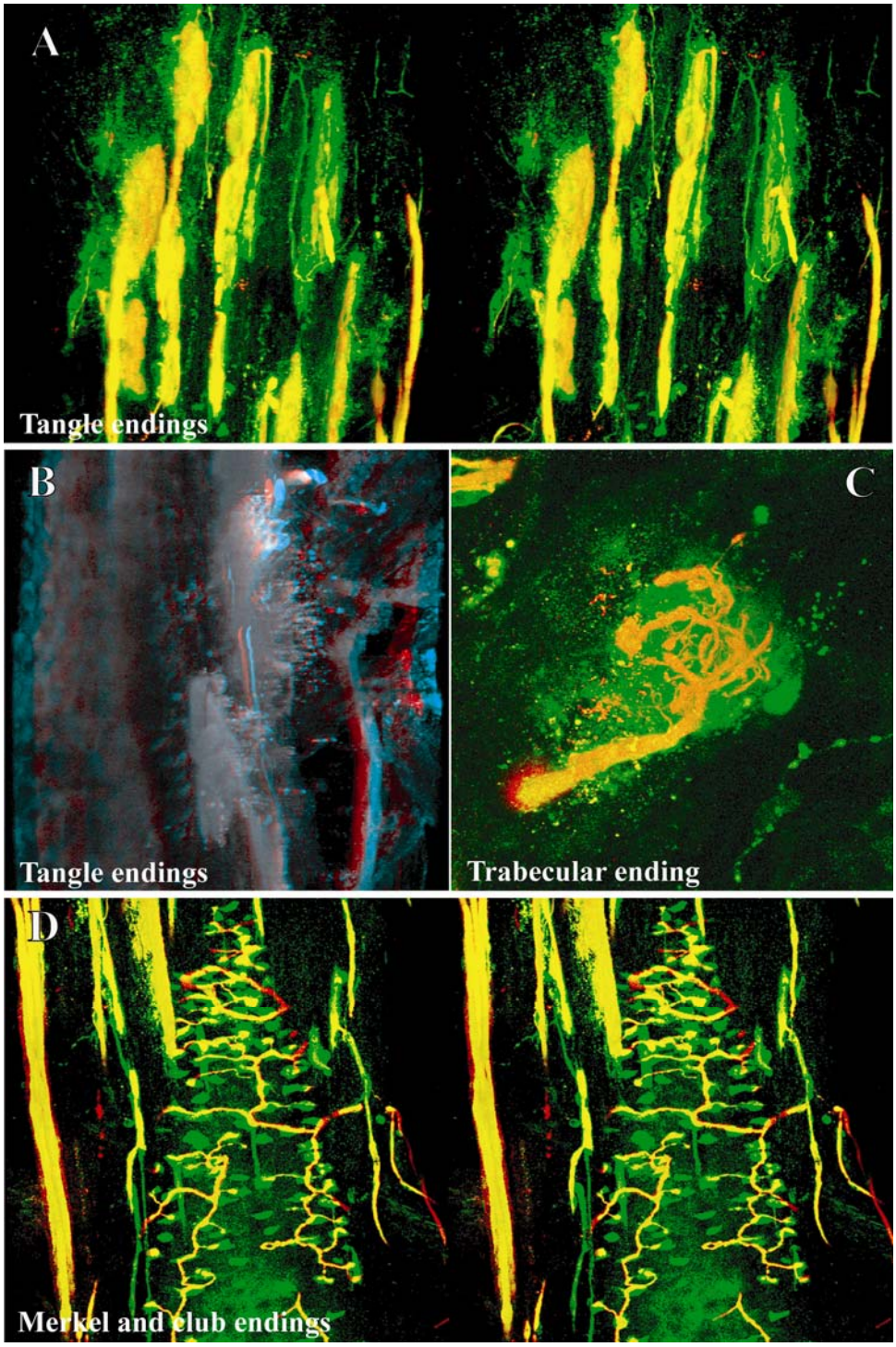
A
Tangle endings
B
Tangle endings
C
Trabecular ending
D
Merkel and club endings

CHAPTER 3
SOMATOSENSORY NUCLEI OF THE MANATEE THALAMUS AND BRAINSTEM

Introduction

Florida manatees are large-bodied herbivorous marine mammals of the Order Sirenia that appear to be tactile specialists due to the presence of tactile hairs (vibrissae) distributed over the entire body with an especially dense distribution on the face (Reep et al., 1998; 2002). This arrangement is unique among mammals and may allow manatees to compensate for their reduced visual system by using vibrissae to aid with navigation in the water. A reliance on haptic input is reflected in the organization of the neocortex as well. Recent evidence suggests that primary somatosensory cortex (SI) occupies roughly 25% of the neocortex (Sarko and Reep, 2007), which is favorably comparable to other somatosensory specialists such as the naked mole-rat (Catania and Remple, 2002). Additionally, manatees exhibit cortical specializations known as Rindenkerne, or "cortical nuclei" that appear as cell clusters in layer VI and are unique to sirenia (Dexler, 1912; Johnson et al., 1994). Rindenkerne share histochemical attributes with "barrels," the functional representations of mystacial vibrissae found in layer IV of SI in rats, mice, and other rodents (Johnson, 1980; Rice, 1995; Kaas and Collins, 2001), as well as in shrews (Catania et al., 1999), opossums (Huffman et al., 1999; Catania et al., 2000; Frost et al., 2000), and hedgehogs (Catania et al., 2000). Rindenkerne may process information related to vibrissae that are behaviorally relevant in active tactile exploration and object recognition, as well as in passive detection of hydrodynamic stimuli. However, this hypothesis remains untested by electrophysiology or axonal tracing methods due to the manatee's status as an endangered species.

Dedication of innervation to a particular sensory modality in the periphery creates a commensurate neural commitment in the brainstem, thalamus, and cerebral cortex. Although the

neocortex of the Florida manatee has been characterized histochemically (Sarko and Reep, 2007) and the sensory innervation of manatee vibrissae is currently being examined using immunofluorescence, no systematic analysis of behaviorally relevant areas of the thalamus and brainstem has been undertaken. It has previously been noted that manatees have a large trigeminal nerve (Reep et al., 1989) and well-developed trigeminal and somatosensory nuclei but reduced visual thalamic and brainstem nuclei (Johnson et al., 1986; 1987; Welker et al., 1986; Reep et al., 1989). Assessments of the relative importance of the visual and somatosensory systems in sirenian behavior parallel these findings, particularly for the trigeminal system that is associated with the use of the facial vibrissae in tactile exploration.

The somatosensory brainstem nuclei of interest for the manatee include Bischoff's nucleus, the cuneate-gracile complex, and the trigeminal nucleus (in particular, the principal sensory component). Bischoff's nucleus is a distinct group of cells in the midline of the caudal medulla that projects heavily to the ventrobasal thalamus in the raccoon (Johnson et al., 1968; Ostapoff and Johnson, 1988) and constitutes the tail representation in most mammals with a well-developed tail (Kappers and Ubbo, 1960). By analogy, Bischoff's nucleus would represent the fluke in the manatee and might occupy a disproportionately large area due to the tactile hairs present on the fluke. Behavioral observations also indicate that manatees carefully manipulate their flukes when navigating through the water, which presumably involves significant sensory feedback via Bischoff's nucleus (Welker, personal observations). The manatee cuneate-gracile complex would be expected to represent somatosensory input from the upper and lower body trunk and the flippers as it does in other species. The commitment of sensory endings to postfacial vibrissae of the flippers and trunk of the body may also create somatotopic parcellation within these nuclei. Finally, it seems reasonable to expect the trigeminal nucleus of the manatee

to be disproportionately large and parcellated into "barreloids" (the functional representation of vibrissae in the brainstem) in order to maintain and process segregated inputs from the facial vibrissae used in direct tactile exploration of objects in the manatee's environment.

The principal somatosensory nucleus in the thalamus is referred to as the ventrobasal (VB) or more commonly the ventroposterior (VP) nucleus which contains a lateral subdivision (VPL) that represents the body and a medial subdivision (VPM) that represents the face and most of the head (e.g., Jones, 1985a). The relative sizes of these nuclei vary in other species according to the relative innervation of the body versus the face, respectively (Rose and Mountcastle, 1952; Cabral and Johnson, 1971; Welker, 1974; Bombardieri et al., 1975). In rodents and some marsupials, VPM has been discovered to contain "barreloids," or neuronal clusters related to individual vibrissae, that are highly reactive for cytochrome oxidase (Jones, 1983; Land and Simons, 1985b; Van der Loos, 1976). Given the manatee's reliance on haptic input, the VPM would be expected to be relatively large and may possess barreloid parcellation.

In the present study we investigate the manatee brainstem and thalamus using stains for Nissl bodies, myelin, acetylcholinesterase, and cytochrome oxidase in order to localize and determine the size and extent of the principal somatosensory nuclei in each region. Because of the manatee's reliance on haptic input, we hypothesize that somatosensory nuclei in the brainstem and thalamus would be relatively large and potentially subdivided in order to accommodate the large amount of information being processed by discrete vibrissae in the periphery—approximately 2,000 on the face and 3,000 on the body (Reep et al., 2001; 2002). Additionally, if Rindenkerne are in fact analogous to cortical barrels, it seems reasonable to expect similar functional representations of vibrissae to be present in the form of discrete cellular aggregates within the brainstem (as barrelettes in the trigeminal nucleus) and the thalamus (as

barreloids). This analysis adds to our comprehensive characterization of the manatee somatosensory system and our overall efforts to understand manatees' specialized adaptations and perceptual capabilities in their unique environmental niche. Examining an evolutionary outlier such as the manatee also contributes significantly to our understanding of general organizing principles of sensory systems.

Materials and Methods

Four postmortem brains of the Florida manatee, *Trichechus manatus latirostris*, were obtained fresh (the head perfused within 24 hours of death) through the statewide manatee salvage program administered by the Florida Department of Natural Resources and collected under U.S. Federal Fish and Wildlife Permit PRT-684532 with IACUC protocol #C233. The heads were perfused in situ by gravity-fed bilateral cannulation of the carotid arteries, with 8–15 L of 0.9% phosphate-buffered saline followed by 8–15 L of 4% phosphate-buffered paraformaldehyde fixative (amounts varied according to specimen size). The dorsal cap of each skull was removed, the brain extracted, and the meninges removed. Each brain was then placed in 4% paraformaldehyde. A summary of relevant specimen information is provided in Table 3-1 (classifications are in accordance with size/age class definitions for the manatee photo-identification system, Sirenia Project, National Biological Survey, 1994). In each case the animal was considered fresh with minimal degradation of the tissues collected and without potentially confounding factors such as chronic pathology or emaciation.

The thalamus was removed from the right hemisphere of specimens TM0339 and TM0406 and remained intact (with the cortex) for specimen TM0410. The brainstem was removed from specimens TM0406, TM0410, and TM0614b. Serial frozen microtome sections were cut coronally at 60μm for these brains and adjacent series of sections were then stained for cytochrome oxidase (CO), for Nissl substance with cresyl violet (CV), for myelin with gold

chloride (GC), and for acetylcholinesterase (AChE) as available (see Table 3-1). Five additional specimens were analyzed from brains in our collection. These specimens included TM84-49, TM85-8, TM84-58, TM86-124, and TM85-32, all of which were celloidin-embedded and sectioned at 40µm. Specimen TM85-8 was sectioned in the horizontal plane, specimen TM84-58 was sectioned in the sagittal plane, and specimens TM84-49, TM86-124, and TM85-32 were sectioned in the coronal plane. Adjacent series of sections for these specimens were stained for Nissl bodies with thionin and for myelin with hematoxylin. The CO procedure (Wong-Riley, 1979) was modified for manatee tissue by staining overnight, and the GC procedure (Schmued, 1990) was used with adjustment of pH to 6.3. The AChE recipe was provided by Dr. Robert Switzer (Neuroscience Associates, Inc., Knoxville, TN). Briefly, sections were cut directly into incubation solution consisting of 0.226 g of acetylthiocholine iodine in 100 ml of deionized water, 25 ml stock glycine, 25 ml stock $CuSO_4$, and 50 ml of 0.2M acetate buffer (pH 5.0). Sections were then placed into incubation solution in a 40ºC hot water bath for 90 minutes, rinsed in distilled water, transferred to 1% silver nitrate for 4 minutes, rinsed again, treated with 1% sodium thiosulfate for 6 minutes, and given a final rinse before being mounted onto slides from 0.02M acetate buffer. Once each staining procedure was complete and sections were mounted onto gelatinized slides, the slides were coverslipped using Eukitt.

All thalamic and brainstem sections were viewed under an Olympus BH-2 microscope, a Bausch and Lomb microprojector, a Zeiss Axiophot microscope, and on a light table in order to examine sequential sections for persistence of the visible patterns and identification of nuclei. Brain atlases of the rat (Paxinos and Watson, 1986; 1998), cat (Berman and Jones, 1982; http://www.brainmaps.org), and monkey (Gergan and MacLean, 1962) were used to assist in identification of boundaries of the thalamic nuclei. Representative sections were imaged using a

Zeiss Axioplan 2 microscope or scanned with an HP ScanJet 5370C and contrast and brightness were optimized using Adobe Photoshop CS.

In an attempt to quantify the percentage of thalamus occupied by VP in the manatee compared to other species, we analyzed three coronal sections spaced across the full extent of VP (the first close to the rostral-most extent of VP, with both VPM and VPL distinguishable; the second a middle section; and the third close to the caudal extent of VP and still retaining distinguishable VPM and VPL). Sections from three manatee brains and two rat brains stained for CO were scanned and outlined using AIS (Analytical Imaging System) software. The extent of the entire thalamus within each coronal section was measured followed by the extent of VP (based on CO-dense staining). These measurements were then completed using Nissl body stained sections from atlases for the rat, cat, and squirrel monkey (Table 3-2).

Results

Brainstem

Since manatee brainstem nuclei have never been fully characterized, we first compiled an atlas illustrating all clearly identifiable nuclei in a representative adult specimen (Fig. 3-1) with a particular focus on the somatosensory components. Nomenclature is based primarily on the Paxinos and Watson (1986; 1998) rat brain atlas and supplemented where appropriate by the cat brain atlas (http://www.brainmaps.org). The mesencephalic nucleus of cranial nerve 5 (Me5) is the rostral-most component of the trigeminal subnuclei (Fig. 3-1, A-D; Fig. 3-2, A-C). As in other species, it is visible along the lateral extent of the periaqueductal gray (PAG; Fig. 3-1A) and locus coereleus (LC; Fig. 3-1D). Disproportionately large components of the auditory system—the inferior colliculus (IC; Fig. 3-1, A-D) and nucleus of the lateral lemniscus (NLL; Fig. 3-1, C-E)—are also visible at this level and are commensurate with the manatee's well-developed auditory system (Gerstein and Gerstein, 1999; Mann et al., 2005).

The motor (Mo5) and principal sensory (Pr5) components of the trigeminal system are seen caudal to Me5 (Fig. 3-1E; Fig. 3-2; Fig. 3-3). Nucleus Mo5 exhibits large motorneuron somata in Nissl body stains (Fig. 1, E-F, left panels) that also characterize the facial motor nucleus (FMN; Fig.3-1, I-J) and lateral vestibular nucleus (LVe; Fig. 3-1, H-K). The Pr5 nucleus appears large and lobulated in both coronal (Fig. 3-1, E-G; Fig. 3-4A) and sagittal (Fig. 3-2, A-C) preparations. It appears as a distinct nucleus caudolateral to the NLL in horizontal sections (Fig. 3-3, B-F), and Pr5 stains moderately for CO (Fig. 3-4A, right panel).

Just caudal to the initial appearance of the facial nerve (7n), Pr5 begins to transition into the presumptive oral division of the spinal trigeminal nucleus (Sp5; Fig. 3-1H; Fig. 3-4B). This shift is also characterized by the appearance of the spinal trigeminal tract (sp5) which assumes a crescent shape surrounding the nucleus. As the facial motor nucleus (FMN) becomes distinct (Fig. 1, I-J) the spinal trigeminal nucleus assumes a flattened and less distinct morphology characteristic of the interpolar subnucleus of Sp5 (e.g., Paxinos and Watson, 1998; Fig. 3-1, J-K; Fig. 3-4C). The extensive caudal subnucleus of Sp5 continues from the interpolar nucleus (Fig. 3-1, L-P; Fig. 3-4D) and appears to be lobulated. The extensiveness of the spinal trigeminal nucleus is also clearly evident in sagittal (Fig. 3-2D) and horizontal sections (Fig. 3-3, C-F). Each of the spinal trigeminal subnuclei stains moderately for CO (Fig. 3-4, right panels). Although Pr5 and the caudal nucleus of Sp5 appear lobulated, and both the oral and interpolar nuclei of Sp5 appear densely penetrated with fiber bundles (Fig. 3-4, B-C), no evidence of barreloids was present.

The cuneate nucleus first becomes evident at the caudal extent of the FMN (Fig. 3-1J). Contrary to previous reports (Johnson et al., 1994) an external cuneate nucleus (ECu) is present, although it is greatly reduced (Fig. 3-1, K-L). As a whole, the cuneate-gracile complex is large,

extensively lobulated, and stains densely for CO (Fig. 3-1L-N; Fig. 3-4D). A large Bischoff's nucleus is also present at the most caudle extent of the gracile nucleus (Fig. 1K) and stains densely for CO (shown in the neonate only but present in all specimens examined, Fig. 3-5E). The proposed somatotopic arrangement of cutaneous inputs from the manatee body is presented later along with the proposed somatotopy for VP within the thalamus (Figure 3-13) based on Welker (1973).

A spaced series of representative sections from a neonatal specimen demonstrates that the location and disproportionately large size of somatosensory nuclei, as well as the organization of brainstem nuclei in general, is consistent between adults and neonates. Figure 3-5A shows a section equivalent to that of Fig. 3-1E with a large Pr5 that stains moderately for CO. The plane of section for Fig. 3-5B is equivalent to Fig. 3-1I, showing Sp5 surrounded by the crescent of spinal trigeminal tract fibers. The adjacent sections shown in Fig. 3-5C are equivalent to Fig. 3-1K with a small external cuneate nucleus present at the lateral aspect and large Sp5 and cuneate-gracile nuclei. Figure 3-5D shows lobulation present in Sp5 and more extensively in the cuneate-gracile complex (CuG) equivalent to Fig. 3-1M. Finally, a large Bischoff's nucleus encompassing the presumptive tail representation is present at the caudal aspect of the medulla (Fig. 3-5E) along with caudal Sp5. Moderate CO staining was present in the trigeminal nucleus and dense staining characterized CuG as seen in adults (Fig. 3-4).

Thalamus

The principal somatosensory nucleus in the thalamus is the ventroposterior (VP) nucleus, one of the most clearly defined thalamic nuclei due to its large size, densely staining cells, and lobulated appearance resulting from penetrating myelin fiber bundles (Jones, 1985b). In Nissl body preparations, subnucleus VPM contains smaller, relatively closely packed cells compared to VPL. In addition, AChE staining reveals robust patterns that allow for the discrimination of

different nuclei and these patterns are generally consistent for rats, cats and primates (Jones, 1985a). Densest staining generally characterizes the ventral lateral geniculate nucleus as well as the intralaminar, anteroventral, anterodorsal, rhomboid, paraventricular, habenular and medioventral nuclei while lighter staining distinguishes the dorsal lateral geniculate nucleus (LGN), medial geniculate nucleus (MGN), reticular nucleus, anterior of the lateral posterior nucleus, and parts of lateral and ventral complexes.

An atlas of the manatee thalamus is provided for the first time (Fig. 3-6) with a more closely spaced series of sections to show the detailed extent of the somatosensory thalamus (Fig. 3-7). Nomenclature is based on Jones, (1985a). The VPL and VPM nuclei first appear in approximately the same plane of section (Fig. 3-6F). Whereas VPL terminates in Fig. 3-6G, VPM extends more caudally to Fig. 3-6H. The medial subnucleus was identifiable in Nissl body preparations as having relatively small, closely packed cells in contrast to the lateral subnucleus which displayed large, darkly staining cells that were more widely spaced (Fig. 3-8). The subnuclei of VP were also distinguishable in AChE staining preparations with VPM exhibiting lighter staining than VPL (Fig. 3-9, left column). As seen in other species, VP was characterized by penetrating fiber bundles visible in myelin preparations (Fig. 3-6, F-H; Fig. 3-7; Fig. 3-9, right column). The entirety of VP was CO-dense as seen in other species and was consistently CO-dense in adults (Fig. 3-9, middle column), neonates and juveniles (Fig. 3-10) although the medial subnucleus did not appear more densely stained as is the case in some other species. No barreloids were clearly distinguishable, although possible functional divisions might be indicated by penetrating fiber laminae that were particularly pronounced in the juvenile specimen (Fig. 3-11). The posterior nucleus (Po) also receives cutaneous input from the periphery and is visible in Fig. 3-6, E-I and in Fig. 3-7.

Overall, the ventroposterior and posterior nuclei appear disproportionately large in the manatee in accordance with their functional relevance to somatic sensation. To quantify the percentage of thalamus occupied by VP in the manatee compared to other species, we analyzed three coronal sections spaced across the full extent of VP (see Materials and Methods) from three manatee brains and two rat brains stained for CO as well as from Nissl body stained sections from atlases for the rat, cat, and squirrel monkey (Table 3-2). Although this yields limited information given that the volume of total thalamus versus VP (and more particularly, VPL versus VPM) could not be calculated, the data indicate that measures were very similar between the rat sections stained for CO and the outlined sections from the rat brain atlas and by extension should be comparable for the cat and squirrel monkey as well. Also, although the measure was across only three coronal sections spaced across VP for each species, it does appear that the percentage of thalamus occupied by VP is higher in manatees, particularly in the adult specimen (28%). Indeed, based on a qualitative assessment of CO-stained coronal sections in the adult (Fig. 3-9), VP appears to occupy approximately one-third of the thalamus. The only other study found to quantify thalamic subnuclei was done by Kruger (1959). Kruger's data quantified VP as a percentage of dorsal thalamus, and dorsal as a percentage of total thalamus. By extrapolation, his measurements indicate that VP occupies 6.6% of total thalamus in rabbits, 2.9% in sheep, 5.0% in cats, 7.0% in monkeys, and 2.6% in dolphins.

Other behaviorally relevant thalamic nuclei include the lateroposterior subnucleus (LP) and the lateral geniculate nuleus (LGN), both of which are relatively small and are overtaken by the large medial geniculate nucleus (MGN; Fig. 3-6, G-K). This anatomical organization reflects the relative degree of development and behavioral importance of the visual and auditory systems, respectively. Our proposed location for MGN differs from other species in that MGN appears

rostral to LGN as seen in coronal (Fig. 3-6, G-K) and horizontal (Fig. 3-12) sections. The medial geniculate is also situated dorsal to LGN with Po visible as a wedge between MGN and LGN (Fig. 3-6I) as seen in the horizontal section. This orientation is conceivable if one considers the overall rostroventral rotation that the manatee brain appears to have undergone, such that the equivalent of the Sylvian (lateral) fissure is oriented vertically. Additionally, if the auditory sense truly dominates visual in the manatee, it is plausible that MGN became greatly expanded at the expense of visual thalamic nuclei thereby forcing them caudal and ventral.

Discussion

Brainstem: Somatotopic Parcellation in Other Species

The brainstem nuclei of interest for the manatee somatosensory system include the trigeminal, cuneate, gracile, and Bischoff's nuclei. Bischoff's nucleus, a distinct group of cells in the midline of the caudal medulla (Johnson et al., 1968), has not been identified previously in the manatee but has been shown, along with the cuneate and gracile nuclei, to project heavily to the ventroposterior thalamus (VP) in the raccoon (Ostapoff and Johnson, 1988). In the raccoon, the tail representation occupies the dorsal portion of VP whereas the hindlimb representation occupies the ventral portion (Johnson et al., 1968). The presence of Bischoff's nucleus has also been noted in rats, shrewmice, kangaroos, great anteaters, some monkeys, and to some extent in cetaceans (Kappers and Ubbo, 1960). In the manatee, Bischoff's nucleus would presumably represent the fluke, and does in fact appear to be disproportionately large as might be expected given the presence of vibrissae on the fluke. The fluke might also be critical during navigation, as manatees have been observed to constantly adjust the angle of their fluke while swimming (Welker, personal observations).

Species like the manatee that rely on tactile exploratory behaviors involving the face (e.g., the star-nosed mole (Crish et al., 2003) and the platypus (Ashwell et al., 2006)) have well

developed trigeminal systems often exhibiting extensive somatotopic organization within the sensory trigeminal nuclei. Studies in the rat revealed that the afferent projection pattern from individual facial vibrissa follicles was topographically related to CO-dense cell clusters ("barrelettes") in the trigeminal principal sensory nucleus (Pr5) with a nearly one-to-one ratio between follicles and corresponding CO-dense clusters (Florence and Lakshman, 1995). These results supported earlier findings by Jacquin et al. (1993) that showed that Pr5 axon collaterals were concentrated within corresponding CO-dense subdivisions, and terminal branches of individual trigeminal afferents rarely crossed over into adjacent regions. In contrast, in three subdivisions of the spinal trigeminal nucleus—the pars oralis (Sp5o), pars interpolaris (Sp5i), and pars caudalis (Sp5c)—a topographical arrangement still existed, but with less specificity and more overlapping representations (Florence and Lakshman, 1995). Whisker-related barrelette patterns are present in Pr5, Sp5i, and Sp5c, but not in Sp5o (e.g., Nomura and Mizuno, 1986). Goyal et al. (1992) showed that the human principal trigeminal nucleus also demonstrated a parcellated CO-dense pattern which was interpreted as a reflection of high-density peripheral innervation of the face despite the lack of punctate structures like vibrissae. In the manatee, the principal sensory and caudal spinal trigeminal nuclei appeared particularly lobulated with possible somatotopic parcellation present. All trigeminal components, and especially the principal sensory nucleus, were elaborated and exceptionally large. In contrast to other studies that have shown CO-dense staining in Pr5 and Sp5c with only light staining in Sp5o and moderate staining in Sp5i (Florence and Lakshman, 1995), CO staining appeared consistently moderate throughout Pr5 and Sp5 in the manatee. The somatotopy proposed for the manatee brainstem (cuneate-gracile complex and Sp5c represented; Fig. 3-13A) is based on the general arrangement seen in mammals (e.g., Woudenberg, 1970).

Somatotopic parcellation is also evident in the cuneate and gracile dorsal column nuclei in other species where somatosensation is the dominant sensory modality. Cutaneous inputs from the upper limbs and rostral trunk of the body are represented in the cuneate nucleus while lower limbs and lower trunk are represented in the gracile nucleus. Strata et al. (2003) studied a prosimian, the Galago, to look at the pattern of peripheral nerve input. Through cell clusters that were identified as CO-dense blotches in both nuclei, they discovered a greater segregation of inputs within the cuneate (fingers and hand representation) than in the gracile (foot representation), which corresponds with the Galago's extensive and highly differentiated use of its hands and fingers relative to its feet. In macaques, inputs from specific parts of the hand relate to CO-dense rostrocaudal clusters of cells (Florence et al., 1991). Although the manatee lacks the manual dexterity of a primate, CO analysis of the manatee cuneate-gracile complex revealed dense staining and extensive suborganization that may be related to discrete functional representations of vibrissae on the postfacial body.

Thalamus: A Comparative Look at Somatosensory Nuclei

The relative sizes of VPM and VPL vary according to the relative innervation of the face versus the body, respectively (Rose and Mountcastle, 1952; Cabral and Johnson, 1971; Welker, 1974; Bombardieri et al., 1975). For rodents whose nose, mouth and lips dominate tactile perception, the VPM is larger, and in monotremes VPM dominates the entirety of VP. In cats, VPM and VPL are approximately equal in size, but in monkeys VPL predominates to accommodate extensive input from the hands and feet. In some species, for example the cat, VPM extends caudal to VPL, whereas in others (such as monkeys) VPL extends more caudally (Jones et al., 1985b). In rodents and some marsupials, VPM has been discovered to contain "barreloids," or neuronal clusters related to individual vibrissae, that are highly reactive for CO (Jones, 1983; Land and Simons, 1985b; Van der Loos, 1976). The VPL of the raccoon and slow

loris contains lobulated subregions representing palmar and digital skin pads (Welker and Johnson, 1965; Krishnamurti et al., 1972). Chronic vibrissae trimming results in reduced staining for CO in both the somatosensory cortical barrels (Land and Simons, 1985a; Wong-Riley and Welt, 1980) and the thalamic barreloids (Land and Akhtar, 1987) associated with the trimmed vibrissae. These findings were similar to those in *Macaca fascicularis* monkeys where peripheral nerves were cut, resulting in reduced staining of "rods" within the VPM (Jones et al., 1986). Using horseradish peroxidase axonal tracing, Jones et al. (1986) also discovered that CO staining was primarily due to terminations of trigeminal afferent fibers that formed somatotopically organized inputs to the rods. They postulated that each rod of the thalamus formed the basis of columnarity of afferent input to the somatosensory cortex by providing bundles of thalamocortical axons terminating in focal domains of the cortex. No barreloids were found in VPM of the manatee thalamus, but the ventroposterior nucleus as a whole was large, reflecting the manatee's reliance on haptic (somatosensory) input. Based on AChE staining, VPM and VPL also appear to divide the ventroposterior nucleus in an approximately equal manner (Fig. 3-9). This seems reasonable given the distribution of vibrissae on the manatee body (2,000 on the face and 3,000 postfacially) balanced by the fact that facial vibrissae are more densely innervated (Reep et al., 2001; 2002). While our proposed "manateeunculus" within the thalamus follows Welker (1973; Fig. 3-13B), it should be noted that such artistic abstractions are limited since the body representation extends in three dimensions throughout VP.

Thalamic nuclei associated with vision (LGN and LP) appear to be overtaken by those associated primarily with somatosensation (Po) and audition (MGN). While this may simply be due to the fact that somatosensation and audition both appear to be dominant sensory modalities in the Florida manatee, it is also possible that there exists extensive multisensory integration. A

previous study from our laboratory found that the manatee cortex exhibits what appears to be extensive—and possibly complete—overlap between primary auditory (AI) and primary somatosensory cortex (SI; Sarko and Reep, 2007). Responses to somatosensory and visual stimuli have also been reported in AI of the macaque (Werner-Reiss et al., 2003; Ghazanfar et al., 2005; Brosch and Scheich, 2005; Brosch et al., 2005; Zhou and Fuster, 2004).

While it is possible that this multisensory integration occurs entirely within AI, with non-auditory information relayed to AI from unimodal sensory areas in subcortical or cortical areas, it is also conceivable that AI receives inputs from multisensory cortex. But perhaps the most intriguing possibility, and one that might be relevant to the present study, involves the integration of auditory and non-auditory inputs at subcortical levels, along the traditional auditory pathways or within multisensory subcortical structures, before projecting to AI (Budinger et al., in press). Possible candidates for these subcortical multimodal areas include Po; the dorsal and medial division of MG; the brachium, dorsal and external nuclei of the inferior colliculus; and the superior colliculus, all of which were found to involve connections with AI in the Mongolian gerbil, a species used frequently for auditory research (Budinger et al., in press). The brachium of the inferior colliculus (bic), Po, and MG and particularly strong candidates as these are reciprocally connected with AI. Indeed the inferior colliculus appears to be extensively involved in acousticomotor and somatosensory systems (e.g., Huffman and Henson, 1990) and neurons within the bic code for auditory space (Schnupp and King, 1997) and project to IC, SC, and AI (Kudo et al., 1984; Mitani et al., 1987; Rouiller et al., 1989**)**. The external subnucleus of the IC has been found to integrate trigeminal and auditory stimuli with projections from both CN and Sp5 (Jain and Shore, 2006), and multisensory integration has also been demonstrated in DCN (Shore, 2005). The inferior and superior colliculi together coordinate aspects of spatial

orientation (e.g., Oliver and Huerta, 1992; Cohen and Knudsen, 1999), and indeed somatosensation has been found to dominate the SC in the star-nosed mole that relies extensively on its haptic sense (Crish et al., 2003). Subdivisions of MG process visual, vestibular, nociceptive and somatosensory stimuli in addition to the auditory stimuli classically associated with MG (e.g., Linke and Shwegler, 2000). In addition, the trigeminal system appears to influence the superior olivary complex (Shore et al., 2000). Overall, cortical and subcortical areas once rigidly defined within unimodal functional boundaries appear to have a broader functional scope, and this may be especially true in the manatee's case where low-frequency sounds in the water might stimulate mechanoreceptors—Merkel and lanceolate endings in particular—as the vibrissae of the face and postfacial body are perturbed. Such integration has been hypothesized to be beneficial in perception and localization of stimuli, potentially by linking object features or adjusting coordinate frames to a different sensory modality (Budinger et al., in press). Projections from AI to subcortical multimodal areas may also modulate subcortical activity by influencing a selected representation of behaviorally relevant frequencies (e.g., Suga and Ma, 2003), improving temporal and spectral resolution of sound representations (Yan et al., 2005), and attention-related gating of auditory information (Yu et al., 2004).

Absence of Barrelettes and Barreloids

If Rindenkerne are in fact analogous to cortical "barrels" and correspond to functional representations of vibrissae, it seems reasonable to expect the brainstem and thalamic counterparts of barrels ("barrelettes" and "barreloids," respectively) to be present. However, the absence of the latter two features in the Florida manatee could be explained by several factors. First, the plane of section may not have been optimal for detection, particularly in the case of the thalamus. We chose to section the majority of our specimens (and all of the specimens stained

for CO) in the coronal plane as this allowed for clearest identification of subnuclei. This was a priority of the current study since nuclei of the manatee thalamus and brainstem have not been characterized previously in a systematic and comprehensive manner. Because of their complex three-dimensional morphology, identification of barreloids in the coronal plane has proven difficult in rodents (Ivy and Killackey, 1982; Land et al., 1995**).** Instead, the oblique horizontal plane has proven optimal for detection of barreloids (Land et al., 1995). Although this hypothesis could be tested by simply altering the plane of section, it is more probable that barreloids are not present in the manatee, because we also did not detect barrelettes in the brainstem, which should be clearly apparent in the coronal plane.

Another possible explanation for the absence of barrelettes and barreloids is that the facial vibrissae of the Florida manatee are not organized in discrete rows as seen in other species including mice, rats and cats whose organization of facial vibrissae into rows and columns is maintained within VPM and the trigeminal sensory nuclei (e.g.,Nomura and Mizuno, 1986; Ma, 1991; Florence and Lakshman, 1995; Land et al., 1995). But perhaps the most likely explanation for the absence of barreloids and barrelettes lies in the difference between Rindenkerne and cortical barrels. While barrels are located in layer IV, an afferent zone, Rindenkerne are located in efferent layer VI. This undoubtedly indicates a fundamental difference in the columnarity of organization between barrels and Rindenkerne. Corticocortical feedback connections originate in infragranular layers, implicating Rindenkerne in descending pathways.

Table 3-1. Summary of specimen information.

Specimen	Areas analyzed	Stains	Sex	Length (in cm)	Weight (in kg)
TM84-49	Thalamus & brainstem intact	Thionin, hematoxylin			
TM85-8	Thalamus & brainstem intact	Thionin, hematoxylin			
TM84-58	Thalamus & brainstem intact	Thionin, hematoxylin			
TM86-124	Thalamus & brainstem intact	Thionin, hematoxylin			
TM85-32	Brainstem	Thionin			
TM0614b	Brainstem	CO, CV, GC	F	326	
TM0339	Thalamus	CO, CV, GC (bad)	F	200	167.8
TM0406	Thalamus& brainstem	CO, CV, AChE, GC	M	290	393.2
TM0410	Thalamus (intact) & brainstem	CO, CV, AChE, GC	M	94	14.5

Table 3-2. Comparative analysis of percentage of thalamus occupied by the ventroposterior nucleus (VP; averaged from 3 evenly spaced coronal sections to encompass VP).

Species	Source of analysis	VP Area* (in mm^2)	Total Thalamus Area* (in mm^2)	Percentage of Thalamus Occupied by VP
Manatee	Neonate (TM0410)	39.0	196.4	20%
	Juvenile (TM0339)	66.9	286.2	23%
	Adult (TM0406)	93.6	333.5	28%
Rat	Adult (340)	1.5	7.1	22%
	Adult (341)	1.6	8.1	20%
	Brain atlas	4.6	24.7	19% (VPL=4.4%, VPM=14.6%)
Cat	Brain atlas	18.4	115.5	16%
Squirrel Monkey	Brain atlas	20.3	101.5	20%

[1] Paxinos and Watson, 1986
[2] Berman and Jones, 1982
[3] Gergan and MacLean, 1962

Figure 3-1. A rostrocaudal series of representative coronal brainstem sections with subnuclei labeled illustrates the size and extent of somatosensory nuclei. A-P) Sections stained with thionin for Nissl bodies (left) shown with adjacent sections stained with hematoxylin for myelin (right). Section numbers are listed at the bottom of each section, and sections were cut at 40µm, specimen 84-49. Scale bars=5mm. 4=trochlear nucleus; 7n=facial nerve; 8n=auditory-vestibular nerve; 10=vagus nucleus; 12=hypoglossal nucleus; Amb=nucleus ambiguous; bic: brachium of the inferior colliculus; BN=Bischoff's nucleus; bp=brachium pontis; CuG=cuneate-gracile; CI=inferior central nucleus; CN=cochlear nucleus; cp=cerebral peduncle; CS=superior central nucleus; Cu=cuneate nucleus; DCN=dorsal cochlear nucleus; DTN=dorsal tegmental nucleus; ECu=external cuneate nucleus; FMN=facial motor nucleus; FTG=gigantocellular tegmental field; g7=genu of facial nerve; IC=inferior colliculus; ICN=interposed cerebellar nucleus; icp=inferior cerebellar peduncle; INC=nucleus incertus; IO=inferior olive; LC=locus coereleus; LCN=lateral (dentate) cerebellar nucleus; ll=lateral lemniscus; LPB=lateral parabrachial nucleus; LVe=lateral vestibular nucleus; Me5=mesencephalic nucleus of 5; ML=medial lemniscus; MLF=medial longitudinal fasciculus; MnR=median raphe nuclei; Mo5=motor nucleus of 5; MRt=medullary reticular nucleus; MVe=medial vestibular nucleus; NLL=nucleus of the lateral lemniscus; PAG=periaqueductal gray; Pn=pontine nuclei; Pr5=principal sensory nucleus of 5; py=pyramidal tract; Rb=rubrospinal tract; Rt=reticular nucleus; s5=sensory root of 5; SC=superior colliculus; scp=superior cerebellar peduncle; SO=superior olivary nucleus; Sol=nucleus of the solitary tract; Sp5=spinal trigeminal nucleus; sp5=spinal trigeminal tract; TRN=tegmental reticular nucleus; Tz=trapezoid nucleus; VCN=ventral cochlear nucleus; Ve=vestibular nucleus; xpy=pyramidal decussation; xscp=decussation of the superior cerebellar peduncle

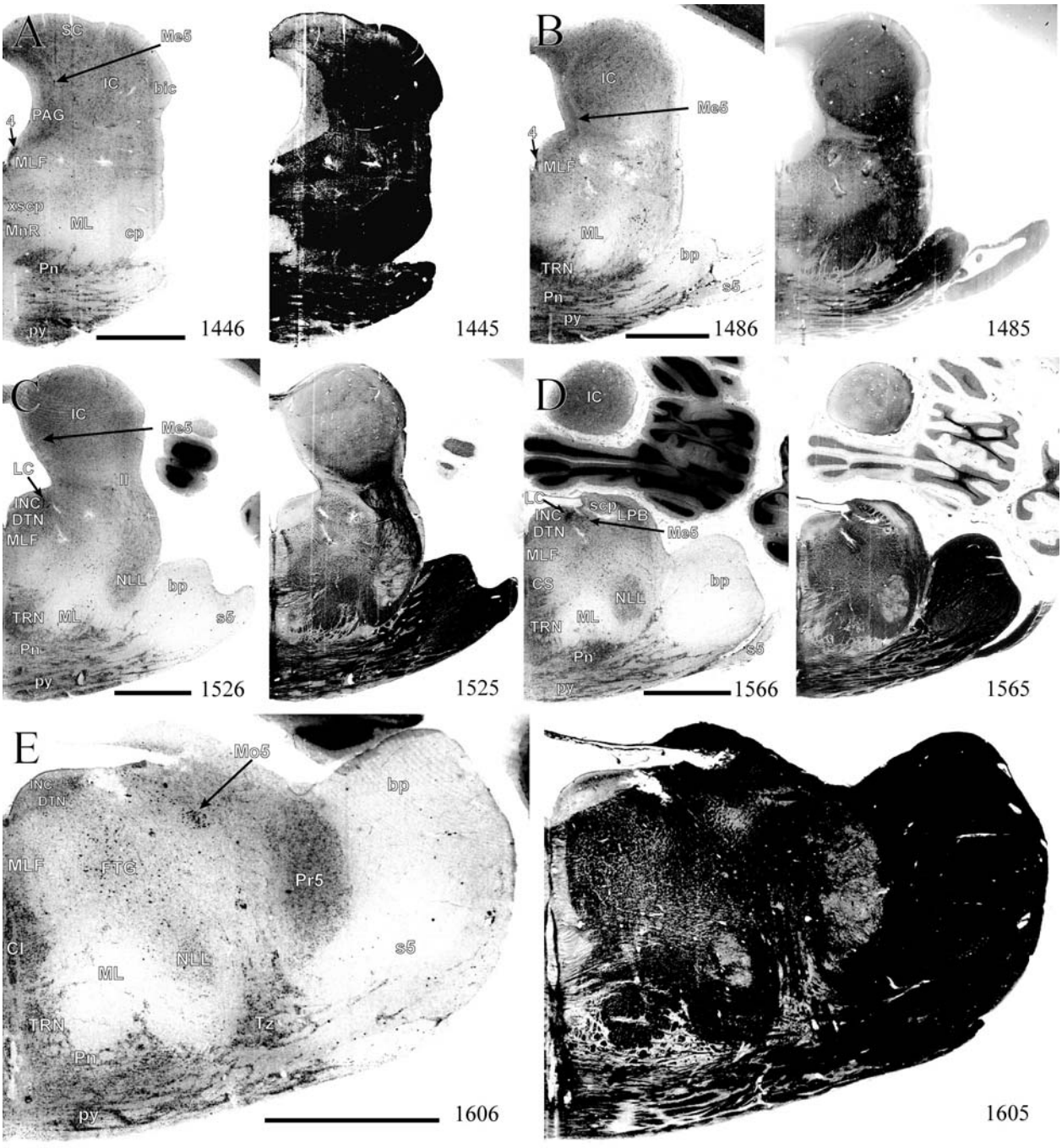
A
SC
Me5
IC
bic
4
PAG
MLF
xscp
MnR
ML
cp
Pn
py
1446
1445
B
IC
Me5
4
MLF
ML
bp
TRN
Pn
py
s5
1486
1485
C
IC
Me5
LC
ll
INC
DTN
MLF
NLL
bp
TRN
ML
s5
Pn
py
1526
1525
D
IC
LC
scp
INC
DTN
LPB
Me5
MLF
CS
bp
NLL
ML
TRN
Pn
s5
py
1566
1565
E
Me5
INC
DTN
bp
MLF
FTG
Pr5
CI
s5
NLL
ML
TRN
Tz
Pn
py
1606
1605

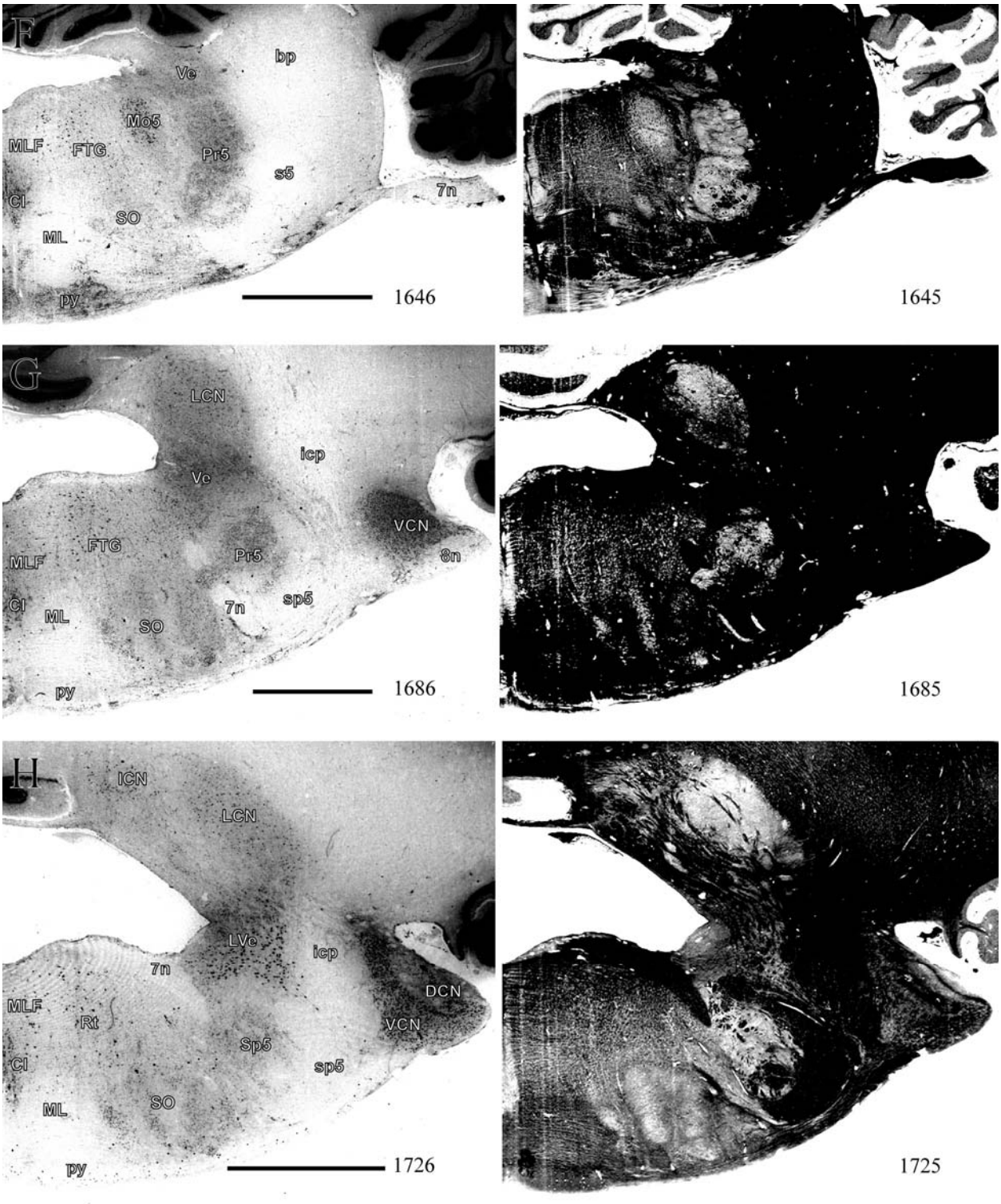

Figure 3-1. Continued

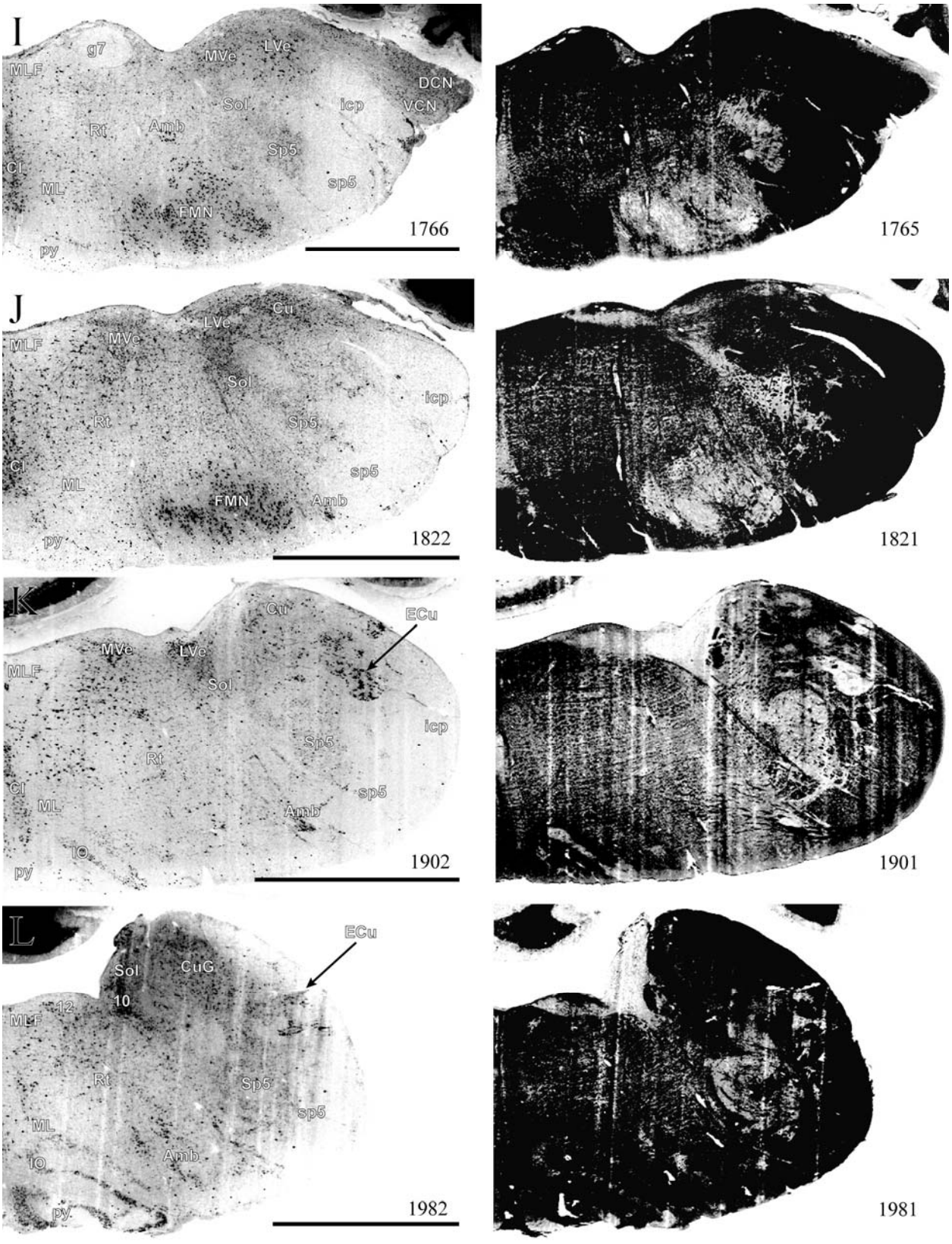

Figure 3-1. Continued

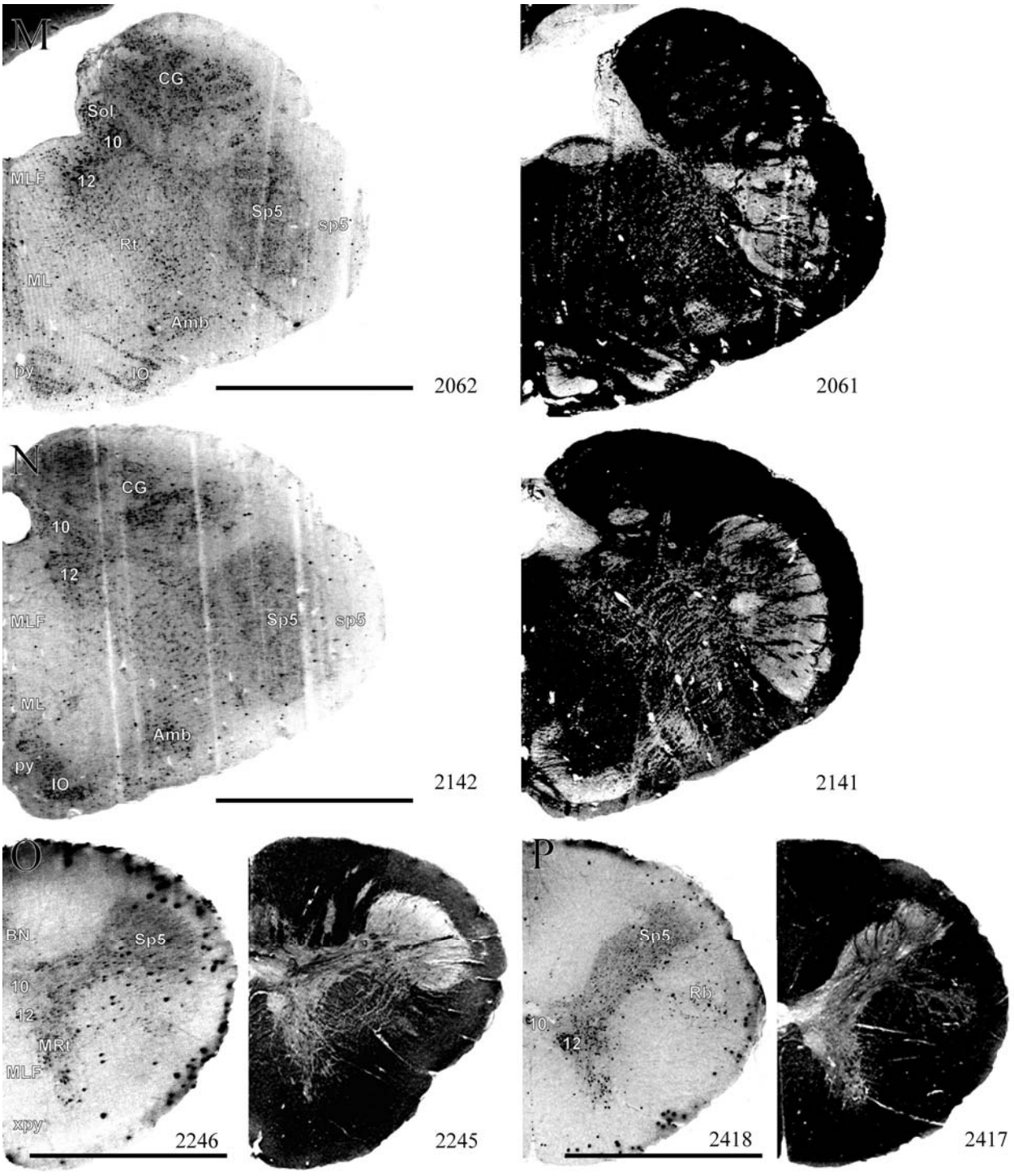

Figure 3-1. Continued

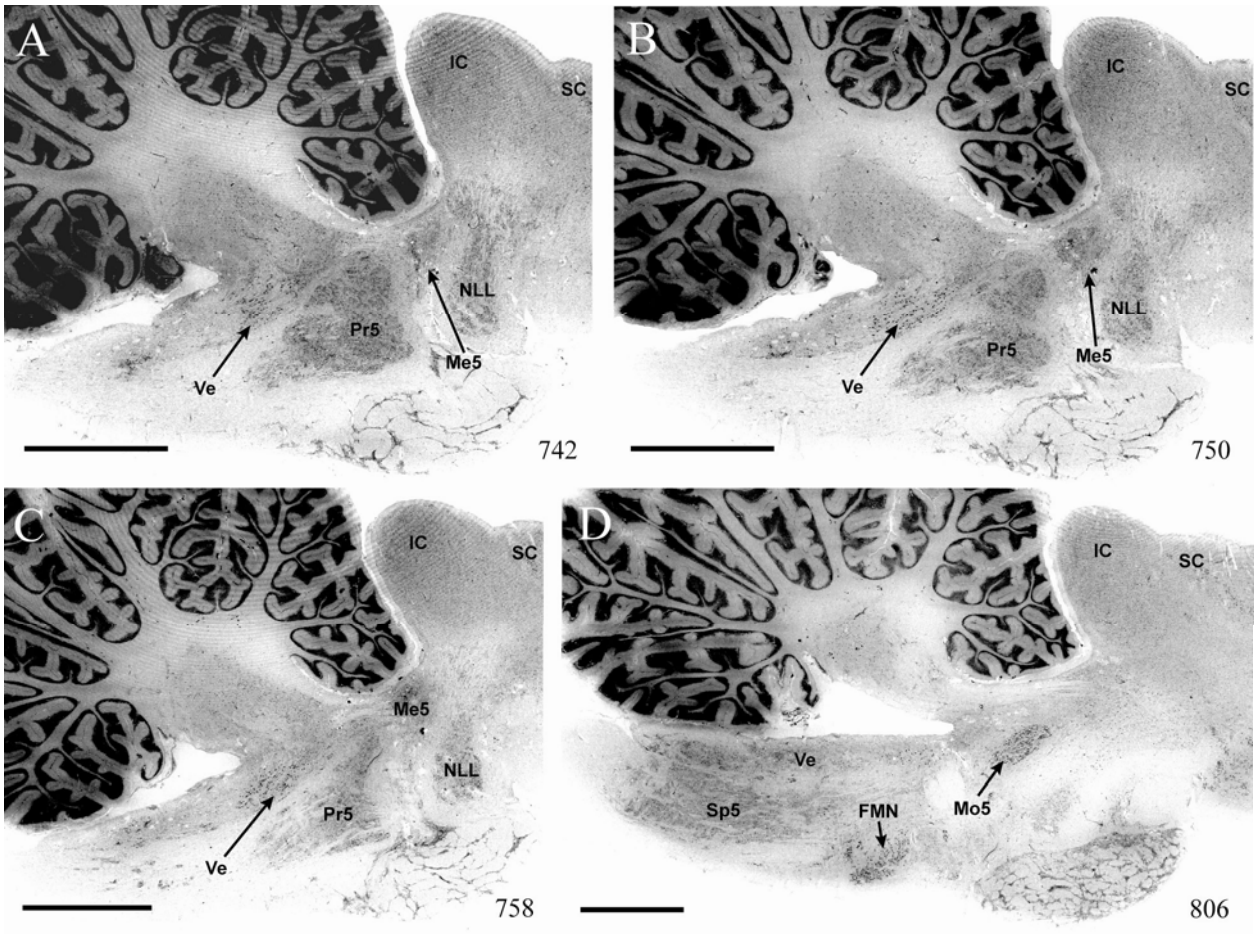

Figure 3-2. Brainstem sections cut in the sagittal plane illustrate the rostrocaudal extent of behaviorally relevant nuclei and in particular the lobulated appearance of the trigeminal nuclei. Sections proceed lateral to medial and were stained with thionin for Nissl bodies Section numbers are listed at the bottom of each section, and sections were cut at 40µm, specimen 84-58. Scale bar=5mm. FMN=facial motor nucleus, IC=inferior colliculus, Me5=mesencephalic nucleus of 5, Mo5=motor nucleus of 5, NLL=nucleus of the lateral lemniscus, Pr5=principal sensory nucleus of 5, SC=superior colliculus, Sp5=spinal trigeminal nucleus, Ve=vestibular nucleus.

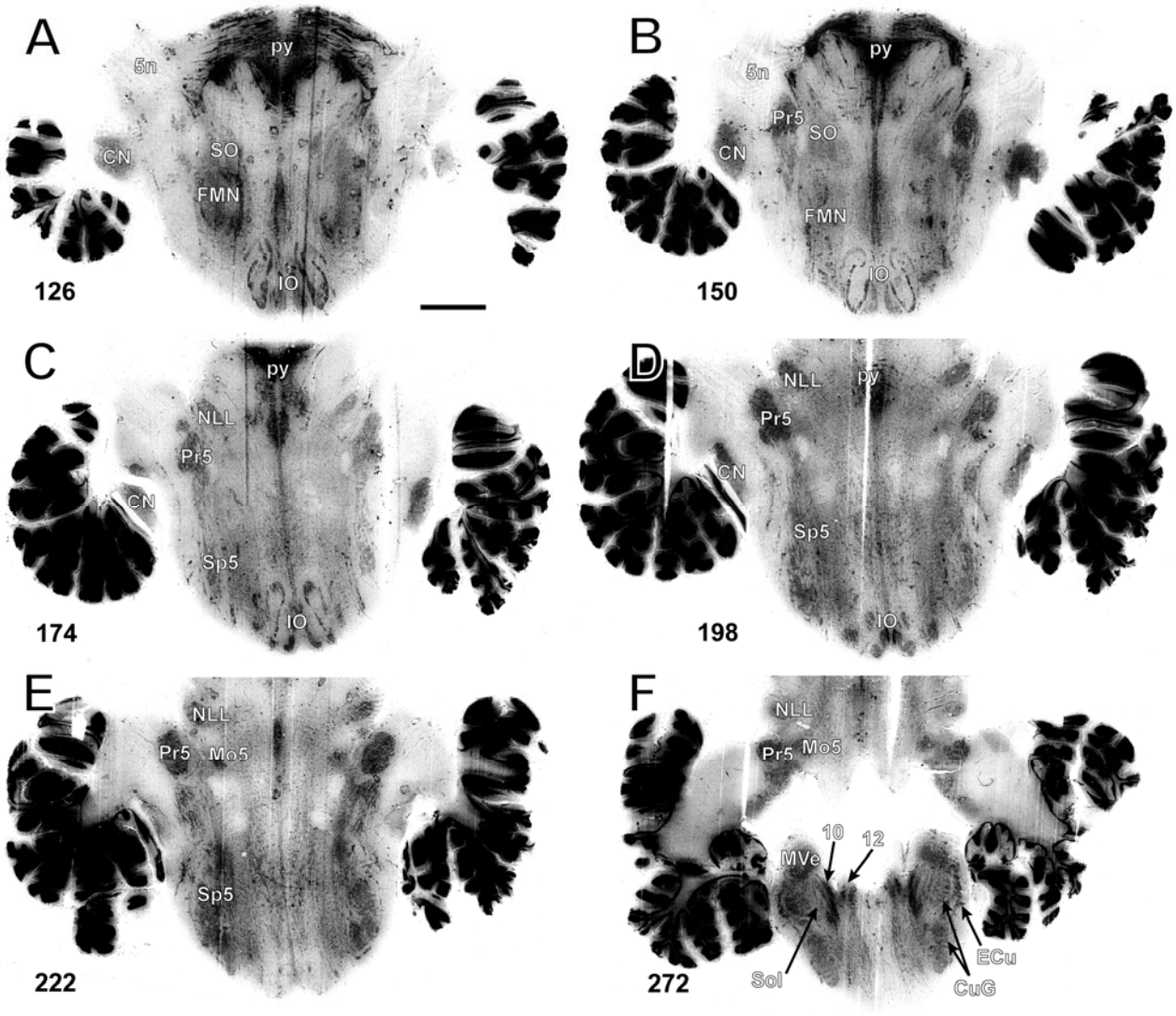

Figure 3-3. Brainstem sections cut in the horizontal plane show the topography and orientation of nuclei of interest. Sections proceed ventral to dorsal and were stained with thionin for Nissl bodies Section numbers are listed at the bottom of each section, and sections were cut at 40µm, specimen 85-8. Scale bar=5mm. 5=trigeminal nerve, CN=cochlear nucleus, CuG=cuneate-gracile complex, FMN=facial motor nucleus, IO=inferior olivary nucleus, Mo5=motor nucleus of 5, NLL=nucleus of the lateral lemniscus, Pr5=principal sensory nucleus of 5, py=pyramidal tract, SO=superior olivary nucleus, Sp5=spinal trigeminal nucleus, Ve=vestibular nucleus.

Figure 3-4. Representative coronal brainstem sections illustrating the appearance of each of the trigeminal subnuclei in an adult specimen. Adjacent sections are shown stained for myelin (with gold chloride, GC) and cytochrome oxidase (CO). A) The principal sensory nucleus (Pr5) is large and exhibits possible somatotopic parcellation. It also stains moderately for CO, as do all of the trigeminal subnuclei. Section numbers are listed at the bottom of each section, and sections were cut at 60µm, specimen TM0614b. Scale bar=5mm. 7=facial nerve, BN=Bischoff's nucleus, CN=cochlear nucleus, CuG=cuneate-gracile complex, DCN=dorsal cochlear nucleus, FMN=facial motor nucleus, LVe=lateral vestibular nucleus, Mo5=motor nucleus of 5, Pr5=principal sensory nucleus of 5, SO=superior olivary nucleus, sp=spinal nerve of 5, sp5=spinal trigeminal tract, Sp5c=spinal trigeminal nucleus caudalis, Sp5i=spinal trigeminal nucleus interpolaris, Sp5o=spinal trigeminal nucleus oralis, VCN=ventral cochlear nucleus.

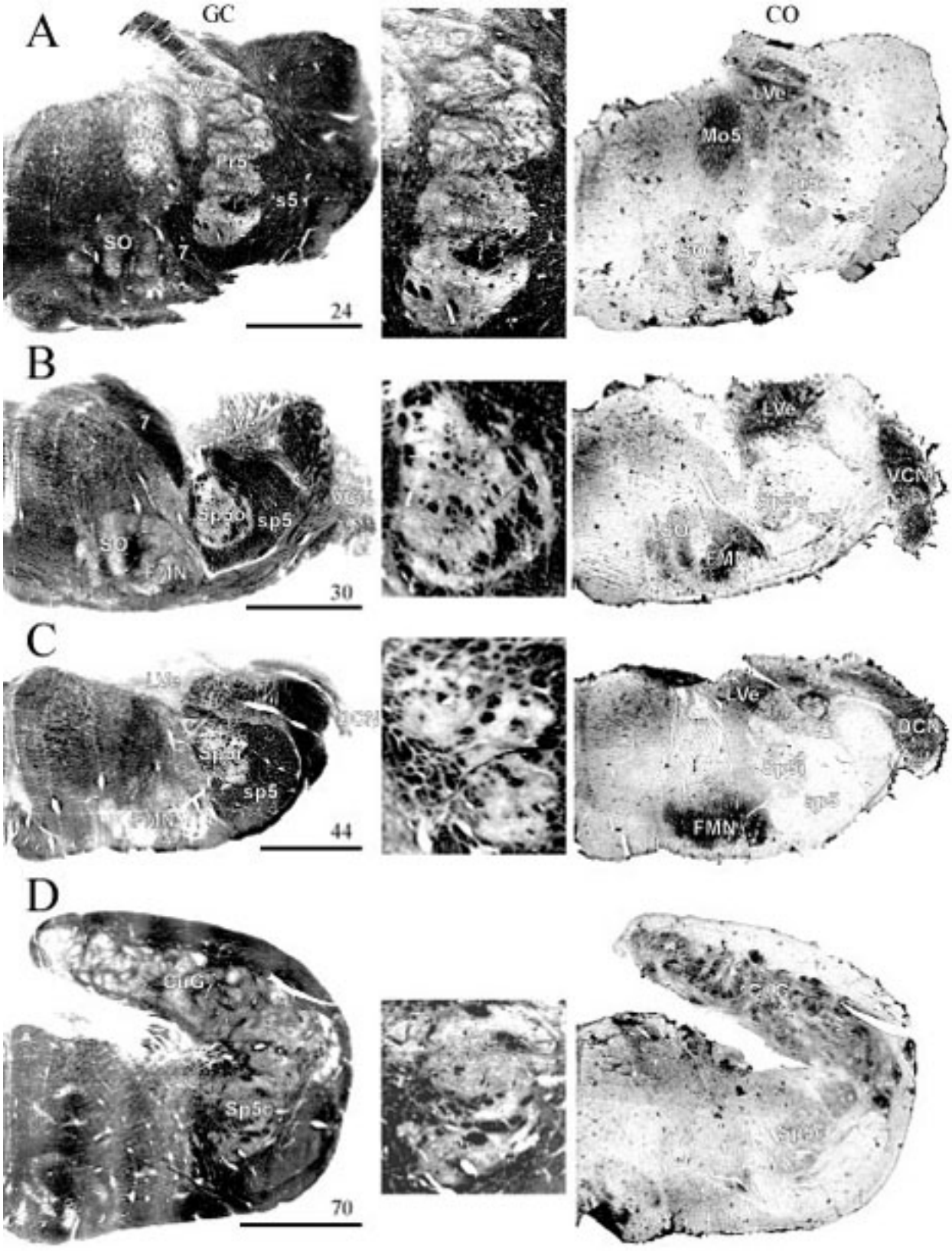
A
GC
CO
Mo5
LVe
sp5
SO
7
24
B
LVe
VCN
Sp5o
sp5
SO
PrH
30
C
LVe
DCN
sp5
FMN
44
D
CrG
Sp5o
70

Figure 3-5. A rostrocaudal series of representative coronal brainstem sections in a neonate shows that somatosensory nuclei are large and have a parcellated appearance as seen in adult specimens. Sections were stained with cytochrome oxidase (CO), gold chloride (GC) for myelin, and cresyl violet (CV) for Nissl bodies. Section numbers are listed at the bottom of each section, and sections were cut at 60µm, specimen TM0410. Scale bar=5mm. BN=Bischoff's nucleus, CN=cochlear nucleus, CuG=cuneate-gracile complex, FMN=facial motor nucleus, Mo5=motor nucleus of 5, Pr5=principal sensory nucleus of 5, Sp5=spinal trigeminal nucleus, Ve=vestibular nucleus.

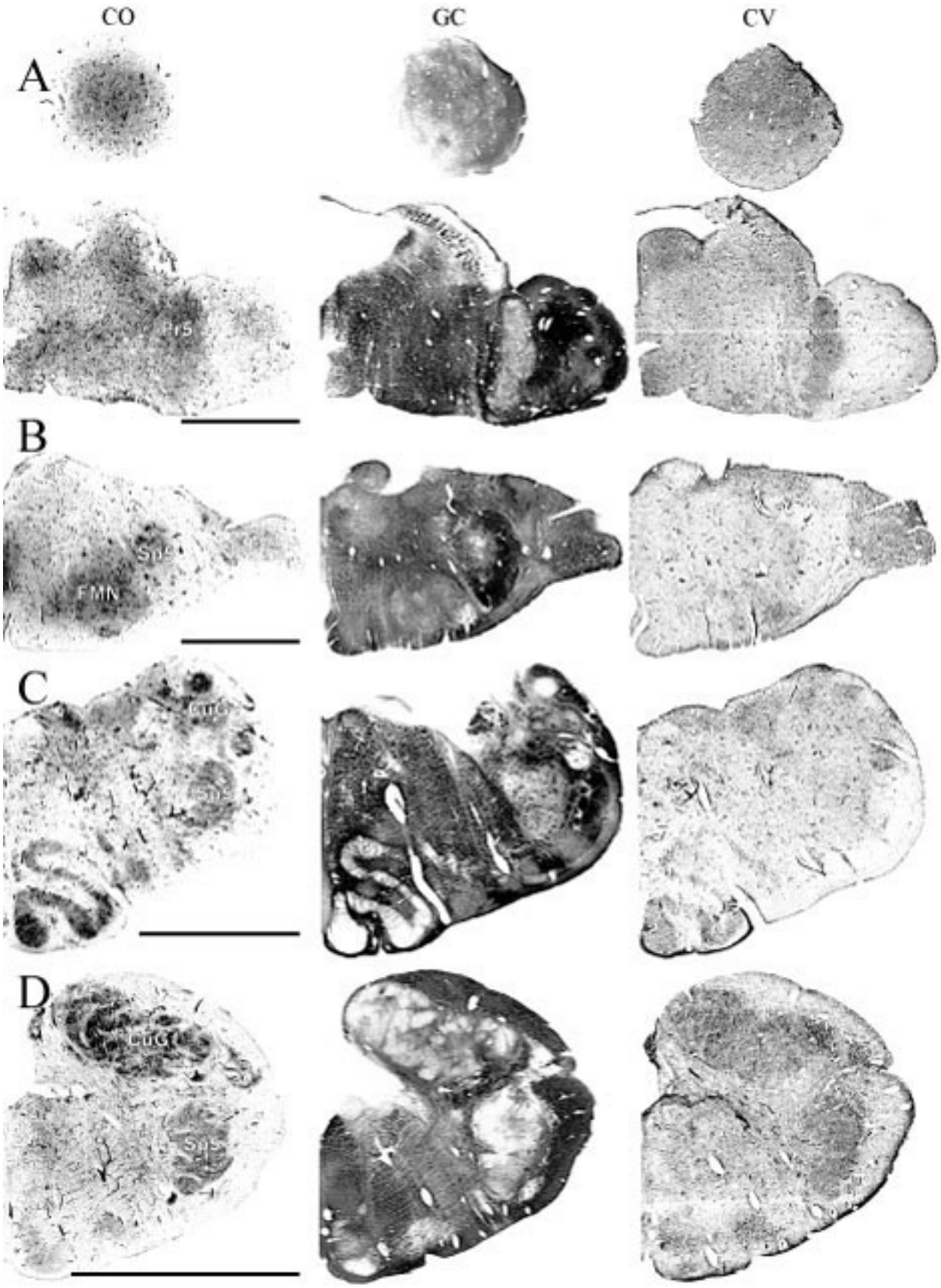
CO
GC
CV
A
PrS
B
SpV
FMN
C
CuC
SpV
D
CuC
SpV

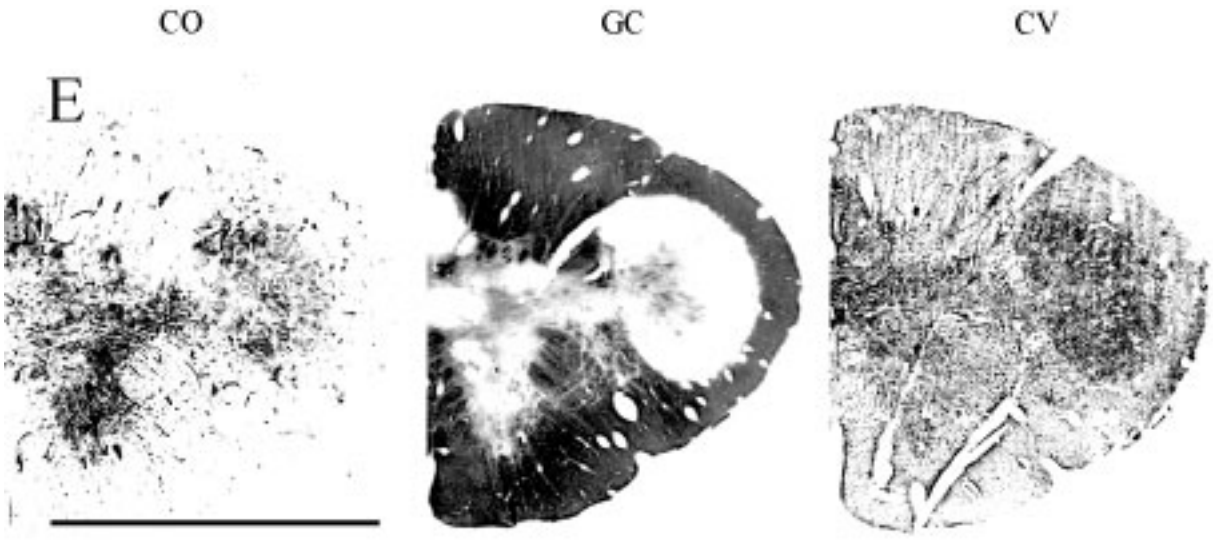

Figure 3-5. Continued

Figure 3-6. A rostrocaudal series of representative coronal thalamic sections with low-magnification images of sections stained with hematoxylin for myelin and high-magnification details of adjacent sections stained with thionin for Nissl bodies with subnuclei labeled. Section numbers are listed at the bottom of each section, and sections were cut at 40μm, specimen 84-49. Scale bar=5mm. AM=anteromedial nucleus, AV=anteroventral nucleus, CeM=central medial nucleus, CL=central lateral nucleus, CM=centre median nucleus, FF=fields of Forel, fr=fasciculus retroflexus, H=habenular nuclei, IC=inferior colliculus, ic=internal capsule, iml=internal medullary lamina, LD=lateral dorsal nucleus, LG=lateral geniculate nucleus, LP=lateral posterior nucleus, MD=mediodorsal nucleus, MG=medial geniculate nucleus, ml=medial lemniscus, MV=medioventral nucleus, PARA=anterior paraventricular nucleus, Pc=paracentral nucleus, Pf=parafascicular nucleus, Po=posterior nucleus, PT=parataenial nucleus, Rh=rhomboid nucleus, SC=superior colliculus, SM=submedial nucleus, st=stria terminalis, SubI=subincertal nucleus, VA=ventral anterior nucleus, VL=ventral lateral nucleus, VM=ventral medial nucleus, VPL=ventral posterior lateral nucleus, VPM= ventral posterior medial nucleus, ZI=zona incerta.

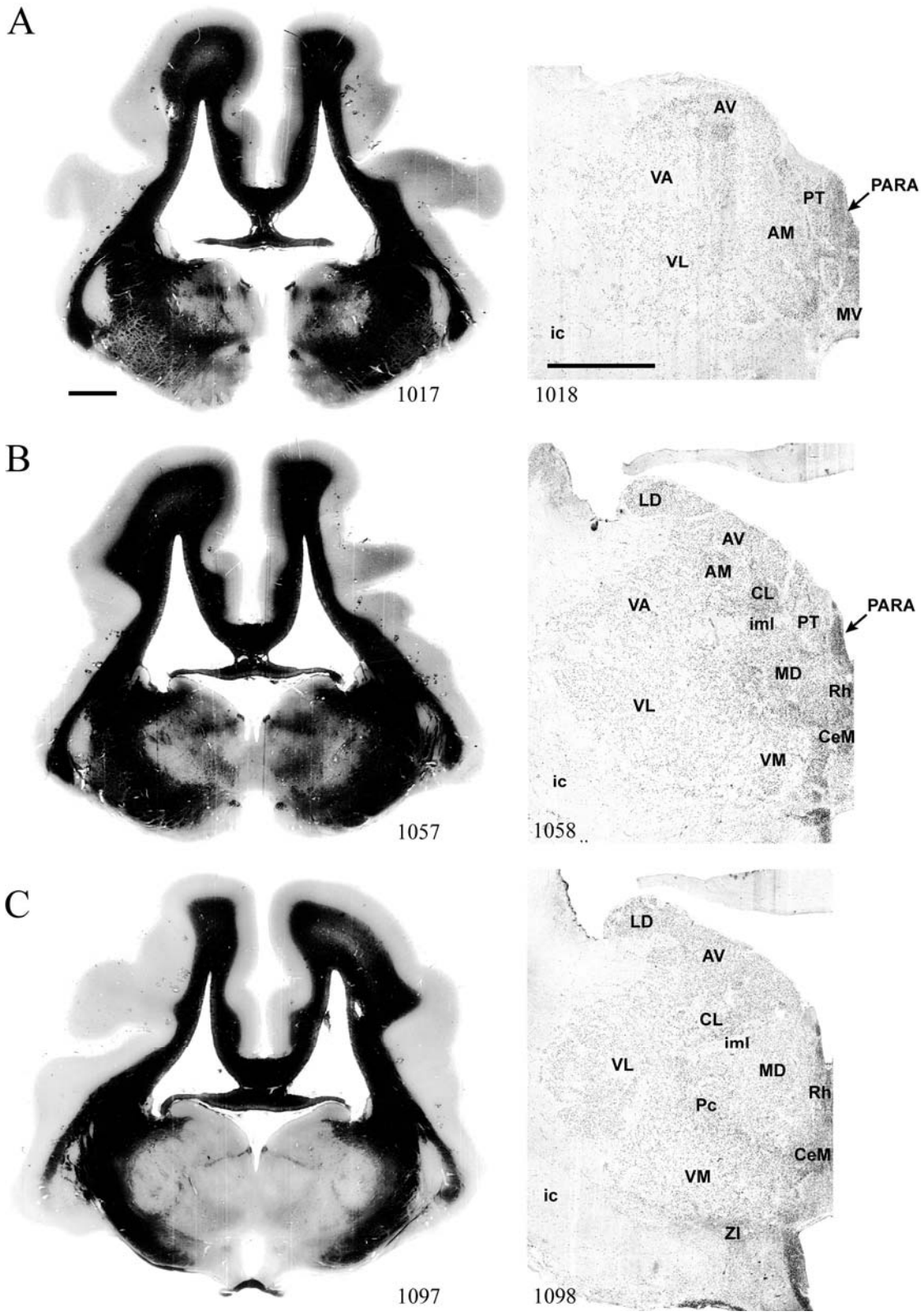
A
AV
VA
PT
PARA
AM
VL
MV
ic
1017
1018
B
LD
AV
AM
CL
VA
iml
PT
PARA
MD
Rh
VL
CeM
VM
ic
1057
1058
C
LD
AV
CL
iml
VL
MD
Rh
Pc
CeM
VM
ic
ZI
1097
1098

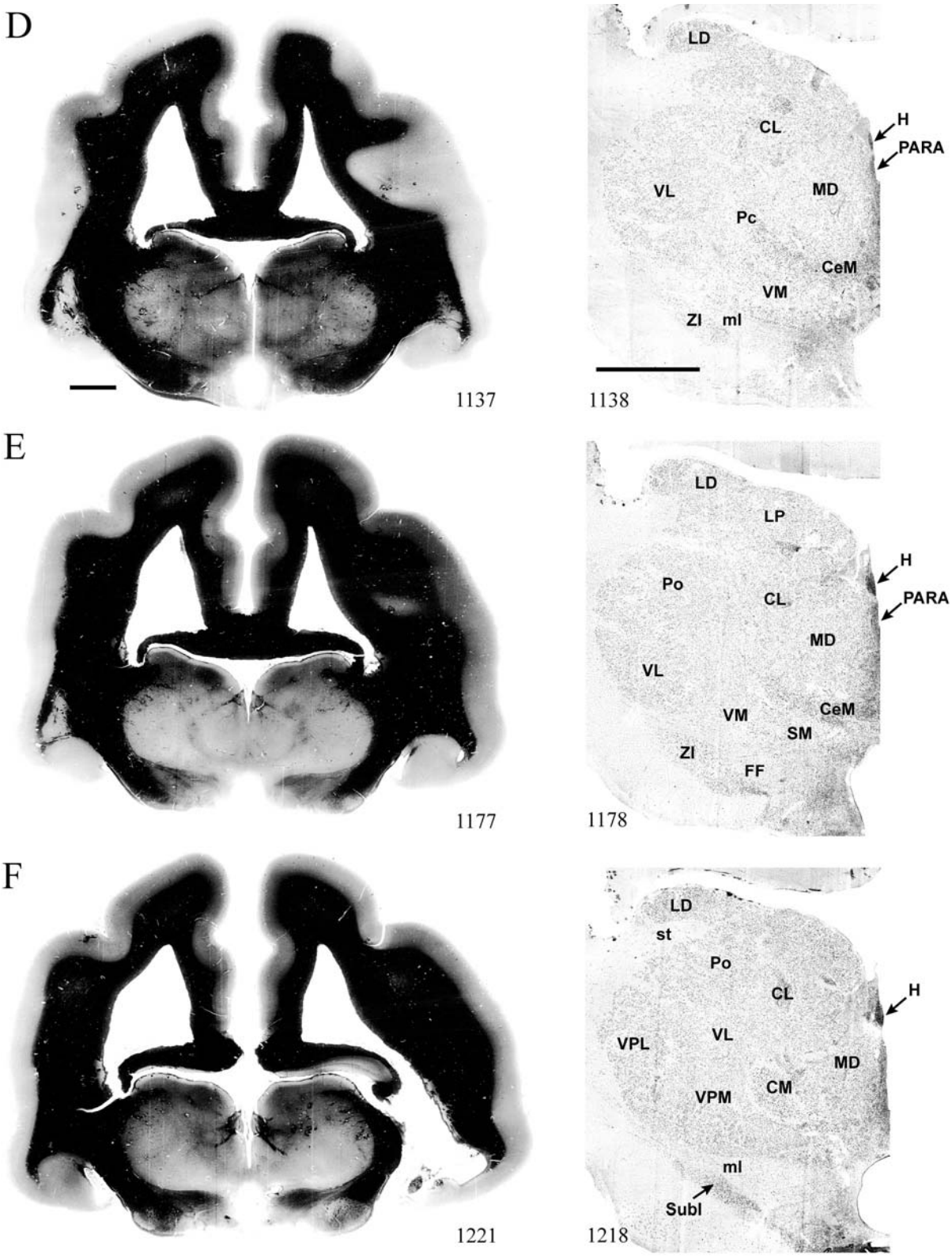

Figure 3-6. Continued

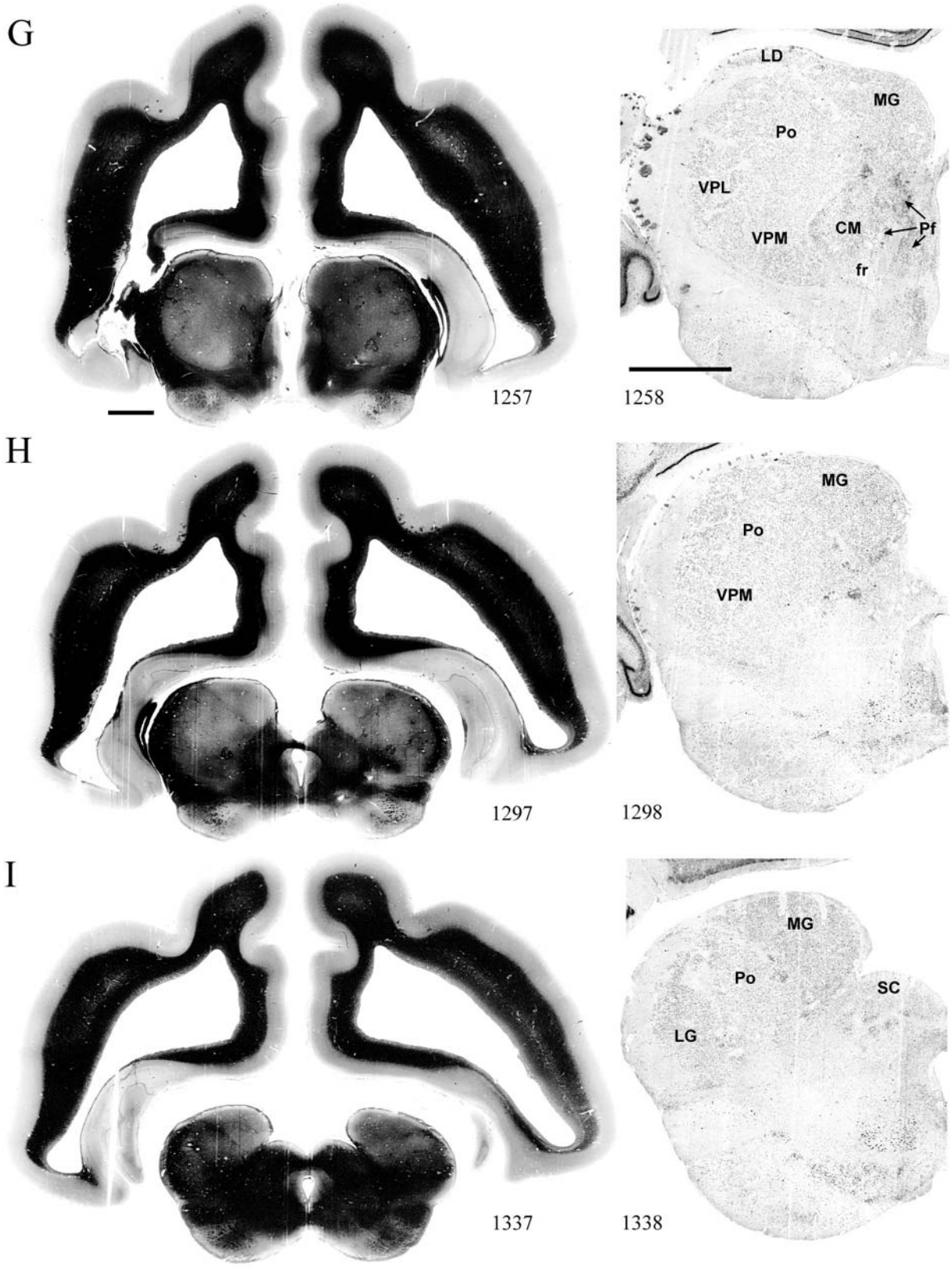

Figure 3-6. Continued

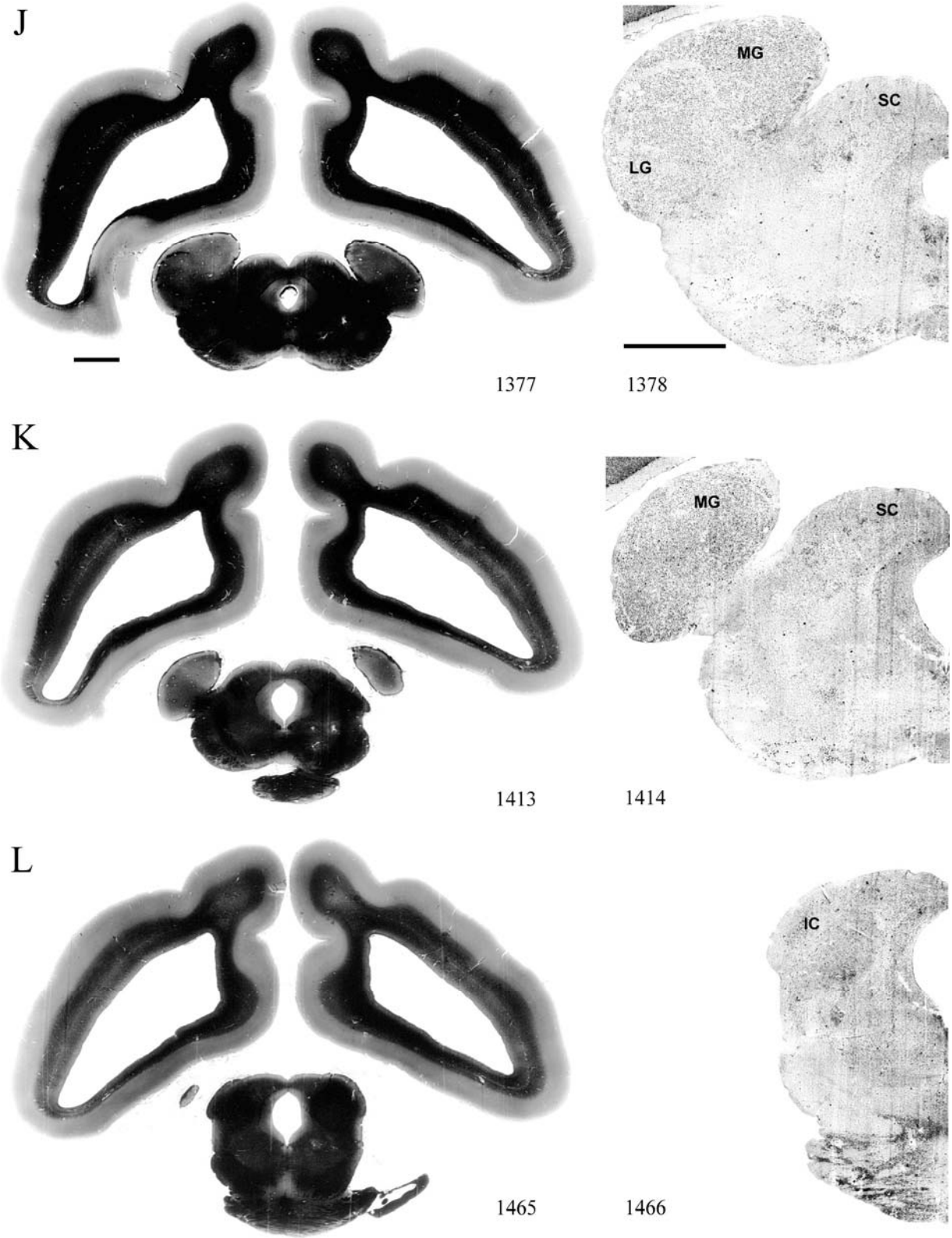

Figure 3-6. Continued

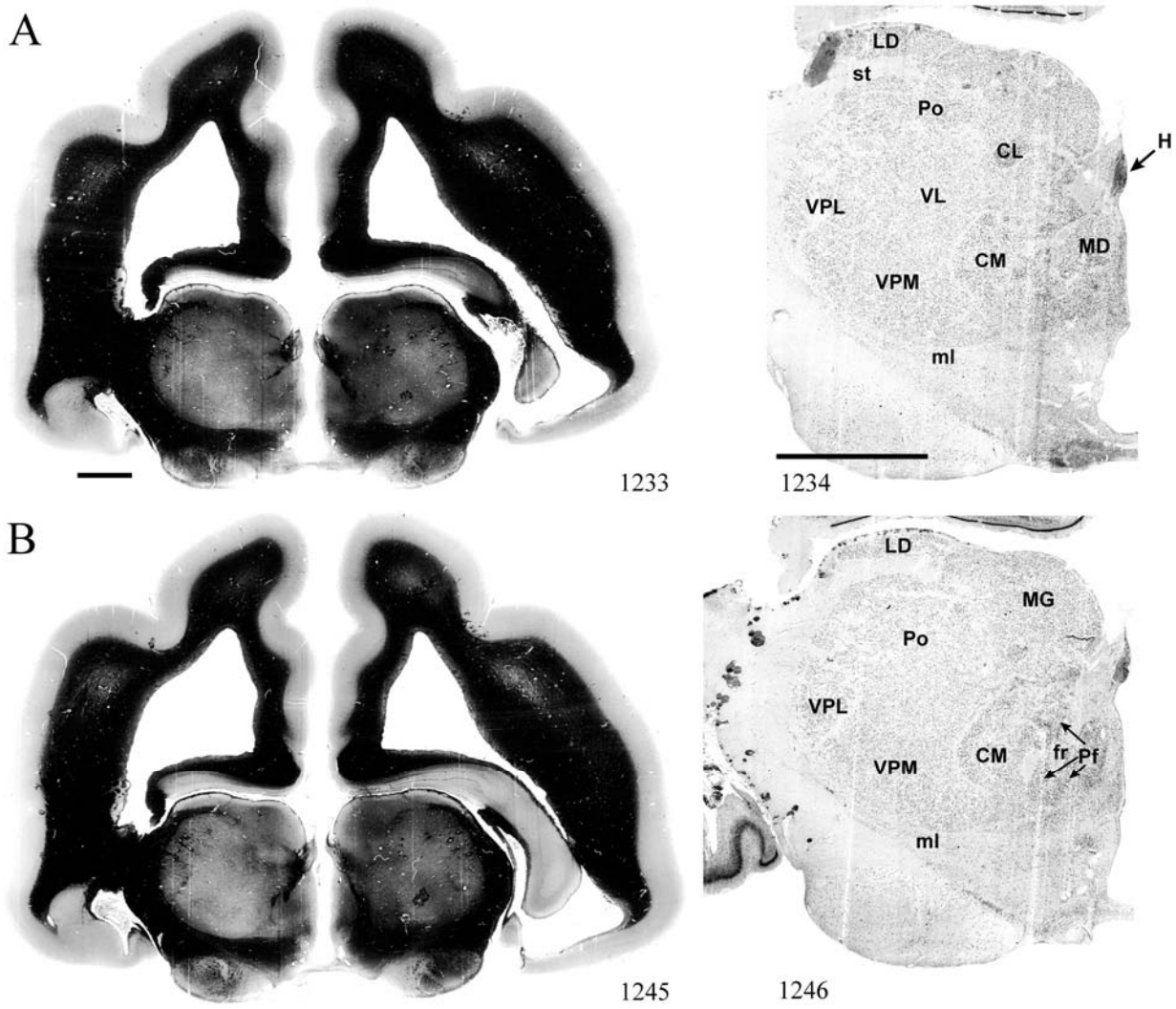

Figure 3-7. A rostrocaudal series of closely spaced coronal sections showing the ventroposterior area (VP) of the thalamus in detail. Low-magnification images of sections stained with hematoxylin for myelin and high-magnification details of adjacent sections stained with thionin for Nissl bodies are labeled for subnuclei. Section numbers are listed at the bottom of each section, and sections were cut at 40µm, specimen 84-49. Scale bar=5mm. CL=central lateral nucleus, CM=centre median nucleus, fr=fasciculus retroflexus, H=habenular nuclei, LD=lateral dorsal nucleus, MD=mediodorsal nucleus, ml=medial lemniscus, Pf=parafascicular nucleus, Po=posterior nucleus, st=stria medullaris, VL=ventral lateral nucleus, VPL=ventral posterior lateral nucleus, VPM= ventral posterior medial nucleus.

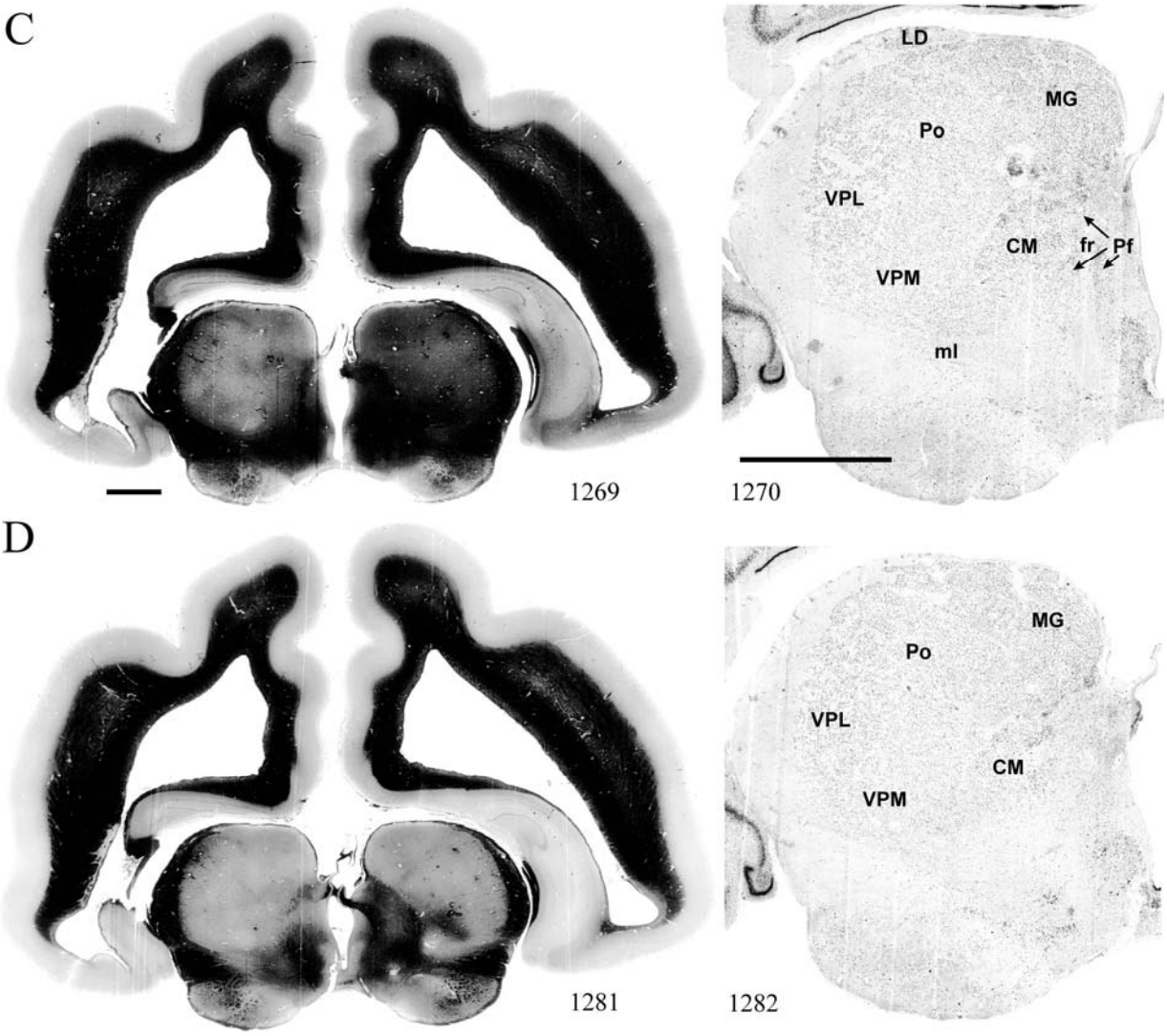

Figure 3-7. Continued

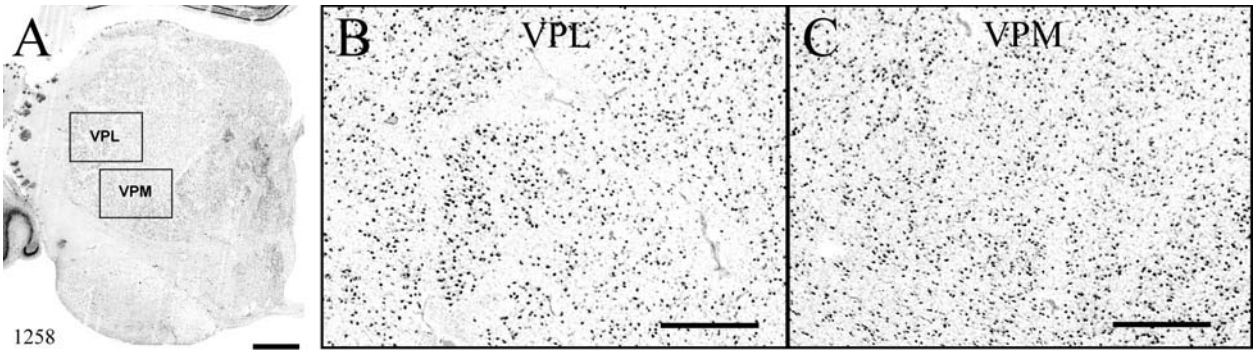

Figure 3-8. Low-magnification and high-magnification images characterizing Nissl body staining of the lateral ventroposterior (VPL) and medial ventroposterior (VPM) subnuclei of the thalamus. A) Low-magnification view shows coronal plane of section and areas imaged at high magnification. B) Cells in VPL are visibly larger, stain more densely, and are less densely packed than those in VPM (C). Sections were stained for thionin and cut at 40µm, specimen 84-49. Scale bars=3mm (A), 1mm (B-C).

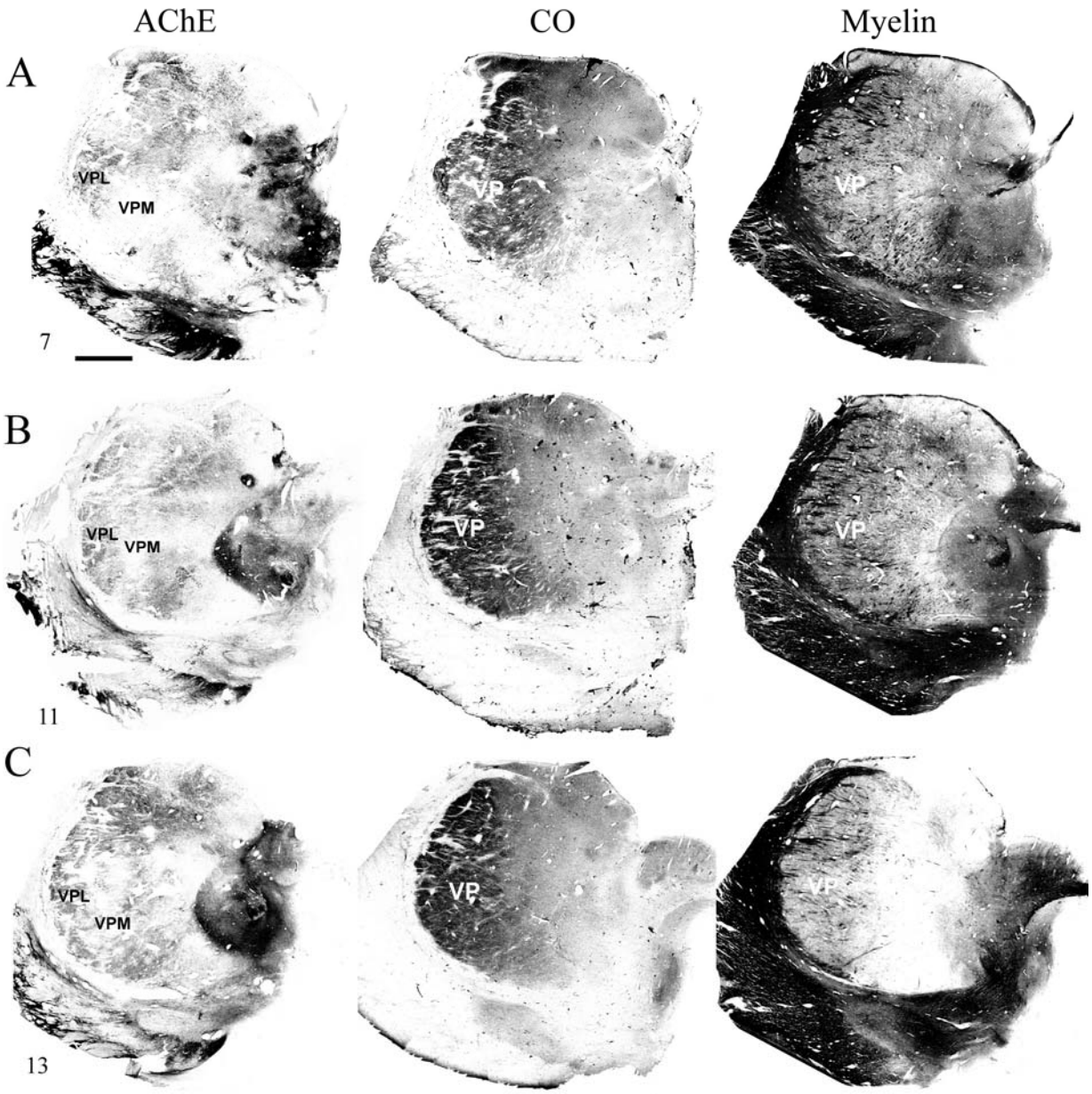

Figure 3-9. Histochemical and histological staining characterization in the ventroposterior nucleus of the thalamus. Coronal sections stained for acetylcholinesterase (AChE) allow the lateral extent of the ventroposterior nucleus (VPL) to be distinguished from the medial subdivision (VPM) by the denser staining in VPL. The entirety of VP also stains densely for cytochrome oxidase (CO) and exhibits dense penetration by fiber bundles in myelin staining (stained with gold chloride, GC). Section number on bottom left for AChE, adjacent sections shown in CO and GC preparations. Up is dorsal, right is medial. Adult specimen TM0406. Scale bar=5mm.

Figure 3-10. Coronal thalamus sections stained for cytochrome oxidase (CO) from a neonate (specimen TM0410) and a juvenile (specimen TM0339) show that the ventroposterior thalamus (VP) exhibits homogenous CO-dense staining without clearly distinguishable barreloids. Up is dorsal, right is medial. Adult specimen TM0406. Scale bar=5mm.

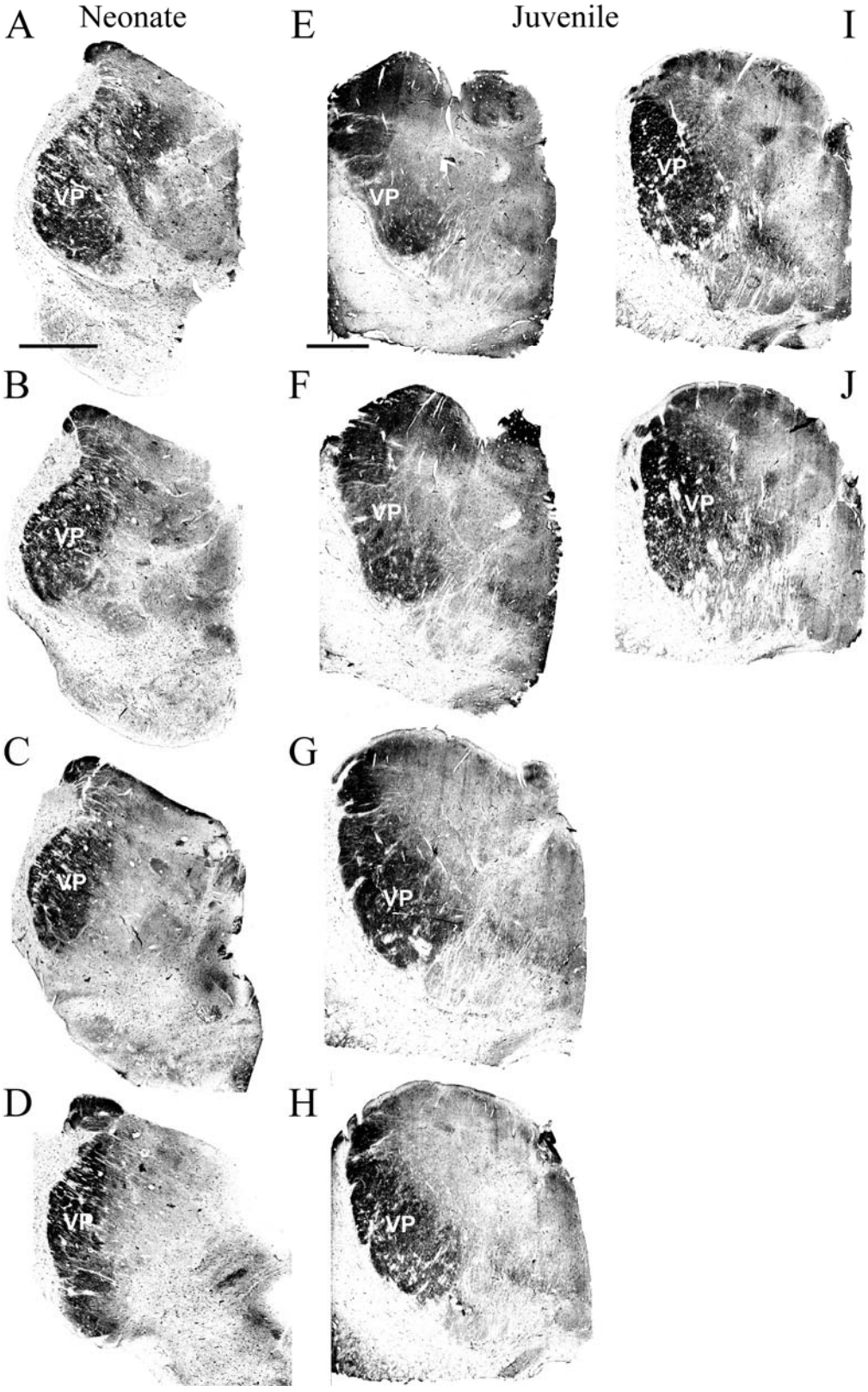
A
Neonate
E
Juvenile
I
VP
VP
VP
B
F
J
VP
VP
VP
C
G
VP
VP
D
H
VP
VP

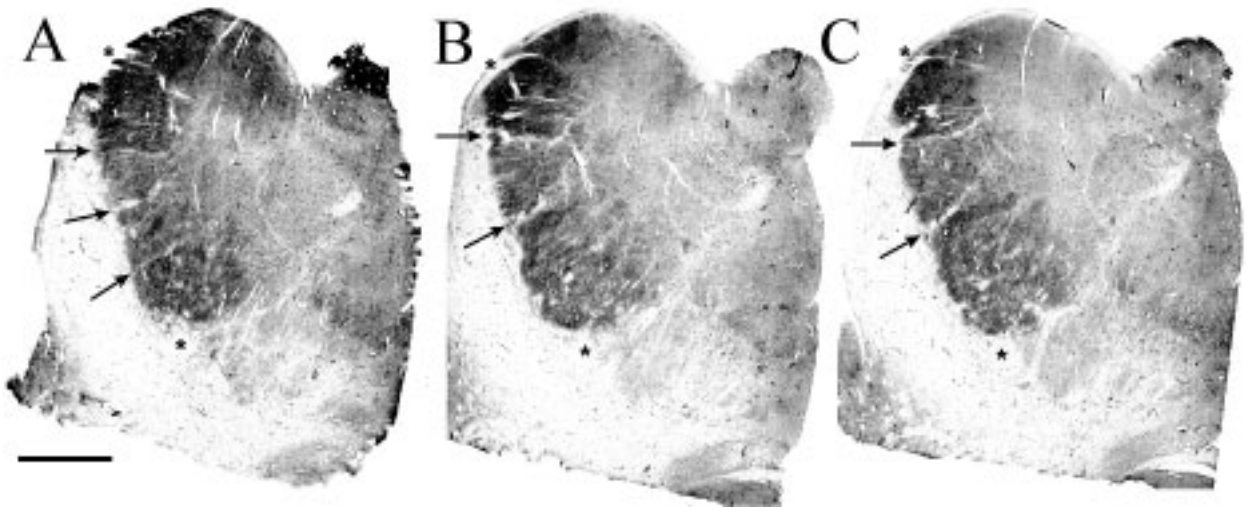

Figure 3-11. Fiber laminae (arrows) seen most distinctly in the juvenile specimen (TM0339) may separate adjacent projections from adjacent body parts into subnuclei of the thalamus as demonstrated in other species. Asterisks denote dorsal and ventral boundaries of the ventroposterior nucleus. Coronal sections stained for cytochrome oxidase. Up is dorsal, right is medial. Scale bar=5mm.

Figure 3-12. Horizontal myelin-stained section showing unusual placement of the medial (MGN) with respect to the lateral geniculate nucleus (LGN). The posterior nucleus (Po) is also visible separating MGN from LGN rostrally. Up is rostral, right is medial. Section number 437, specimen 85-8. Scale bar=5mm.

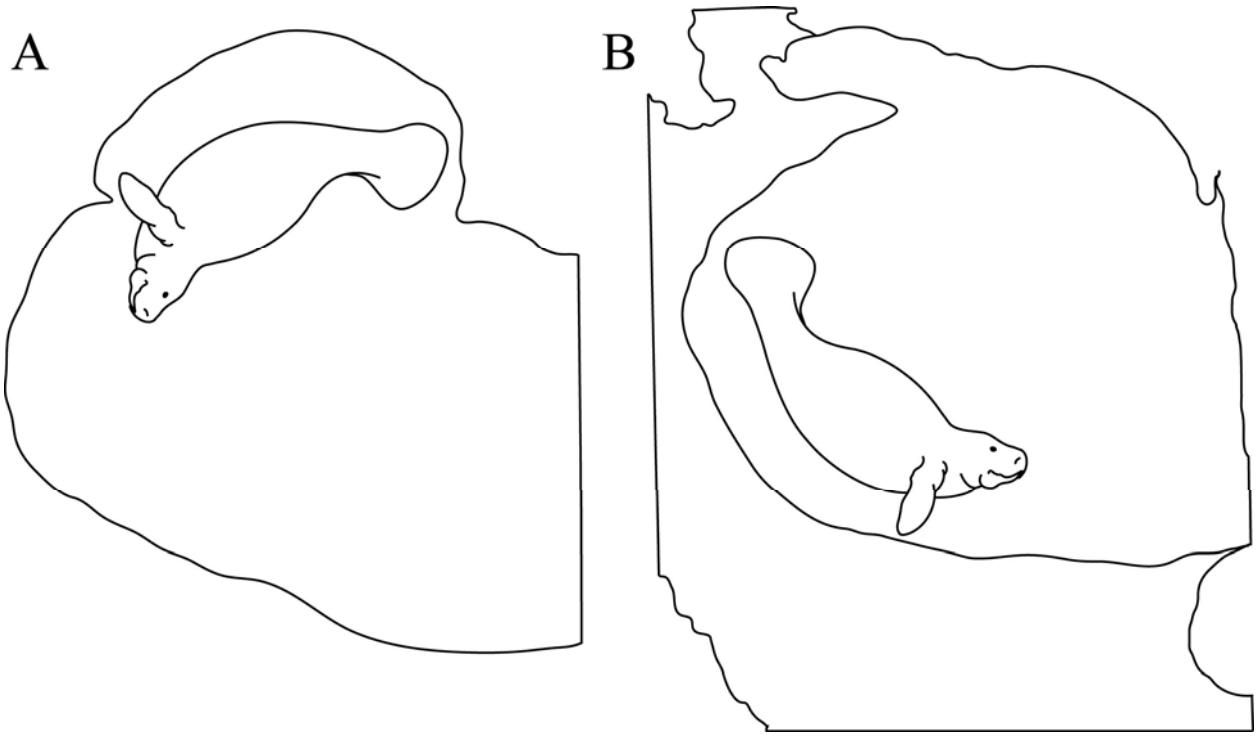

Figure 3-13. Proposed somatotopy of functional representations within the brainstem somatosensory nuclei (cuneate-gracile and trigeminal) and the ventroposterior nucleus (VP) of the thalamus in the coronal plane of section. A) As seen in other mammals, the presumptive somatotopical arrangement within the manatee brainstem would include the head at the most lateral aspect within the trigeminal nucleus with the dorsal aspect of the face medial and the ventral face lateral. The rest of the body arrangement would proceed dorsomedially within the cuneate-gracile complex with the flippers, trunk of the body, and the fluke. The plane of section is equivalent to Fig. 3-1M. B) In the thalamus, the somatotopy is presumably arranged such that the face is represented at the ventromedial extent of VP with the dorsal aspect of the face positioned dorsally and the ventral aspect positioned ventrally. The somatotopy continues along the lateroventral aspect of the thalamus proceeding laterally and dorsally with the flipper representation followed by the trunk of the body and the fluke. The plane of section is equivalent to Fig. 3-6F. Up is dorsal, right is medial.

CHAPTER 4
SOMATOSENSORY AREAS OF MANATEE CEREBRAL CORTEX: HISTOCHEMICAL CHARACTERIZATION AND FUNCTIONAL IMPLICATIONS

Introduction

The Florida manatee appears to have developed a unique combination of neuroanatomical, physiological, and behavioral traits to accommodate its life as a tactile specialist and the only mammalian obligate aquatic herbivore. For example, whereas most mammals exclusively exhibit tactile hairs on the face, particularly the mystacial region, manatee tactile hairs are distributed over the entire body. Furthermore, tactile hairs (or "vibrissae," distinguished by a prominent circumferential blood sinus complex, connective tissue capsule and dense innervation) are the only type of hair seen in manatees (Reep et al., 2001). This system might function as a distributed array for detecting water movements associated with the presence of other animals, river currents, and tidal flows (Reep et al., 2002). Manatees could also use this system to orient and navigate in the murky waters of their habitat with an enhanced tactile sense compensating for poor visual acuity (Bauer et al., 2003). Tactile hairs are 30 times more densely distributed on the face than on the postcranial body and are crucial in manatee feeding and tactile exploration of the environment, accomplishing dual and synergistic motor and sensory roles (Marshall et al., 1998a, b). The hair and bristles of the manatee face span 9 distinct regions (Reep et al., 1998), 2 of which are used in a prehensile grasping fashion during feeding and "oripulation" that is unique among mammals as well as in social behaviors including mouthing, nuzzling, and pinching a conspecific's back in an attempt to gain access to food (Marshall et al., 1998b; Reep et al., 2001). Such observations suggest a high level of perioral dexterity and tactile discrimination. This is supported by evidence that the relative tactile difference threshold (or Weber fraction) is 14% for manatees using their perioral hairs, which is comparable to that of an Asian elephant's trunk (Bachteler and Dehnhardt, 1999). Notably, the eyes are often closed

during feeding and tactile exploration (Marshall et al., 1998b; Bachteler and Dehnhardt, 1999), further suggesting an emphasis on haptic over visual input. Therefore we hypothesized that the Florida manatee has a large area of cortex devoted to somatosensory processing, with the facial region assuming a disproportionately large amount of this area.

Somatosensory maps have been delineated for a wide variety of species, traditionally through the use of electrophysiology but more recently in combination with histochemical and axonal tracing studies. Although the endangered status of the Florida manatee precludes it from becoming a subject for electrophysiological study, studies relating electrophysiology to histochemistry—specifically cytochrome oxidase and myelin staining (Krubitzer, 1995; Kaas and Collins, 2001)—have identified anatomical characteristics that hold predictive value in determining the functional parcellation of primary sensory areas, and can therefore be applied to the manatee through comparative analysis. Given the variety of behavioral and sensory uses for which the facial vibrissae of the manatee are specialized, we would expect to find a large cortical primary somatosensory area (SI) with a particularly large and potentially specialized facial representation to accommodate a high level of cutaneous input, as seen in a diverse range of animals including the llama (Welker et al., 1976), platypus (Bohringer and Rowe, 1977; Johnson, 1990), star-nosed mole (Catania, 2000), and naked mole-rat (Catania and Remple, 2002; Henry et al., 2006). Presumptive SI of the Florida manatee was first identified on the basis of location and cytoarchitectural characteristics (Reep et al., 1989; Marshall and Reep, 1995) and was hypothesized to consist of areas cluster cortex areas 1 and 2 (CL1 and CL2) as well as dorsolateral areas 1 and 2 (DL1 and DL2). In addition, cortical cell clusters of layer VI called Rindenkerne ("cortical nuclei"), first identified by Dexler (1912) and recently investigated in more detail (Reep et al., 1989; Marshall and Reep, 1995), are unique to sirenians (Johnson et al.,

1994) and stain darkly for cytochrome oxidase. Rindenkerne are reminiscent of "barrels" found in layer IV of the vibrissae subfield of somatosensory cortex in rats, mice, and other rodents (Johnson, 1980; Rice, 1995; Kaas and Collins, 2001), as well as in shrews (Catania et al., 1999), opossums (Huffman et al., 1999; Catania et al., 2000; Frost et al., 2000), and hedgehogs (Catania et al., 2000).

In our efforts to delineate SI and to assign Rindenkerne within a presumptive functional scheme for the Florida manatee, preliminary findings revealed four distinct cytochrome oxidase-dense patches in the neonate, corresponding to the presumptive forelimb flipper, face, body, and tail representations of SI but only one distinct patch in presumptive SI of juvenile and adult specimens (Sarko and Reep, 2005). This might indicate modification and refinement of sensory inputs as manatees develop. In order to pursue these observations in more detail, we performed a systematic analysis of flattened cortex preparations and coronal sections stained for Nissl bodies, myelin and cytochrome oxidase to accurately localize primary sensory areas, laminar restriction of staining, and differential patterning observed between younger versus older animals.

Materials and Methods

Four postmortem brains of the Florida manatee, *Trichechus manatus latirostris*, were obtained fresh (the head perfused within 24 hours of death) through the statewide manatee salvage program administered by the Florida Department of Natural Resources and collected under U.S. Federal Fish and Wildlife Permit PRT-684532 and IACUC protocol #C233. The heads were removed at the necropsy facility of Sea World, FL, and then transported to the University of Florida to be perfused in situ by gravity-fed bilateral cannulation of the carotid arteries, with 8–15 L of 0.9% phosphate-buffered saline followed by 8–15 L of 4% phosphate-buffered paraformaldehyde fixative (amounts varied according to specimen size). The dorsal cap of each skull was removed, the brain extracted, and the meninges removed. Each brain was then

placed in 4% paraformaldehyde. A summary of relevant specimen information is provided in Table 4-1 (classifications are in accordance with size/age class definitions for the manatee photo-identification system, Sirenia Project, National Biological Survey, 1994). Specimen TM0310 was classified as a neonatal mortality with nonspecific pulmonary and renal congestion, no underlying infectious or degenerative process, and the cause of death was attributed to hypothermia. The death of the second neonate (TM0410) was classified as perinatal and natural including the involvement of salmonellosis and hypoglycemia. The juvenile TM0339 died due to gastric rupture. The death of the adult TM0406 was attributed to watercraft impact. In each case the animal was considered fresh with minimal degradation of the tissues collected and without potentially confounding factors such as chronic pathology or emaciation. In an additional specimen, TM2, sections spanning the caudal extent of the basal ganglia to the rostral extent of the thalamus had been previously stained for Nissl bodies and cytochrome oxidase in the laboratory of Dr. Robert Switzer (Neuroscience Associates, Inc., Knoxville, TN). These sections were analyzed and found to corroborate findings for the juvenile and adult.

The left hemisphere cortex of each brain was removed and flattened in fixative overnight under a uniformly weighted glass plate. Once flattened, 60 μm serial frozen microtome sections were cut tangentially to the pial surface. Adjacent series of sections were then stained for cytochrome oxidase (all specimens), for Nissl substance with cresyl violet (all specimens), and for myelin with gold chloride (TM0339, TM0406, and TM0410 only). The cytochrome oxidase procedure (Wong-Riley, 1979) was modified for manatee tissue by staining overnight, and the gold chloride procedure (Schmued, 1990) was used with adjustment of pH to 6.3. Once staining was complete and sections were mounted onto gelatinized slides, the slides were coverslipped using Eukitt. The right hemisphere of each brain remained unflattened and was processed to

allow for detailed analysis of cytochrome oxidase staining within cytoarchitectural boundaries. Sections were cut coronally, but otherwise followed the above protocol (frozen-sectioned at 60 μm and with identical staining procedures).

All cortical sections were viewed under an Olympus BH-2 microscope, a Bausch and Lomb microprojector, and a Zeiss Axiophot microscope. Tangential sections from the flattened left hemisphere stained for cytochrome oxidase were placed on a light Table and sequential sections were examined for persistence of the visible patterns. Representative sections were scanned with a HP ScanJet 5370C and merged using Adobe Photoshop. Composites were completed for each brain (Fig. 4-1) with the exception of TM0410, where inadequate perfusion of the left hemisphere only permitted analysis of the right hemisphere coronal sections. Images of flattened composites were then analyzed using image analysis software (MCID, Imaging Research, Inc.) to determine the percentage of area that presented cytochrome oxidase-dense staining when using threshold and areal morphometry analysis and also when areas were outlined by hand (Fig. 4-1B; Table 4-2).

Coronal sections were examined for cytochrome oxidase-dense patches and compared to adjacent Nissl body sections in order to localize patches according to cytoarchitectural boundaries previously noted (Reep et al., 1989; Marshall and Reep, 1995). We subsequently related the above results on coronal sections of the right hemisphere to tangential patterning seen in the left hemisphere. This allowed for accurate localization of patterns seen on tangential sections, and compensated for distortion inherent in the flattening process. The laminar locations of cytochrome oxidase-dense bands were also assessed through direct comparison of adjacent coronal cytochrome oxidase and Nissl body sections using the Bausch and Lomb microprojector and the Zeiss Axiophot microscope. Rindenkerne were observed, localized cytoarchitecturally,

and then related to the functional areal delineations proposed in the above analyses. Representative sections used in figures were imaged with a Zeiss Axioplan2 morphometric microscrope. A spaced series of coronal sections from the right hemisphere of specimen TM0410 was imaged using MCID software in order to create a true three-dimensional reconstruction of cytoarchitectural area overlap with cytochrome oxidase staining (Fig. 4-7). Each section was aligned and imaged using a CCD black and white camera model 72S (Dage MTI, Inc.) attached to a lightbox. The lateral surface of each section was then outlined by hand with user-specified colors to delineate the extent of cytoarchitectural areas determined from Nissl-stained sections. The outlining was then repeated for cytochrome oxidase-dense staining and the reconstructions were then overlapped.

Results

Areal Patterning

Tangential sections taken from flattened cortex preparations for a neonate (TM0310, Fig. 4-1A), a juvenile (TM0339, Fig. 4-1C), and an adult (TM0406, Fig. 4-1D) were stained for cytochrome oxidase and analyzed for general identification of primary sensory areas. Presumptive functional areas of somatosensory cortex were assigned based on the location of cytochrome oxidase-dense patches with “F” representing the face, “FL” the flipper, “B” the body, and “T” the tail (Fig. 4-1A, C-D). Although the frontoparietal region of the neonate had 4 distinct patches (Fig. 4-1A), the juvenile and adult specimens shared a similar pattern of one large patch blending the presumptive functional areas into one continuous domain (Fig. 4-1C, D). Primary auditory (Fig. 4-1A, C-D patch “A1”) and visual (Fig. 4-1A, C-D, patch “V1”) areas were also assigned based on cytochrome oxidase-dense staining and location.

The percentage of flattened cortical surface that stained darkly for cytochrome oxidase, and therefore presumably represented primary sensory areas, was determined using a computer-

based morphometry program (Fig. 4-1B; Table 4-2). Percentages were calculated for primary sensory areas versus total cortical surface area, SI versus total cortical surface area, primary somatosensory area (SI) versus cortical surface area of the frontal hemisphere (rostral to the lateral fissure), and primary sensory areas (presumably encompassing A1 and V1) versus cortical surface area of the caudal hemisphere (caudal to the lateral fissure). A density threshold was chosen across all specimens such so as to minimize false positives and generate a conservative estimate of percentage of cortical area stained. A measurement for SI versus frontal hemisphere area was also drawn by hand and recalculated as the computer-generated outline appeared to underestimate surface area devoted to SI as can be visually assessed for the frontoparietal hemisphere density threshold generated for specimen TM0310 (Fig. 4-1B) versus staining (Fig. 4-1A). Roughly one third of cortical area was devoted to primary sensory areas overall. Although the MCID software did appear to underestimate the percentage of SI area in the frontal hemisphere compared to manually delineated outlines of SI, in both cases the neonatal specimen produced smaller percentages of SI area than in the juvenile and adult. If the self-drawn outlines were indeed more accurate, then the adult specimen showed the most area devoted to SI at 75% of the frontal hemisphere, but taking the computer-generated percentages as a conservative estimate still assigned over 50% of the frontal cortex to SI in the adult and juvenile specimens. In contrast, only 12% of the caudal hemisphere was devoted to primary auditory and visual areas combined, and this percentage was consistent across age groups.

Neonates

Coronal sections from the right hemisphere of 2 neonate brains (Table 4-1) were analyzed to match cytochrome oxidase-dense staining with cytoarchitectural boundaries. Although ventral aspects of TM0310 were damaged, and tangential sections of TM0410 were not useful for analysis due to shredding, the neonate brains exhibited consistent trends. Cytochrome

oxidase-dense staining in layer IV corresponded to myelin-rich areas overall, with presumptive primary sensory areas also staining for myelin in layers V and VI (Fig. 4-5) consistent with other species (Hassiotis et al., 2004). Staining for cytochrome oxidase activity is characterized as dense (or intense; e.g., area DL1 layer IV staining, Fig. 4-2A), moderate (e.g., layer III staining in rhinal cortex (RH), Fig. 4-2A), or absent (e.g., area dorsomedial (DM2), Fig. 4-2D). Within the frontal cortex (FR), cytochrome oxidase staining rostrally was broad and dense spanning the dorsal to dorsomedial extent of FR (Fig. 4-2A). Intense staining in area FR spanned layer V and moderate staining persisted in layer VI. In area DL1 intense cytochrome oxidase staining became restricted to layer IV with moderate staining in layer III (Fig. 4-6B). The DL1 band extended throughout DL1 rostrally and then began to terminate more dorsally within caudal DL1 (Fig. 4-2, A-E). A band of moderate cytochrome oxidase staining emerged caudally in layer VI of DL1 in neonatal specimens (Figs. 4-2D, E; 4-6B) but not in juvenile (Fig. 4-3, B-D) or adult (Figs. 4-4A, B; 4-5) specimens. Within area DL2, dense staining was located in layer IV only caudally along with moderate staining in layer III and additional moderate layer VI seen only in neonates (Figs. 4-2, A-D; 4-6C). As dorsomedial FR transitioned to area DM3 the dense staining of layers V and VI that characterized FR became laminar and restricted to layer IV with moderate layer III staining in DM3 (Figs. 4-2, A-C; 4-6E), and the extent of DM3 was cytochrome oxidase-dense throughout layer IV of each brain (Fig. 4-2, C-I). DM2 consistently lacked staining (Fig. 4-2, C-I). Dorsal cortex (DD) area staining was irregular, showing no staining rostrally (Fig. 4-2, B-F) but exhibiting moderate laminar staining in layer IV for a limited caudal extent (Fig. 4-2G, H). Areas RH and olfactory cortex (OLF) were moderately cytochrome oxidase-dense in layer III (Fig. 4-2, A-C). Rindenkerne in CL1 stained densely for cytochrome oxidase in layer VI but were clearest in myelin and Nissl body stains for areas CL2 through CL5 in all specimens

examined. Intense layer IV, moderate layer III and additional layer VI staining in neonates only also appeared throughout the caudal extent of CL2 rostral to the lateral fissure (Figs. 4-2E; 4-6A). Caudal to the lateral fissure moderate CL2 staining appeared in layer IV (Fig. 4-2, F-G) whereas CL1 stained only lightly for cytochrome oxidase (Fig. 4-2G). Area DD2 displayed moderate staining in layer III (Figs. 4-2, I-L; 4-6F). All of CL3 was cytochrome oxidase-dense in layer IV whereas the dorsal extent of areas CL4 and CL5 showed moderate staining in their combined layer III/IV (Fig. 4-2, H-L). Splenial sulcal cortex (SS) was consistently cytochrome oxidase-dense in layer IV, as was all of DL3 and to a moderate extent the ventral portion of DL4, both in layer IV (Fig. 4-2, J-L).

Juvenile and Adult

Adult (TM0406) and juvenile (TM0339) specimens displayed similar cytochrome oxidase-dense staining patterns, and therefore a representative series from only the juvenile is shown for reference (Fig. 4-3) with selected examples from the adult used to illustrate similar trends (Fig. 4-4). Results for areas CL1, CL2, CL3, DD, DD2, DM2 and DM3 were also confirmed in specimen TM2. Rostral area FR exhibited diffuse, dense staining (Fig. 4-3A). Area DL1 demonstrated intense laminar staining restricted to layer IV with moderate staining in layer III (Fig. 4-3, B-D). Only the caudal portion of DL2 stained densely for cytochrome oxidase and staining was restricted to layer IV with moderate layer III staining (Fig. 4-3B, C). Area DM3 was consistently cytochrome oxidase-dense in layer IV with moderate staining in layer III, and DM2 displayed diffuse cytochrome oxidase activity rostrally (Fig. 4-3, B-C) but not caudally (Fig. 4-3, D-K), whereas DM1 exhibited no cytochrome oxidase activity. Area DD displayed dense cytochrome oxidase activity in layer IV (Figs. 4-3E, F; 4-6D) whereas DD2 demonstrated moderate layer III activity (Fig. 4-3, G-N). In area CL2, dense staining was present in layer IV both rostral and caudal to the lateral fissure, except at the most rostral extent of CL2, along with

moderate layer III staining (Figs. 4-3, C-J; 4-6A). Area CL1 stained moderately for cytochrome oxidase in the dorsocaudal region bordering the lateral fissure (Fig. 4-3, G-J). The entire span of CL3 exhibited intense cytochrome oxidase staining in layer IV (Fig. 4-3J, K). Area CL4 exhibited moderate layer III/IV staining dorsally (Fig. 4-3K) and CL5 also expressed moderate staining in layer III/IV (Fig. 4-3, L-O). Area DL3 had intense staining in layer IV (Fig. 4-3L, M) whereas DL4 showed moderate layer IV staining (Fig. 4-3N, O). Caudal pole cortex (CP) exhibited moderate to light staining, SS stained intensely in layer IV (Fig. 4-3, L-O), and medial wall cortex area two (MW2) stained moderately in layer III (Fig. 4-3, K-M).

The new histochemical information provided above might indicate a reassessment of previously assigned cytoarchitectural regions, as the caudal portion of areas CL2 and DL2 stained for cytochrome oxidase whereas the rostral portion (and lateral portion in the case of older specimens) of each region did not (Fig. 4-6A, C). Given this additional histochemical information, we suggest that the rostral and caudal portions of areas CL2 and DL2 be referred to as alpha and beta subdivisions, respectively.

Neonate versus Juvenile and Adult Comparison

As noted previously (Sarko and Reep, 2005), cytochrome oxidase staining patterns in neonate versus juvenile and adult specimens differed. Area DL1 staining occurred more dorsally in the more developed animals (Figs. 4-2D; 4-3, B-D; 4-4B) as did CL2 staining (Figs. 4-2E; 4-3D; 4-4C). Area DD staining was also prominent in the older animals (Figs. 4-3E, F; 4-4A, B) but not in neonatal specimens (Fig. 4-2, B-F). Finally, neonatal specimens exhibited a moderately staining cytochrome oxidase band in layer VI of areas DL1, DL2 and CL2 that was absent in juvenile and adult specimens. Variations in cytoarchitecture between neonates and older animals also became apparent. Area DM2 never extended to the dorsal aspect of the cortex

in neonates (Fig. 4-2, A-C) but was present in the juvenile (Fig. 4-3B) and the adult. Also, the medial aspect of area FR extended much further caudally in the neonatal specimens.

Discussion

Utilizing the ability of cytochrome oxidase to preferentially stain primary sensory areas, we have determined which cytoarchitectural regions are likely to have specific functional significance for the Florida manatee (Fig. 4-7). Though sample size was necessarily limited due to the manatee's endangered status, these results expand on, and are often in agreement with, those areas proposed by Marshall and Reep (1995) based on cytoarchitecture alone.

Somatosensory Cortex

Primary somatosensory cortex appears to correspond to areas DM3, DL1, CL2, CL1, and portions of DD, DL2, and DM2. Areas DM3, DL1, and CL2 each have a well organized layer IV and were previously identified as potential candidates for SI (Marshall and Reep, 1995). Although the presence of areas with and without Rindenkerne in presumptive SI remains puzzling, it seems likely that CL areas represent vibrissal input whereas areas DL, DM, and DD mainly accommodate cutaneous information, with roughly half of presumptive SI devoted to each type of input. Area DM3 likely encompasses the tail representation of SI, due to its dorsomedial location, pronounced layer IV, and cytochrome oxidase-dense staining in layer IV. However, a caveat to the proposal that non-cluster cortex represents cutaneous input would be that, by extension, the tail representation of the cortex lacks clear vibrissal representation because area DM3 lacks Rindenkerne. The manatee tail contains a hair density distribution comparable to that of the trunk of the body, making the absence of any cortical representation of tail vibrissae unlikely (Reep et al., 2002). Manatees also manipulate their tails as they navigate through the water, implicating the tail in sensory feedback through a turbid water environment. Therefore, we hypothesize that the tail vibrissae are in fact represented in the cortex but that their

small size and innervation (Reep et al., 2001) potentially correspond to relatively small Rindenkerne just as smaller, less innervated mystacial vibrissae project to relatively small barrels in the rodent cortex (Woolsey and Van der Loos, 1970; Lee and Woolsey, 1975; Woolsey et al., 1975; Welker and Van der Loos, 1986; Rice, 1995), and that such Rindenkerne might be detectable by more sensitive methods. Welker and Van der Loos (1986) also discovered that histological cortex preparations only produced visible barrels if the corresponding whiskers had a threshold number of afferents. Therefore it is possible that the tail vibrissae of the manatee are below this innervation threshold as has been proposed for buccal pad sensory hairs in the naked mole-rat (Henry et al., 2006). Area DL1 is located more laterally and has a well-developed layer IV that consistently stains for cytochrome oxidase, making it a likely candidate for the body representation. The adjacent cytoarchitectural area CL2 also has a well-developed layer IV that stains for cytochrome oxidase and might lend itself to the body representation in its more medial portion and possibly the flipper and face representations in its lateral portion. Area DL2 exhibited cytochrome oxidase-dense staining exclusively at its caudal extent, making it possible that this area represents facial information.

Due to differential staining patterns, rostral DL2 is reclassified here as $DL2_{\alpha}$ with the caudal, cytochrome oxidase-dense portion denoted $DL2_{\beta}$ (Figs. 4-1E; 4-6C). Similarly, the lateral extent of CL2 was found to lack cytochrome oxidase reactivity in layer IV and is thus renamed $CL2_{\alpha}$, with $CL2_{\beta}$ signifying the larger, cytochrome oxidase-dense region (Figs. 4-1E; 4-6A). Area CL1, though lacking layer IV, maintains cytochrome oxidase staining of the largest Rindenkerne present in the cortex and therefore remains a likely candidate for the facial representation as well, possibly specialized for the extensive sensorimotor integration involved with oripulation during use of the largest vibrissae. Prominent cytochrome oxidase staining in

DD and moderate dorsal DM2 staining that was seen only in the juvenile and adult specimens likely contribute to the body representation as well, given the dense staining in a well-developed layer IV in each area. The differences seen in areal patterning between neonate versus juvenile and adult specimens (Fig. 4-1A, C-D) are also reflected in the analysis of coronal sections (Figs. 4-2, A-E; 4-3, A-G; 4-4) and appear to be due to more dorsal staining of areas CL2 and DL1 as well as more extensive staining of DD and dorsolateral DM2 seen in the older animals. Riddle et al. (1992) compared the growth of functional representations within SI in juvenile and mature rats and found that the representation of the head enlarged to a greater extent than that of the paw. They also found that SI grew to a greater extent than the neocortex overall, demonstrating that the cortical expansion is not uniform but rather exhibits regional growth differences. Due to the close relationship between the periphery and the cortical map, and the instructional role that the periphery plays in organizing the layout of somatosensory cortex (Killackey et al., 1990; Catalano et al., 1995), the differences seen in SI of neonate versus juvenile and adult manatees may reflect modifications of the sensory periphery reflected in reorganization of SI in the more developed animals, although the limitation of small sample size precludes assignment of a definitive causal mechanism.

Area DD2 presented moderate staining restricted to layer III. As shown by Eskenasy and Clarke (2000), area SII in humans demonstrates cytochrome oxidase activity in layer III whereas cytochrome oxidase-dense activity in SI was restricted to layer IV. Due to its location and cytochrome oxidase reactivity in layer III, area DD2 of the manatee brain might be a candidate for SII. Supragranular cytochrome oxidase staining was also found in secondary sensory areas in other species such as the tammar wallaby (Ashwell et al., 2005), whereas the motor cortex exhibited broad, dense staining as shown here for the manatee. SI appears to occupy roughly

25% of total cortical area (Table 4-2), which is comparable to other somatosensory specialists such as the naked mole-rat in which SI comprises approximately 31% of neocortex (Catania and Remple, 2002). As hypothesized, SI also appears to occupy proportionately greater neocortical area than A1 and V1 (Table 4-2) in the manatee. This is characteristic of other tactile specialists such as the echidna and the platypus whose 4 somatosensory areas occupy approximately 75% of total sensory cortex (Hassiotis et al., 2004; Krubitzer et al., 1995b; Ulinski, 1984).

Auditory and Visual Cortex

As hypothesized by Marshall and Reep (1995), primary auditory cortex appears to span area CL3, but appears to include area CL2 caudal to the lateral fissure as well. Both CL2 and CL3 presented dense cytochrome oxidase staining of layer IV and of Rindenkerne in layer VI. Layer IV staining characterized the entirety of each area. Caudal to the lateral fissure, only the Rindenkerne of area CL1 stained for cytochrome oxidase, making this an unlikely primary auditory area but a potential auditory association area. The presence of only cluster cortex areas in what is hypothesized to be primary auditory cortex is puzzling if Rindenkerne are in fact cortical representations of vibrissae. However, it is plausible that this could represent an overlap of auditory and somatosensory information analogous to the parietal ventral (PV), ventral somatosensory (VS), or caudomedial (CM) areas found in other taxa (Cusick et al., 1989; Krubitzer et al., 1995a, b; Beck et al., 1996; Kaas and Collins, 2001; Schroeder et al., 2001). Such multisensory integration could conceivably involve low-frequency sounds or other hydrodynamic stimuli detected through movement of vibrissae on the manatee body (Reep et al., 2002). Indeed, in determining the underwater audiogram of the West Indian manatee, it was discovered that behavioral responses to low-frequency (<0.4 kHz) sounds changed such that one manatee pivoted its body roughly 45 degrees and lowered its head (a response not exhibited for frequencies >0.4 kHz), which the authors attributed to switching detection of sound stimuli to

vibrotactile sensation (Gerstein and Gerstein, 1999). However, if Rindenkerne are in fact functional representations of tactile hairs, then the entirety of A1 would overlap with presumptive somatosensory function caudal to the lateral fissure in cytoarchitectural areas CL3 and CL2, each of which has a well-developed layer IV that stains densely for cytochrome oxidase. Although the bimodal areas such as PV, VS, or CM could offer a partial explanation, it seems unusual that a separate A1 would not exist in the manatee cortex unless somatosensory information is so crucial to perception of the environment that a complete overlap became adaptive. In the opossum *Monodelphis domestica*, Catania et al. (2000) showed that A1 overlaps with the trunk, body, and ear representations in the opossum's unusually large S2, but this case appears to be an exception.

Primary visual cortex appears to span cytoarchitectural areas DL3 and DL4, as postulated by Marshall and Reep (1995). Each area has a well-organized layer IV that stains densely for cytochrome oxidase. The dorsal aspects of areas CL4 and CL5 are also cytochrome oxidase-dense, but the ventral, larger proportion of each stains only moderately, making these areas likely candidates as visual association areas. Area SS has prominent staining in layer IV as well, but layer IV is only moderately organized with cells that appear more pyramidal than granular (Marshall and Reep, 1995), making it unlikely to be part of the primary visual cortex. The broad, moderate staining of area CP, in addition to its well-developed cortical layers, mark it as a potential multimodal association area that, based on its location, is mostly dedicated to visual information.

In order to completely characterize the manatee somatosensory system and to elucidate specializations that have presumably arisen as adaptations to the unique ecological niche of this species, it will be necessary to thoroughly examine this system at each level of processing.

Whether there exist somatosensory specializations in the manatee thalamus and brainstem, particularly those that might be associated with the cortical Rindenkerne, remains an open question that we are currently investigating. Characterization of nerve endings present in vibrissae, especially interregional differences and specializations, would also further our understanding of the manatee's perceptual capabilities and adaptations.

Table 4-1. Summary of specimen data.

Animal Number	Gender	Length (in cm)	Weight (in kg)	Classification
TM0310	F	127	13.6	Neonate
TM0339	F	200	167.8	Juvenile
TM0406	M	290	393.2	Adult
TM0410	M	94	14.5	Neonate

Table 4-2. Percentage of cortical area represented by presumptive sensory cortex.

	1° areas/total cortex	SI/total	SI/frontal area	SI (manual delineation)/ frontal area	1° areas/ caudal area
TM0310	35	18	35	49	12
TM0339	36	28	55	66	12
TM0406	31	27	53	75	12

Figure 4-1. Tangential sections stained with cytochrome oxidase and merged to encapsulate the full extent and persistence of areal patterning in left hemisphere flattened cortex preparations for A) neonate (TM0310), C) juvenile (TM0339), and D) adult (TM0406) specimens. Presumptive functional areas within SI have been assigned such that "F" represents the face, "FL" the flipper, "B" the body, and "T" the tail. Primary auditory (A1) and visual (V1) areas have also been assigned based on cytochrome oxidase-dense staining patterns (A, C-D). B) A computer-generated density threshold generated for cytochrome oxidase-dense staining in specimen TM0310. E) A cytoarchitectural schematic of the manatee brain modified from Marshall and Reep (1995) to include α and β subdivisions of CL2 and DL2. This schematic illustrates differences in laminar organization as revealed by Nissl body staining and was used as a template for localization of cytochrome oxidase staining in the present study. A-E: left is rostral, up is dorsal.

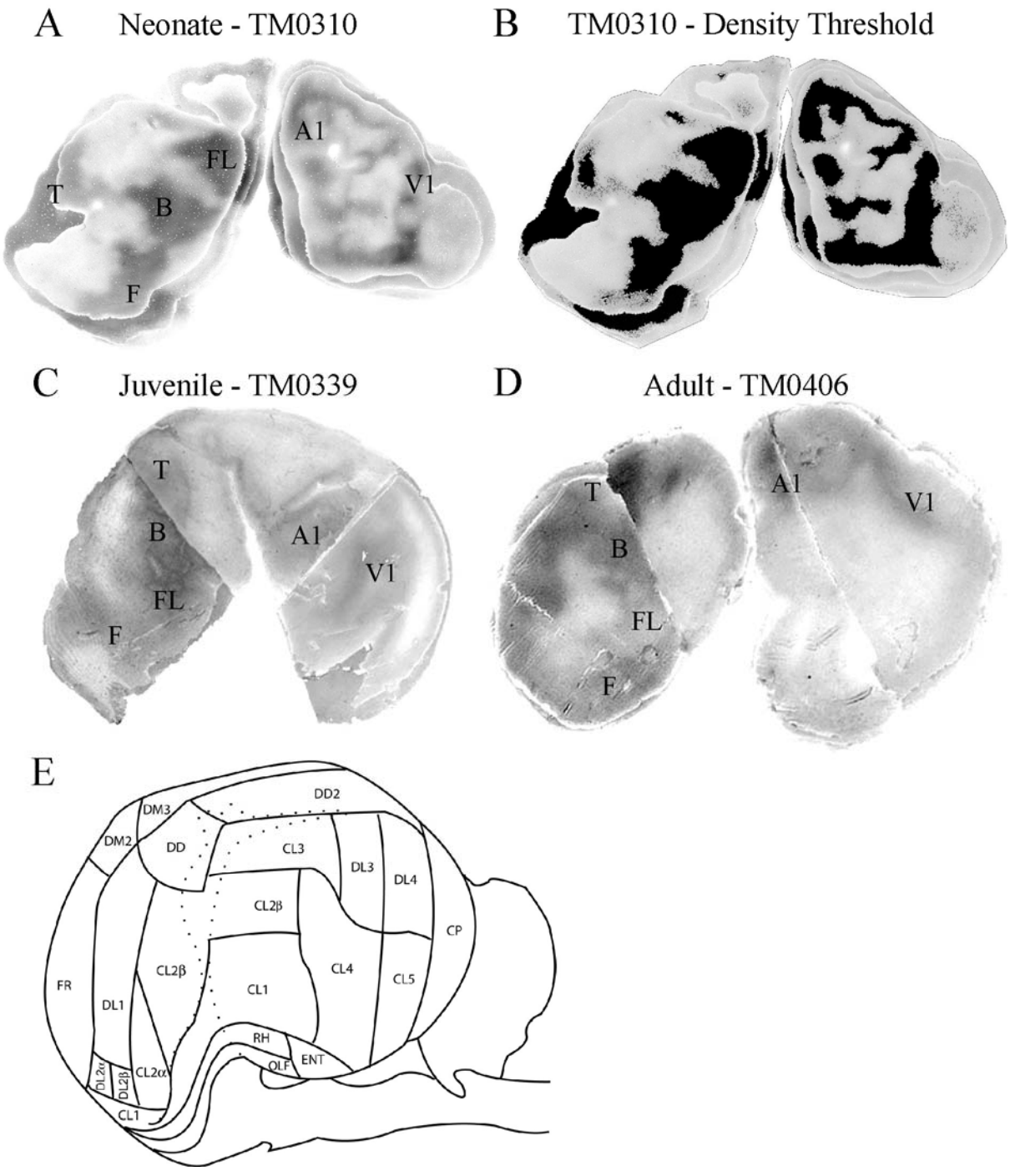
A
Neonate - TM0310
T
B
FL
F
A1
V1
B
TM0310 - Density Threshold
C
Juvenile - TM0339
T
B
FL
F
A1
V1
D
Adult - TM0406
T
B
FL
F
A1
V1
E
DM3
DD2
DM2
DD
CL3
DL3
DL4
CL2β
CP
CL2β
CL4
CL5
FR
CL1
DL1
RH
QLF
ENT
DL2α
DL2β
CL2α
CL1

Figure 4-2. Rostrocaudal series of coronal sections relating cytochrome oxidase staining to cytoarchitectural boundaries (determined by Nissl body and myelin stains of adjacent sections) in a neonate brain (TM0410). Black arrows indicate examples of Rindenkerne seen in areas CL1 and CL2 best illustrated in B but evident in A-E. Right is medial, up is dorsal. The insets of a manatee brain schematic reveal planes of section for A-L. Dotted lines within the schematic approximate locations of the lateral and horizontal fissures separating the frontal and caudal hemispheres.

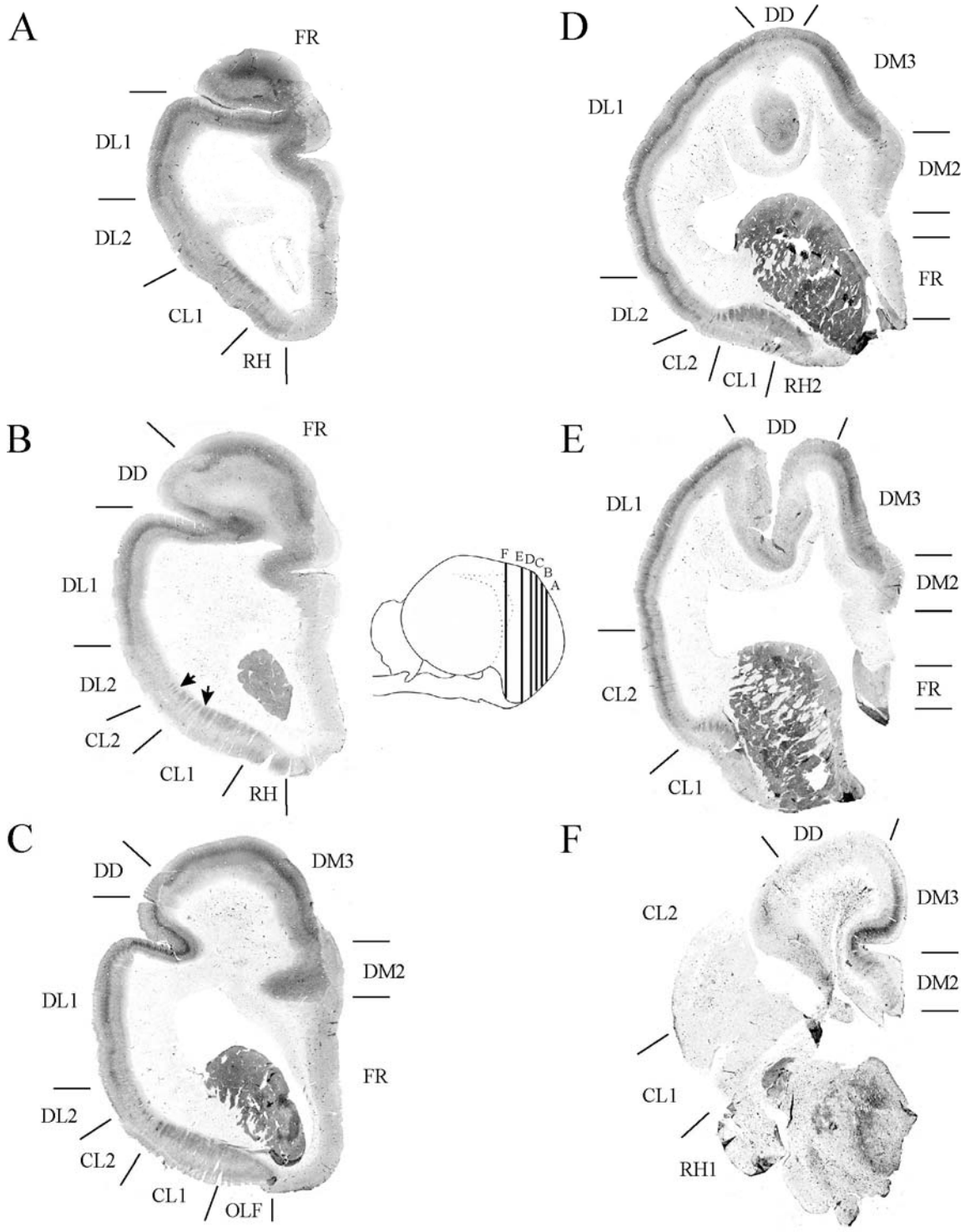
A
FR
DL1
DL2
CL1
RH
B
FR
DD
DL1
DL2
CL2
CL1
RH
F E D C B A
C
DD
DM3
DM2
DL1
FR
DL2
CL2
CL1
OLF
D
DD
DM3
DL1
DM2
FR
DL2
CL2
CL1
RH2
E
DD
DL1
DM3
DM2
CL2
FR
CL1
F
DD
CL2
DM3
DM2
CL1
RH1

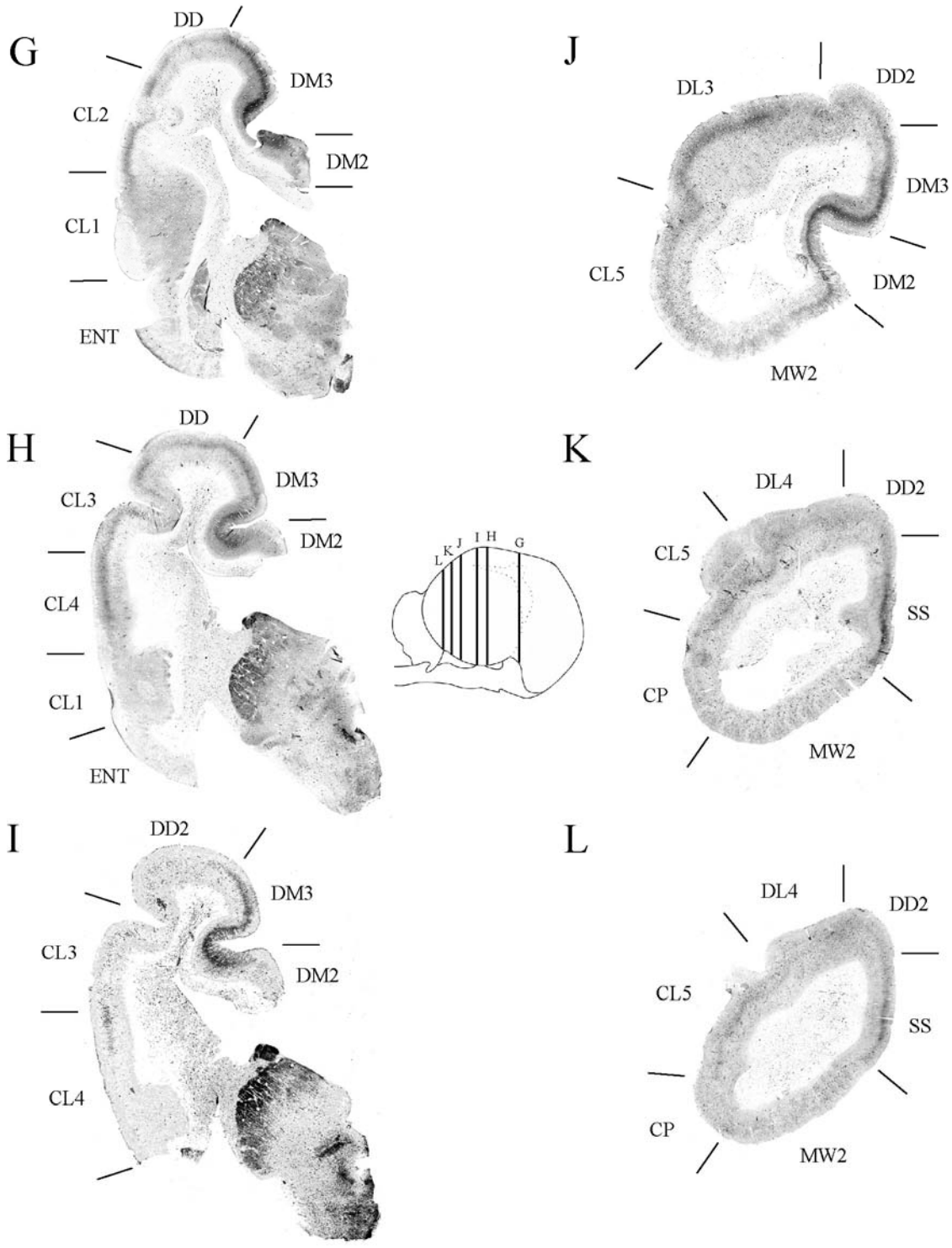

Figure 4-2. Continued

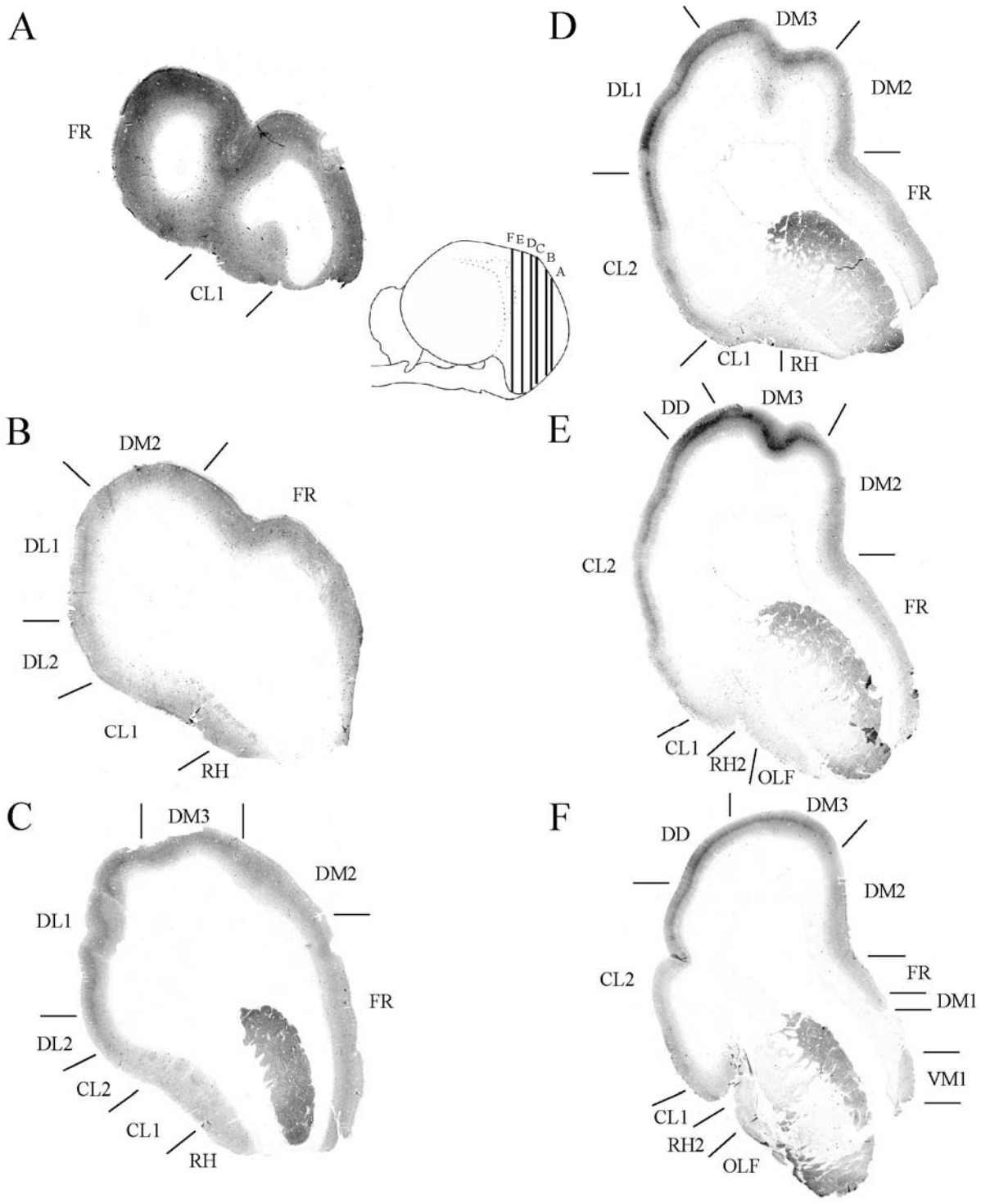

Figure 4-3. Rostrocaudal series of coronal sections relating cytochrome oxidase staining to cytoarchitectural boundaries in a juvenile brain (TM0339). Right is medial, up is dorsal. The inset of a manatee brain reveals planes of section for A-O.

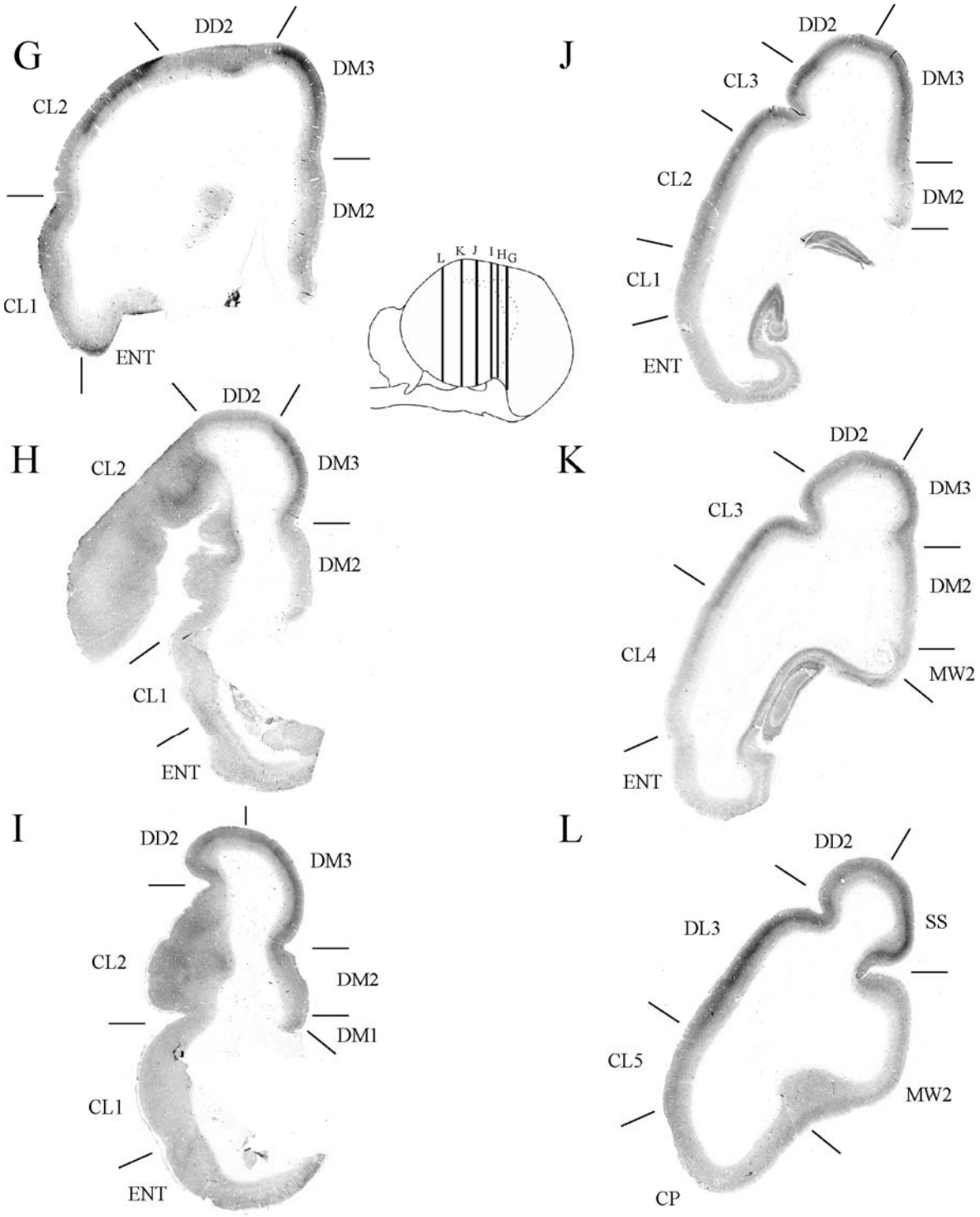

Figure 4-3. Continued

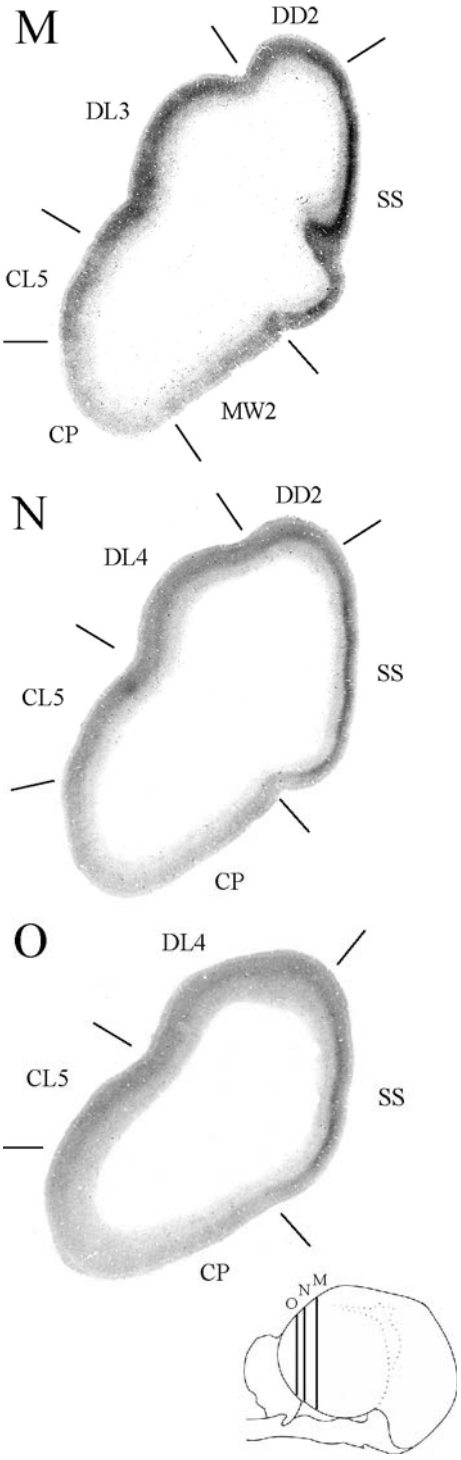

Figure 4-3. Continued

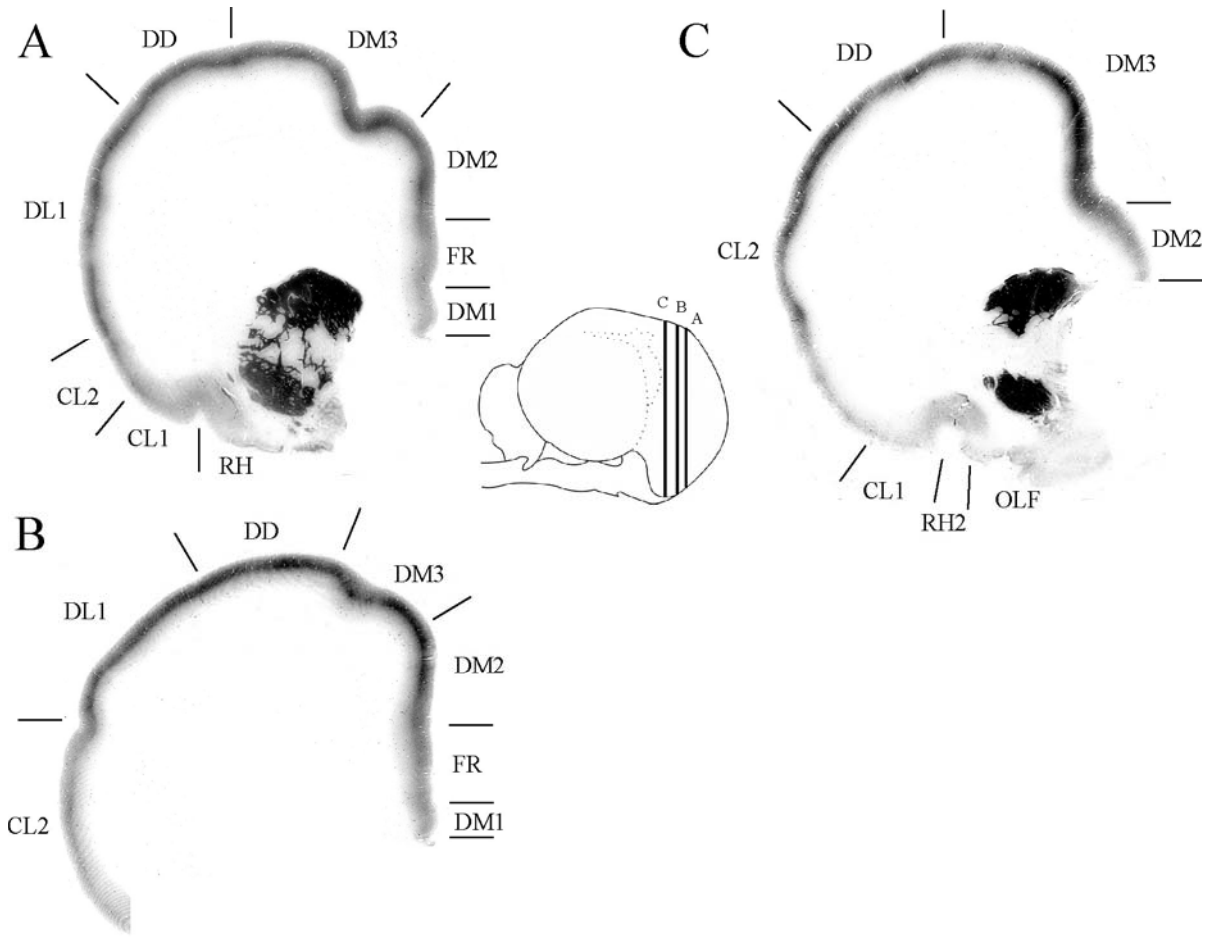

Figure 4-4. Coronal cytochrome oxidase sections from an adult specimen (TM0406) revealing trends consistent with the juvenile specimen but distinct from the neonate (see text for details). Right is medial, up is dorsal. The inset of a manatee brain reveals planes of section for A-C.

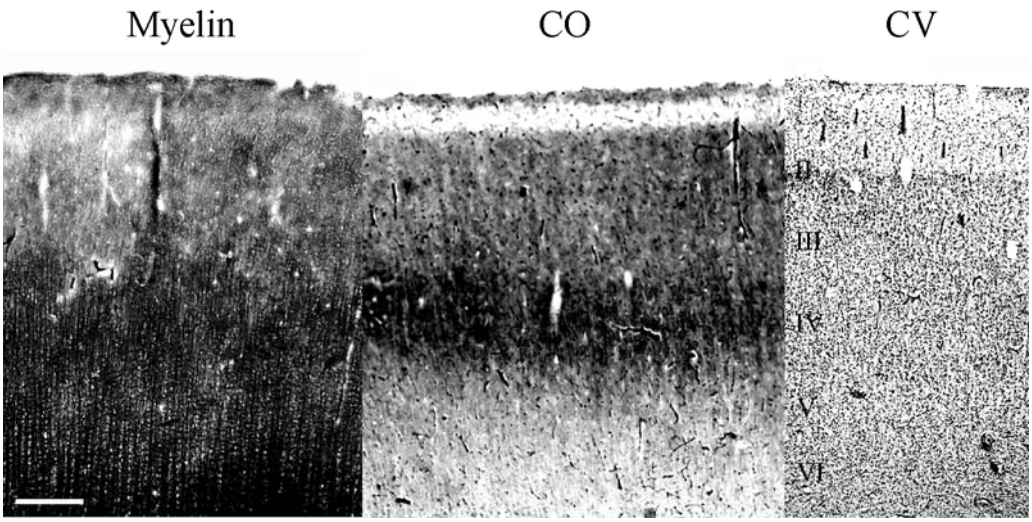

Figure 4-5. Adjacent sections stained for myelin, cytochrome oxidase, and Nissl bodies illustrate consistently dense staining in layer IV in both myelin and cytochrome oxidase preparations of presumptive primary sensory areas (specimen TM0406, area DL1 shown). Myelin preparations also exhibit moderate layer V and dense layer VI staining.

Figure 4-6. Localization of cytochrome oxidase-dense staining within cortical layer boundaries for each cytoarchitectural area. A) Area CL2 is shown with absence of cytochrome oxidase staining rostrally (left; specimen TM0339, Fig. 4-4-3F equivalent section), presence of cytochrome oxidase staining caudally (right; specimen TM0410, Fig. 4-4-2E equivalent), and stained for Nissl bodies (center; TM0410, Fig. 4-4-2E equivalent) to show laminar restriction of cytochrome oxidase-dense staining to layer IV, with a moderately staining band also present in layer VI in neonates. Scale bar = 1mm for all sections. White arrowheads show staining artifact in A and B. B) Area DL1 exhibits cytochrome oxidase-dense staining restricted to layer IV (specimen TM0410, Fig. 4-4-2D equivalent) in addition to a moderately staining band also present in layer VI (for neonatal specimens). C) Caudal area DL2 is shown with little cytochrome oxidase staining rostrally (left) versus cytochrome oxidase-dense staining caudally restricted to layer IV and a moderately dense cytochrome oxidase band in layer VI (right; specimen TM0410, Fig. 4-4-2D; layer VI band present only in neonatal specimens). D) Area DD exhibits cytochrome oxidase-dense staining restricted to layer IV (specimen TM0339, fig 3F equivalent sections). E) Area DM3 has cytochrome oxidase-dense staining restricted to layer IV (specimen TM0410, Fig. 4-4-2D). F) Area DD2 (specimen TM0310) demonstrates moderate, supragranular staining.

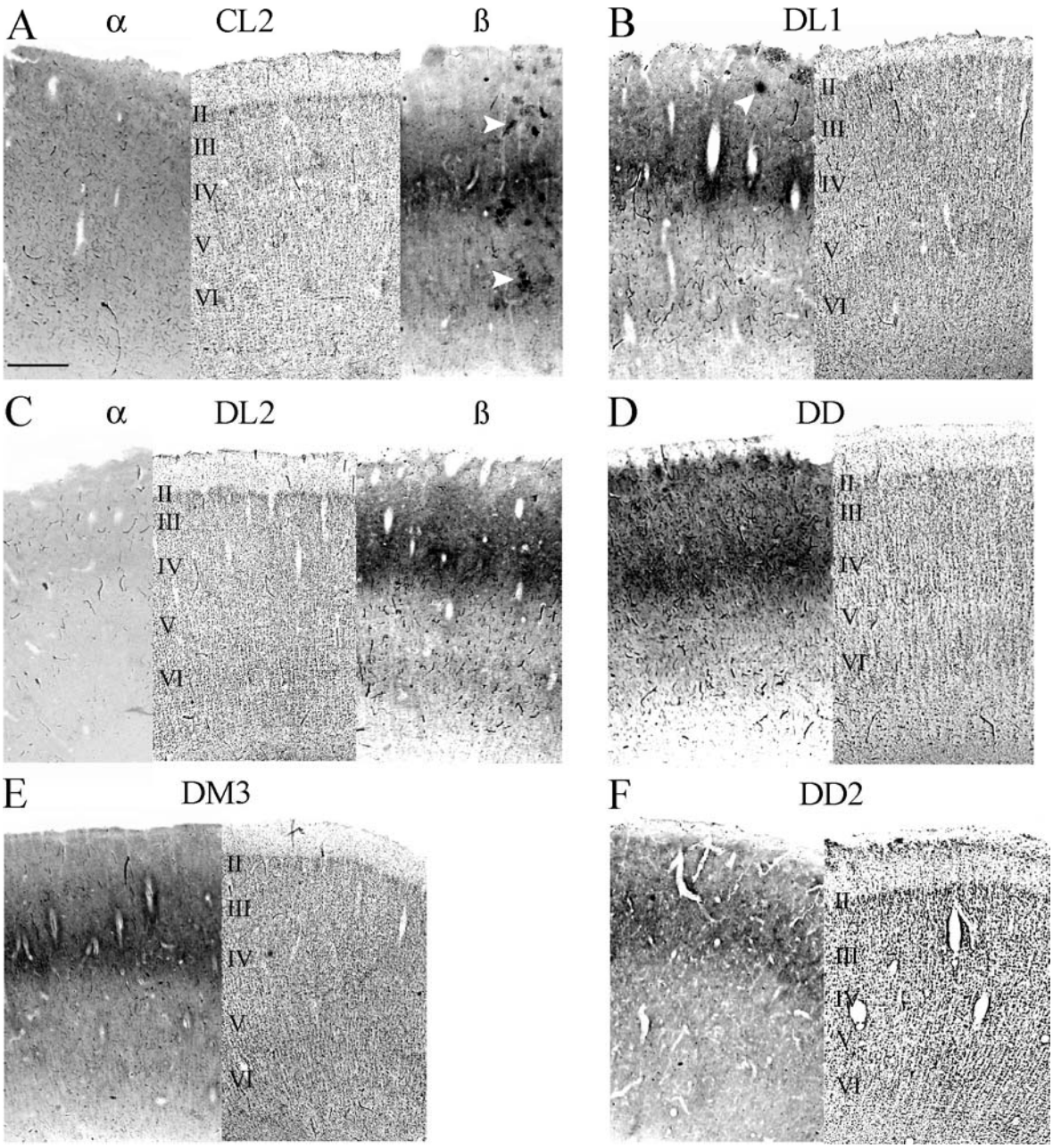
A
α
CL2
ß
II
III
IV
V
VI
B
DL1
II
III
IV
V
VI
C
α
DL2
ß
II
III
IV
V
VI
D
DD
II
III
IV
V
VI
E
DM3
II
III
IV
V
VI
F
DD2
II
III
IV
V
VI

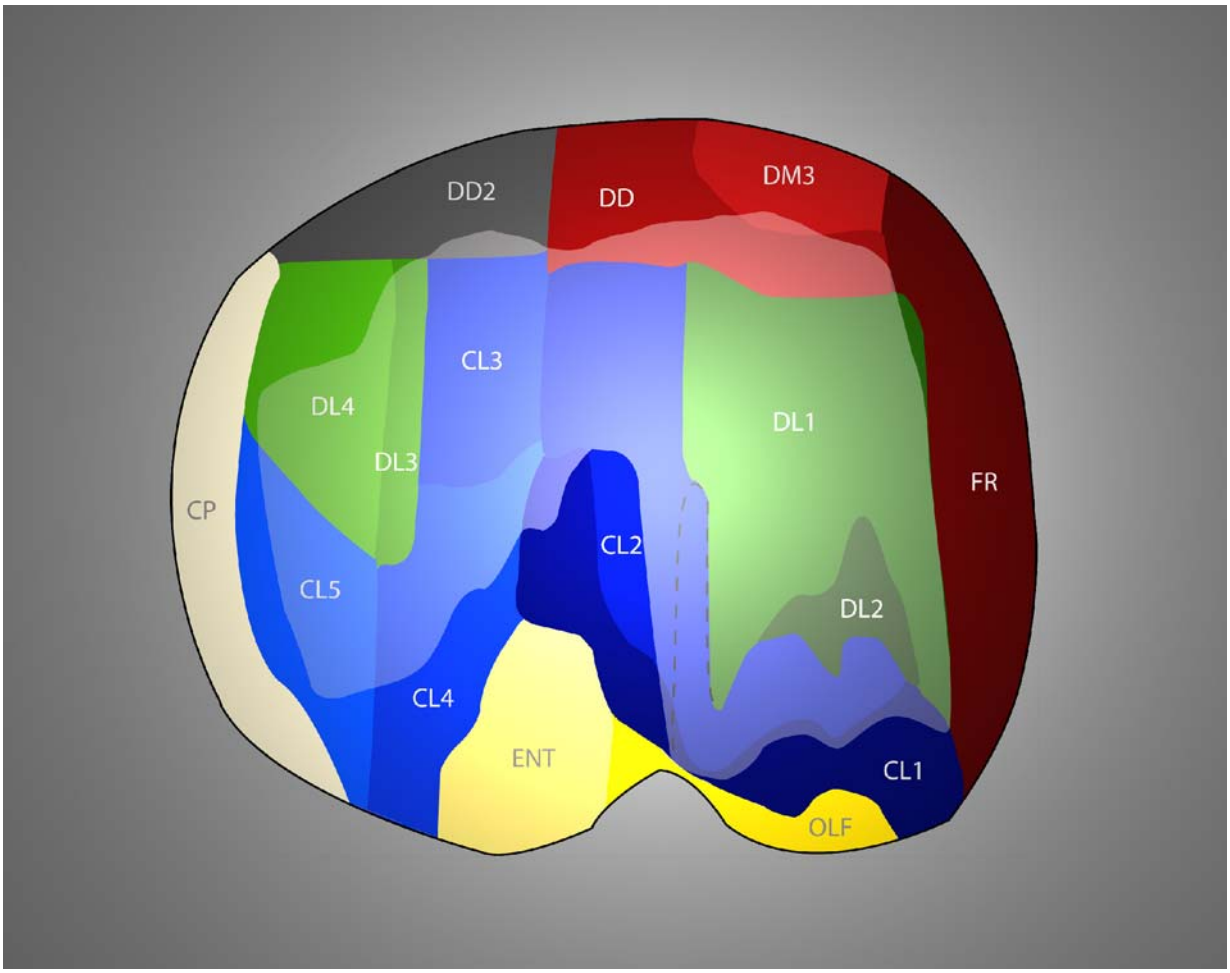

Figure 4-7. Three-dimensional reconstruction of neonatal specimen TM0410. The color-coded cytoarchitectural map was reconstructed from a series of spaced coronal sections from the right hemisphere, stained for cresyl violet. Superimposed upon this (in gray shading) is a map of cytochrome oxidase staining reconstructed from an adjacent coronal series stained for cytochrome oxidase. The composite was then smoothed to compensate for discrepancies between cytoarchitectural and cytochrome oxidase boundaries drawn by hand. Right is rostral, up is dorsomedial.

CHAPTER 5
CONCLUSIONS AND FUTURE DIRECTIONS

Summary and Conclusions

This work has contributed extensively to our understanding of the Florida manatee somatosensory system. For the first time, immunofluorescent labeling was used to characterize sensory innervation of tactile hairs (vibrissae) of the manatee body and face. From this we discovered that facial vibrissae exhibited dense C- and Aδ-fiber innervation of the epidermis and rete ridge collar, dense Merkel cell and moderate longitudinal lanceolate ending distribution at the ring sinus, and fine-caliber innervation located along the trabeculae of the cavernous sinus. Postfacial vibrissae contained Merkel endings and dense C- and Aδ-fiber distribution at the rete ridge collar. Dense Merkel ending networks were present at the inner conical body and ring sinus levels along with moderate longitudinal lanceolate ending innervation. The cavernous sinus contained fine-caliber innervation. By knowing the response properties of each type of sensory ending in other species, this general characterization of innervation in manatee vibrissae gives us an indication of what stimuli manatees are capable of detecting in their environment.

Two types of novel, presumptive low-threshold mechanoreceptors (BNaC+), were also discovered. Novel "tangle" endings were found along the mesenchymal sheath at the lower inner conical body/upper ring sinus level of both facial and postfacial vibrissae, and novel trabecular endings were found at the level of the cavernous sinus along the connective tissue in facial vibrissae only. Endings with these characteristics (size, location along the axis of the follicle-sinus complex, and immunolabeling characterization) have not been previously documented in any species. "Tangle" endings may confer additional directionality detection to the follicle-sinus complex (FSC) through association with deflection of the hair shaft against the upper trabeculae while the trabecular endings may be responsive to tension induced by deflection of exceptionally

rigid vibrissae which might involve modified sensory endings in order to optimally detect deflection. Since only the facial vibrissae exhibited the trabecular endings, these mechanoreceptors may have evolved to facilitate oripulative behavior that is unique to sirenia and combines sensorimotor functions.

Facial vibrissae are in fact more densely innervated, with more varied sensory endings, in accordance with their behavioral importance in active tactile exploration. Furthermore it seems that manatees are heavily invested in directionality detection, an adaptation that would enhance their perception of underwater hydrodynamic stimuli.

Histochemical and cytoarchitectural analysis of the brainstem, including stains for cytochrome oxidase (CO), myelin, and Nissl bodies, showed that somatosensory nuclei of the brainstem (Bischoff's, trigeminal, and cuneate-gracile nuclei) appear disproportionately large. The trigeminal and cuneate-gracile complex show evidence of parcellation that may be somatotopically related to discrete body areas, though no clear evidence of "barrelettes" was discovered.

Similar histochemical and cytoarchitectural analysis of the thalamus, including stains for CO, myelin, acetylcholinesterase, and Nissl bodies showed that the somatosensory nucleus, the ventroposterior (VP) nucleus with its medial (VPM) and lateral (VPL) subdivisions, appears disproportionately large. No evidence of "barreloids" was found. Reduced areas related to vision (e.g., LP and LGN) appear to be overtaken by areas related to somatosensation (VP and Po) and audition (MGN). We further postulate that many of these subnuclei may be multimodal and function in subcortical integration of auditory and somatosensory information.

Histochemical and cytoarchitectural analysis was also completed for the neocortex of the Florida manatee in order to localize primary sensory areas and particularly primary

somatosensory cortex (SI). Based on the location of CO-dense staining in flattened cortex preparations, and in coronal sections systematically analyzed in order to accurately localize the laminar and cytoarchitectural extent of CO staining, preliminary functional divisions were assigned for SI with the face represented laterally followed by the flipper, body and tail representations proceeding medially. Overall, SI appears to occupy roughly 25% of total cortical area, which is comparable to other somatosensory specialists such as the naked mole-rat, and spans seven cytoarchitectural areas. We hypothesize that area dorsomedial cortex (DM3) is dedicated to the tail representation; areas dorsolateral cortex (DL1), dorsal cortex (DD) (in the juvenile and adult specimens) and the dorsal portion of cluster cortex (CL2) serve as the body representation; the lateral extent of CL2 represents the flipper; and DL2, ventrolateral CL2, and CL1 represent the face. Area DD2 may represent a secondary somatosensory area (SII).

The neonate cortex exhibited four distinct patches in the frontoparietal region (presumptive SI) of flattened cortex preparations, whereas juvenile and adult specimens demonstrated a distinct pattern in which CO-dense staining appeared to be blended into one large patch extending dorsomedially. This differential staining between younger versus older, more developed animals was also seen on coronal sections stained for CO, myelin, or Nissl bodies and may indicate modifications of the sensory periphery reflected in reorganization of SI in the more developed animals.

Primary auditory cortex appears to span area CL3 and area CL2 caudal to the lateral fissure. The presence of only cluster cortex areas in what is hypothesized to be primary auditory cortex indicates extensive overlap of auditory and somatosensory information analogous to the parietal ventral (PV), ventral somatosensory (VS), or caudomedial (CM) areas found in other taxa (Cusick et al., 1989; Krubitzer et al., 1995a, b; Beck et al., 1996; Kaas and Collins, 2001;

Schroeder et al., 2001). This proposed multisensory integration may involve low-frequency sounds or other hydrodynamic stimuli detected through deflection of vibrissae on the manatee body.

Primary visual cortex appears to span cytoarchitectural areas DL3 and DL4. Areas CL4 and CL5 are likely candidates as visual association areas while area caudal pole cortex (CP) may function as a multimodal association area primarily dedication to visual processing.

This study is the first 1) to characterize sensory endings present in manatee vibrissae using immunofluorescence, and 2) to localize and characterize primary somatosensory areas of the brainstem, thalamus and cortex in the Florida manatee using a metabolic marker (cytochrome oxidase) that distinguishes primary sensory areas. This information substantially enhances our understanding of the manatee's somatosensory specializations, and adaptations to its environmental niche. Such knowledge is becoming increasingly critical as the numbers of this endangered species dwindle. It is our hope that elucidating the perceptual capabilities of manatees will aid in conservation efforts to preserve them as a species. Furthermore, as an evolutionary outlier, manatees offer the unique opportunity to add significant information to comparative neurobiology and allow a better understanding of organizing principles of sensory systems in general.

Future Directions

Although innervation of manatee vibrissae was characterized for the types of nerve endings present at each level of the follicle sinus complex and compared across 3 facial regions and 7 postfacial regions of the manatee body, exact quantification of the distribution density of nerve endings was not completed. This quantification would provide a direct method for comparison with other mammalian somatosensory specialists and allow us to further elucidate

the extent of somatosensory specialization in the Florida manatee. Furthermore, the information presented here is only a microlevel assessment of the anatomical substrates involved in manatee perceptual abilities; behavioral analyses are needed to confirm what behaviorally relevant stimuli manatees actually detect.

The locations of primary somatosensory areas defined here for the brainstem, thalamus and cortex would be greatly enhanced by electrophysiological or axonal tracing studies examining the exact functional boundaries of both the overall somatosensory region and the functional representation of each body region within it. Such invasive techniques are not feasible at present due to the manatee's status as an endangered species, but true functional delineations can only be hypothesized based on comparative neurobiological principles until more direct assessments are possible. Examination of the connectivity of individual Rindenkerne, especially in areas containing the largest Rindenkerne (CL1 and CL2) that may be related to facial vibrissae, is also critical in understanding this uniquely sirenian neuroanatomical specialization. Although a "fastDiI" experiment was completed by injecting DiI into non-perfused manatee brain sections in order to examine the connectivity of CL1 Rindenkerne, these data have not yet been analyzed.

Further characterization of behaviorally relevant subnuclei of the brainstem would also benefit our understanding of the Florida manatee's physiology and perceptual abilities. The present study shows that such areas as the vestibular nuclei and the vagus nucleus are exceptionally large in the manatee, but these were not examined in detail.

While manatees and dugongs represent evolutionary outliers as the only remaining families under the order Sirenia, their closest (yet distant) relatives, elephants and hyraxes, have been largely neglected as well in terms of physiological and neurobiological analysis. This

neglect of an entire supraordinal group, the Afrotheria (Kemp, 2005), represents a major gap in our knowledge of comparative evolution. Gross morphological and functional analyses are sparse (see Sale, 1970; Shoshani et al., 2006 for exceptions) and must be expanded upon. Current investigations in our laboratory involve analyzing the somatosensory system of the rock hyrax for comparison with the Florida manatee.

Additional Considerations

The present study suggests broader questions about the development and evolutionary divergence involved in creating the unique attributes seen in the Florida manatee. For instance, it is a uniquely sirenian attribute to possess a distribution of tactile hairs on the entire body. The question becomes: how was the developmental plan modified such that tactile hairs are distributed over the entire manatee body, and not just in restricted regions? Zelena (1994) describes the development of vibrissal follicles in four stages. First, sensory axons grow from the nerve plexus towards the epidermis and branch into the mesenchyme. Mesenchyme then aggregates around the nerve branches, followed by thickening of the epidermis above the mesenchymal condensation. Finally, the budding follicle grows down toward the nerve branches and into the mesenchymal condensation. However, whether sensory axons induce mesenchymal condensation or the mesenchyme itself induces follicle development remains an open question. It does appear that neural cell adhesion molecule (NCAM) is critical in formation of the coordinated pattern of nerves and whiskers in rat maxillary vibrissae (Scarisbrick and Jones, 1993). Other signals such as WNT, DKK, BMP, FGF, and Lef1 appear to be involved in hair follicle spacing (Sick et al., 2006). However, why certain animals retain vibrissae in only restricted regions (e.g., maxillary, carpal and supraorbital regions), while manatee vibrissae are distributed over the entire body, remains unclear. It is possible, though it seems unlikely, that this

is the basic mammalian plan and has only been retained in its complete form in sirenia, but has been lost (except in restricted, specialized regions of the body) in other mammals. One must assume that because innervation to tactile hairs on the entire body is a metabolically costly commitment, vibrissae have only been retained where they confer information critical to the animal's successful adaptation to its environment.

Regarding the issue of Rindenkerne development an additional question becomes: how did manatees evolve to form barrel-like structures in layer VI? If Rindenkerne are truly analogous to barrels, it seems reasonable to hypothesize that similar developmental principles govern the formation of both neuroanatomical structures. Little is known about the exact mechanisms involved in barrel field formation, although it does appear that growth-associated protein (GAP-43) is critical to the formation of an ordered vibrissal representation in the rat (Maier et al., 1999). Recent studies using monoamine oxidase-A (MAO-A), 5-HT transporter, vesicular monoamine transporter-2 (VMAT2) and 5-HT1B receptor single, double and triple knockout mice also indicate that the serotonergic system plays an important role in barrel field formation in the developing somatosensory cortex (Luo et al., 2003), but the possible genetic basis for barrel field formation remains elusive.

APPENDIX
LETTER OF PERMISSION TO REPRODUCE COPYRIGHTED MATERIAL (THE ENTIRETY OF CHAPTER 4)

Dear Dr. Sarko,

Thank you for your e-mail below. As for your request, I am pleased to inform you that permission is granted herewith to use the article

Sarko DK, Reep RL. 2007. Somatosensory areas of manatee cerebral cortex: Histochemical characterization and functional implications. Brain Behav Evol, 69:20–36.

in your doctoral dissertation provided that complete credit is given to the original source and S. Karger AG, Basel is mentioned.

Best wishes,

Isabelle Flückiger

Rights and Permissions

S. Karger AG

Medical and Scientific Publishers

Allschwilerstrasse 10

CH - 4009 Basel

Tel +41 61 306 14 75

Fax +41 61 306 12 34

E-Mail permission@karger.ch

LIST OF REFERENCES

Albrecht PJ, Hines S, Eisenberg E, Pud D, Finlay DR, Connolly MK, Pare M, Davar G, Rice FL. 2006. Pathologic alterations of cutaneous innervation and vasculature in affected limbs from patients with complex regional pain syndrome. Pain 120:244-266.

Ashwell KW, Hardman CD, Paxinos G. 2006. Cyo- ad chemoarchitecture of the sensory trigeminal nuclei of the echidna, platypus and rat. J Chem Neuroanat, 31:81-107.

Ashwell KW, Zhang LL, Marotte LR. 2005. Cyto- and Chemoarchitecture of the cortex of the tammar wallaby (*Macropus eugenii*): areal organization. Brain Behav Evol 66:114-136.

Bachteler D, Dehnhardt G. 1999. Active touch performance in the Antillean manatee: evidence for a functional differentiation of facial tactile hairs. Zoology 102:61-69.

Bauer GB, Colbert DE, Gaspard JC, Littlefield B, Fellner W. 2003. Underwater visual acuity of Florida manatees. Int J Comp Psychol 16:130-142.

Beck PD, Pospichal MW, Kaas JH. 1996. Topography, architecture, and connections of somatosensory cortex in opossums: evidence for five somatosensory areas. J Comp Neurol 366:109-133.

Berman AL, Jones EG. 1982. The thalamus and basal telencephalon of the cat: a cytoarchitectonic atlas with stereotaxic coordinates. University of Wisconsin Press.

Bohringer RC, Rowe MJ. 1977. The organization of sensory and motor areas of cerebral cortex in the platypus (*Ornithorhynchus anatinus*). J Comp Neurol 174:1-14.

Bombardieri RA, Johnson JI, Campos GB. 1975. Species differences in mechanosensory projections from the mouth to the ventrobasal thalamus. J Comp Neurol 163:41-64.

Brecht M, Preilowski B, Merzenich MM. 1997. Functional architecture of the mystacial vibrissae. Behav Brain Res 84:81-97.

Brosch M, Scheich H. 2005. Non-acoustic influence on neural activity inauditory cortex. In: The auditory cortex: A synthesis of human and animal research (König R, Heil P, Budinger E, Scheich H, eds), p 127-144. Mahwah, NJ: Lawrence Erlbaum.

Brosch M, Selezneva E, Scheich H. 2005. Nonauditory events of a behavioral procedure activate auditory cortex of highly trained monkeys. J Neurosci, 25:6796-6806.

Budinger E, Heil P, Heiss A, Scheich H. 2006. (in press). Multisensory processing via early cortical stages: Connections of the primary auditory cortical field with other sensory systems. Neurosci.

Burgess PR, Perl ER. 1973. Cutaneous mechanoreceptors and nociceptors. In: Iggo A, editor. Handbook of sensory physiology, 2, somatosensory systems. Berlin: Springer-Verlag. p 29-78.

Byers MR. 1984. Dental sensory receptors. Int Rev Neurobiol 25:39-94.

Byers MR, Närhi MV. 1999. Dental injury models: experimental tools for understanding neuroinflammatory interactions and polymodal nociceptor functions. Crit Rev Oral Biol Med 10:4-39.

Cabral RJ, Johnson JI. 1971. The organization of mechanoreceptive projections in the ventrobasal thalamus of the sheep. J Comp Neurol 141:17-36.

Catalano SM, Robertson RT, Killackey, HP. 1995. Rapid alteration of thalamocortical axon morphology follows peripheral damage in the neonatal rat. Proc Natl Acad Sci USA 92:2549-2552.

Catania KC. 2000. Cortical organization in insectivore: the parallel evolution of the sensory periphery and the brain. Brain Behav Evol 55:311-321.

Catania KC, Jain N, Franca JG, Volchan E, Kaas JH. 2000. The organization of somatosensory cortex in the short-tailed opossum (*Monodelphis domestica*). Somatosens Mot Res 17:39-51.

Catania KC, Lyon DC, Mock OB, Kaas JH. 1999. Cortical organization in shrews: evidence from five species. J Comp Neurol 410:55-72.

Catania KC, Remple MS. 2002. Somatosensory cortex dominated by the representation of teeth in the naked mole-rat brain. Proc Natl Acad Sci USA 99:5692-5697.

Cohen YE, Knudsen EI. 1999. Maps versus clusters: different representations of auditory space in the midbrain and forebrain. TREND Neurosci, 22:128-135.

Crish SD, Comer CM, Marasco PD, Catania KC. 2003. Somatosensation in the superior colliculus of the star-nosed mole. J Comp Neurol, 464:415-425.

Cusick CG, Wall JT, Felleman DJ, Kaas JH. 1989. Somatotopic organization of the lateral sulcus of owl monkeys: area 3b, S-II, and a ventral somatosensory area. J Comp Neurol 282:169-190.

Dehnhardt G, Mauck B, Bleckmann H. 1998. Seal whiskers detect water movements. Nature 394:235-236.

Dehnhardt G, Hyvärinen H, Palviainen A, Klauer G. 1999. Structure and innervation of the vibrissal follicle-sinus complex in the Australian water rat, *Hydromys chrysogaster*. J Comp Neurol 411:550-562.

Dehnhardt G, Mauck B, Hanke W, Bleckmann H. 2001. Hyrdrodynamic trail-following in harbor seals (*Phoca vitulina*). Science 293:102-104.

Dexler H. 1912. Das Hirn von *Halicore dugong*. Erxl Gegenbaurs Morphol Jahrb 45:97-190.

Dykes RW. 1975. Afferent fibers from mystacial vibrissae of cats and seals. J Neurophysiol 38:650-662.

Ebara S, Kumamoto K, Matsuura T, Mazurkiewicz JE, Rice FL. 2002. Similarities and differences in the innervation of mystacial vibrissal follicle-sinus complexes in the rat and cat: a confocal microscopic study. J Comp Neurol 449:103-119.

Eskenasy AC, Clarke S. 2000. Hierarchy within human SI: supporting data from cytochrome oxidase, acetylcholinesterase and NADPH-diaphorase staining patterns. Somatosens Mot Res 17:123-132.

Florence SL, Lakshman S. 1995. Topography of primary afferent projections in the trigeminal sensory nuclei of rats. Acta Neurobiologiae Experimentalis 55: 193-200.

Florence SL, Wall JT, Kaas JH. 1991. Central projections from the skin of the hand in squirrel monkeys. J Comp Neurol 311:563-578.

Frost SB, Milliken GW, Plautz EJ, Masterton RB, Nudo RJ. 2000. Somatosensory and motor representations in cerebral cortex of a primitive mammal (*Monodelphis domestica):* a window into the early evolution of sensorimotor cortex. J Comp Neurol 421:29-51.

Fundin BT, Pfaller K, Rice FL. 1997. Different distributions of the sensory and autonomic innervation among the microvasculature of the rat mystacial pad. J Comp Neurol 389:545-568.

García-Añoveros J, Samad TA, Žuvela-Jelaska L, Woolf CJ, Corey DP. 2001. Transport and localization of the DEG/ENaC ion channel BNaC1α to peripheral mechanosensory terminals of dorsal root ganglia neurons. J Neurosci 21:2678-2686.

Gergan JA, MacLean PD. 1962. A stereotaxic atlas of the squirrel monkey's brain (*Saimiri sciureus*). Washington DC: NIH Public Health Service.

Gerstein ER, Gerstein L. 1999. The underwater audiogram of the West Indian manatee (*Trichechus manatus*). J Acoust Soc Am 105:3575-3583.

Ghazanfar AA, Maier JX, Hoffman KL, Logothetis NK. 2005. Multisensory integration of dynamic faces and voices in rhesus monkey auditory cortex. J Neurosci, 25:5004-5012.

Gottschaldt K-M, Vahle-Hinz C. 1981. Merkel cell receptors: structure and transducer function. Science 214:183-186.

Gottschaldt K-M, Iggo A, Young DW. 1973. Functional characteristics of mechanoreceptors in sinus hair follicles of the cat. J Physiol (Lond) 235:287-315.

Goyal R, Rasey SK, Wall JT. 1992. Current hypotheses of structural pattern-formation in the somatosensory system and their potential relevance to humans. Brain Res 583:316-319.

Griffin DR. 1958. Listening in the dark. Yale UP, New Haven.

Hassiotis M, Paxinos G, Ashwell KW. 2004. Cyto- and chemoarchitecture of the cerebral cortex of the Australian echidna (*Tachyglossus aculeatus*). I. Areal organization. J Comp Neurol 475:493-517.

Henry EC, Remple MS, O'Riain MJ, Catania KC. 2006. Organization of somatosensory cortical areas in the naked mole-rat (*Heterocephalus glaber*). J Comp Neurol 495:434-452.

Huffman KJ, Nelson J, Clarey J, Krubitzer L. 1999. Organization of somatosensory cortex in three species of marsupials, *Dasyurus hallucatus*, *Dactylopsila trivirgata*, and *Monodelphis domestica*: neural correlates of morphological specializations. J Comp Neurol 403:5-32.

Huffman RF, Henson OW Jr. 1990. The descending auditory pathway and acousticomotor system: Connections with the inferior colliculus. Brain Res Rev, 15:295-323.

Hyvärinen H. 1989. Diving in darkness: whiskers as sense organs of the ringed seal. J Zool (Lond) 218:663-678.

Hyvärinen H. 1995. Structure and function of the vibrissae of the ringed seal (*Phoca hispada* L). In: Kastelein RA, Thomas JA, Nachtigall PA, editors. Sensory systems of aquatic mammals. Woerden: De Spil Publishers. p 429-445.

Hyvärinen H, Katajisto H. 1984. Functional structure of the vibrissae of the ringed seal (*Phoca hispida* Schr.). Acta Zool Fenn 171:17-30.

Iggo A. 1963. New specific sensory structure in hairy skin. Acta Neuroveg (Wien) 24:175-180.

Iggo A. 1966. Cutaneous receptors with a high sensitivity to mechanical displacement. In: de Reuck AVS, Knight J, editors. Touch, heat and pain. London: Churchill. P 237-256.

Iggo A, Muir AR. 1969. The structure and function of a slowly-adapting touch corpuscle in hairy skin. J Physiol (Lond) 200:763-796.

Ivy GO, Killackey HP. 1982. Ephemeral cellular segmentation in the thalamus of the neonatal rat. Dev Brain Res, 2:1-17.

Jain R, Shore SE. 2006. External inferior colliculus integrates trigeminal and acoustic information: Unit responses to trigeminal nucleus and acoustic stimulation in the guinea pig. Neurosci Lett, 395:71-75.

Jacquin MF, Renehan WE, Rhoades RW, Panneton WM. 1993. Morphology and topography of identified primary afferents in trigeminal subnuclei principalis and oralis. J Neurophysiol 70:1911-1936.

Johansson RS, Landstrom U, Landstrom R. 1982a. Responses of mechanoreceptive afferent units in the glabrous skin of the human hand to sinusoidal skin displacements. Brain Res 244:17-25.

Johansson RS, Landstrom U, Landstrom R. 1982b. Sensitivity to edges of mechanoreceptive afferent units innervating the glabrous skin of the human hand. Brain Res 244:27-32.

Johansson RS, Vallbo AB. 1983. Tactile sensory coding in the glabrous skin of the human hand. TINS 6:27-32.

Johnson JI. 1990. Comparative development of somatosensory cortex. In: Cerebral Cortex: Comparative Structure and Evolution of Cerebral Cortex, Vol 8B (Jones EG, Peters A, eds), New York City: Plenum Press. p 335-449.

Johnson JI. 1980. Morphological correlates of specialized elaborations in somatic sensory cerebral neocortex. In: Comparative Neurology of the Telencephalon (Ebbesson SOE, ed), New York City: Plenum Press. p 423-447.

Johnson JI, Welker W, Reep RL. 1987. The motor nuclei of the cranial nerves in manatees, *Trichechus manatus*. Anat Rec 218:A68-A68.

Johnson JI, Welker W, Reep RL, Switzer RC III. 1986. Dorsal column nuclei of the aquatic herbivorous manatee (*Trichechus manatus*). Soc Neurosci Abstr 12:110.

Johnson JI, Kirsch JA, Reep RL, Switzer RC III. 1994. Phylogeny through brain traits: more characters for the analysis of mammalian evolution. Brain Behav Evol 43:319-47.

Johnson JI, Welker WI, Pubols BH. 1968. Somatotopic organization of raccoon dorsal column nuclei. J Comp Neurol 132:1-43.

Jones EG .1983. Organization of the thalamocortical complex and its relation to sensory process. In: Handbook of physiology: The Nervous System. (ed. Darian-Smith, I.) Washington DC: American Physiological Society vol III: 149-212.

Jones EG. 1985a. Transmitters, Receptors, and Related Compounds in the Thalamus. In: The Thalamus. NY: Plenum Press 227-233.

Jones EG. 1985b. The Ventral Nuclei. In: The Thalamus. NY: Plenum Press 325-423.

Jones EG, Friedman DP. 1982. Projection pattern of functional components of thalamic ventrobasal complex on monkey somatosensory cortex. J Neurophys 48:521-544.

Kaas JH, Collins CE. 2001. The organization of sensory cortex. Curr Opin Neurobiol 11:498-504.

Kappers A, Ubbo C. 1960. The comparative anatomy of the nervous system of vertebrates, including man. V.3 New York, Hafner Pub. Co. p 263.

Kemp TS. 2005. Living and fossil placentals. In: The origin and evolution of mammals. New York: Oxford. p 251-257.

Killackey HP, Rhoades RW, Jacquin M. 1990. Development of somatosensory system structures. In: Development of Sensory Systems in Mammals (Coleman J, ed), New York: Wiley Press. p 406-433.

Krishnamurti A, Kanagasuntheram R, Wong WC. 1972. Functional significance of the fibrous laminae in the ventrobasal complex of the thalamus in the slow loris. J Comp Neurol 145:515-524.

Krubitzer L. 1995. The organization of neocortex in mammals—are species differences really so different? Trends Neurosci 18:408-417.

Krubitzer LA, Clarey J, Tweedale R, Elston G, Calford M. 1995a. A redefinition of somatosensory areas in the lateral sulcus of macaque monkeys. J Neurosci 15:3821-3839.

Krubitzer L, Manger P, Pettigrew J, Calford M. 1995b. Organization of somatosensory cortex in Monotremes: in search of the prototypical plan. J Comp Neurol 351:261-306.

Kruger L. 1959. The thalamus of the dolphin (*Tursiops truncatus*) and comparison with other mammals. J Comp Neurol, 111:133-194.

Kudo M, Tashiro T, Higo S, Matsuyama T Kawamura S. 1984. Ascending projections from the nucleus of the brachium of the inferior colliculus in the cat. Exp Brain Res, 54:203-211.

Land PW, Buffer SA Jr., Yaskosky JD. 1995. Barreloids in adult rat thalamus: Three-dimensional architecture and relationship to somatosensory cortical barrels. J Comp Neurol, 355:573-588.

Land PW, Akhtar ND. 1987 Chronic sensory deprivation affects cytochrome-oxidase staining and glutamic acid decarboxylade immunoreactivity in adult rat ventrobasal thalamus. Brain Res 425:178-181.

Land PW, Simons DJ. 1985a. Cytochrome-oxidase staining in the rat SmI barrel cortex. J Comp Neurol 238:225-235.

Land PW, Simons DJ. 1985b. Metabolic and structural correlates of the vibrissae representation in the thalamus of the adult rat. Neurosci Lett 60:319-324.

Lee KJ, Woolsey TA. 1975. A proportional relationship between peripheral innervation density and cortical neuron number in the somatosensory system of the mouse. Brain Res 99:349-353.

Levin MJ, Pfieffer CJ. 2002. Gross and microscopic observations on the lingual structure of the Florida manatee *Trichechus manatus latirostris*. Anat Histol Embryol 31:278-285.

Lichtenstein SH, Carvell GE, Simons DJ. 1990. Responses of rat trigeminal ganglion neurons to movement of the vibrissae in different directions. Somatosens Mot Res 7:47-75.

Ling JK. 1977. Vibrissae of marine mammals. In Harrison JB, editor. Functional anatomy of marine mammals, vol 3 Academic Press, London, 387-415.

Linke R, Schwegler H. 2000. Convergent and complementary projections of the caudal paralaminar thalamic nuclei to rat temporal and insular cortex. Cereb Cortex, 10:753-771.

Luo X, Persico AM, Lauder JM. 2003. Serotonergic regulation of somatosensory cortical development: lessons from genetic mouse models. Dev Neurosci 25:173-83.

Ma PM. 1991. The barrelettes—Architectonic vibrissal representations in the brainstem trigeminal complex of the mouse. I. Normal structural organization. J Comp Neurol 309:161-99.

Mackay-Sim A, Duvall D, Graves BM. 1985. The West Indian manatee, *Trichechus manatus*, lacks a vomeronasal organ. Brain Behav Evol 27:186-194.

Mahler P, Hamilton WJ. 1966. Mechanisms of animal behavior. John Wiley & Sons, NY. p397-425.

Maier DL, Shyamala M, Donovan SL, Soppet D, Tessarollo L, McCasland JS, Meiri KF. 1999. Disrupted cortical map and absence of cortical barrels in growth-associated protein (GAP)-43 knockout mice. PNAS 96:9397-9402.

Mann DA, Colbert DE, Gaspard JC, Casper BM, Cook ML, Reep RL, Bauer GB. 2005. Temporal resolution of the Florida manatee (*Trichechus manatus latirostris*) auditory system. J Comp Physiol A Neuroethol Sens Neural Behav Physiol 191:903-908.

Marshall CD, Amin H, Kovacs KM, Lydersen C. 2006. Microstructure and innervation of the mystacial vibrissal follicle-sinus complex in bearded seals, *Erignathus barbatus* (Pinnipedia: Phocidae). Anat Rec 288A:13-25.

Marshall CD, Clark LA, Reep RL. 1998a. The muscular hydrostat of the Florida manatee (*Trichechus manatus latirostris*): a functional morphological model of perioral bristle use. Marine Mamm Sci 14:290-303.

Marshall CD, Clark LA, Reep RL. 1998b. The muscular hydrostat of the Florida manatee (*Trichechus manatus latirostris*) and its role in the use of perioral bristles. Mar Mamm Sci 14:290-303.

Marshall CD, Huth GD, Edmonds VM, Halin DL, Reep RL. 1998b. Prehensile use of perioral bristles during feeding and associated behaviors of the Florida manatee (*Trichechus manatus latirostris*). Marine Mamm Sci 14:274-289.

Marshall CD, Reep RL. 1995. Manatee cerebral cortex: cytoarchitecture of the caudal region in *Trichechus manatus latirostris*. Brain Behav Evol 45:1-18.

Marshall CD, Maeda H, Iwata M, Furuta M, Asano A, Rosas F, Reep RL. 2003. Orofacial morphology and feeding behaviour of the dugong, Amazonian, West African and Antillean manatees (Mammalia: Sirenia): functional morphology of the muscular-vibrissal complex. J Zool (Lond) 259:1-16.

McNab BK. 1978. Energetics of arboreal folivores: physiological problems and ecological consequences of feeding on an ubiquitous food supply. In The Ecology of Arboreal Folivores (GG Montgomery, ed.) Smithsonian Institution P, Washington DC p.153-162.

McNab BK. 1980 Food habits, energetics, and the population biology of mammals. Amer Nat 116:106-124.

Melaragno HP, Montagna W. 1953. The tactile hair follicles in the mouse. Anat Rec 115:129-149.

Mitani A, Itoh K, Mizuno N. 1987. Distribution and size of thalamic neurons projecting to layer I of the auditory cortical fields of the cat compared to those projecting to layer IV. J Comp Neurol, 257:105-121.

Munger BL, Publos LM, Publos BH. 1971. The Merkel rete papilla: a slowly adapting sensory receptor in mammalian glabrous skin. Brain Res 29:47-61.

Nomura S, MizunoN. 1986. Histochemical demonstration of vibrissae-representing patchy patterns of cytochrome oxidase activity within the trigeminal sensory nuclei in the cat. Brain Res 380:167-171.

Nweeia MT, Eidelman N, Eichmiller FC, Giuseppetti AA, Jung YG, Zhang Y. 2005. Hydrodynamic sensor capabilities and structural resilience of the male narwhal tusk. Soc Mar Mamm Abstr.

Oliver DL, Huerta MF. 1992. Inferior and superior colliculi. In: The mammalian auditory pathway: Neuroanatomy. (Webster DB, Popper AN, Fay RR, eds), New York; Springer. p 168-221.

Ostapoff EM, Johnson JI. 1988. Distribution of cells projecting to thalamus vs. those projecting to cerebellum in subdivisions of the dorsal column nuclei in raccoons. J Comp Neurol 267:211-230.

Paré M, Smith AM, Rice FL. 2002. Distribution and terminal arborizations of cutaneous mechanoreceptors in the glabrous finger pads of the monkey. J Comp Neurol 445:347-359.

Paré M, Elde R, Mazurkiewicz JE, Smith AM, Rice FL. 2001. The Meissner corpuscle revised: a multiafferented mechanoreceptor with nociceptor immunochemical properties. J Neurosci 21:7236-7246.

Paxinos G, Watson C. 1998. The rat brain in stereotaxic coordinates. San Diego: Academic Press.

Paxinos G, Watson C. 1986. The rat brain in stereotaxic coordinates. 2nd ed Sydney: Academic Press Australia.

Reep RL, Johnson JI, Switzer RC, Welker WI. 1989. Manatee cerebral cortex: cytoarchitecture of the frontal region in *Trichechus manatus latirostris*. Brain Behav Evol 34:365-386.

Reep RL, Marshall CD, Stoll ML. 2002. Tactile hairs on the postcranial body in Florida manatees: a mammalian lateral line? Brain Behav Evol 59:141-154.

Reep RL, Marshall CD, Stoll ML, Whitaker DM. 1998. Distribution and innervation of facial bristles and hairs in the Florida manatee (*Trichechus manatus latirostris*). Marine Mamm Sci 14:257-273.

Reep RL, Stoll ML, Marshall CD, Homer BL, Samuelson DA. 2001. Microanatomy of facial vibrissae in the Florida manatee: the basis for specialized sensory function and oripulation. Brain Behav Evol 58:1-14.

Rice FR. 1995. Comparative aspects of barrel structure and development. In: Cerebral Cortex: The Barrel Cortex of Rodents (Jones EG, Peters A, eds), New York: Plenum Press. p 1-75.

Rice FL, Fundin BT, Arvidsson J, Aldskogius H, Johansson O. 1997. Comprehensive immunofluorescence and lectin binding analysis of vibrissal follicle sinus complex innervation in the mystacial pad of the rat. J Comp Neurol 385:149-184.

Rice FL, Mance A, Munger BL. 1986. A comparative light microscopic analysis of the sensory innervation of the mystacial pad. I. Innervation of the vibrissal follicle-sinus complexes. J Comp Neurol 252:154-174.

Riddle D, Richards A, Feri Z, Purves D. 1992 Growth of the rat somatic sensory cortex and its constituent parts during postnatal development. J Neurosci 12:3509-3524.

Rose JE, Mountcastle VB. 1952. The thalamic tactile region in rabbit and cat. J Comp Neurol 97:441-489.

Rouiller EM, Hornung JP, de Ribaupierre F. 1989. Extrathalamic ascending projections to physiologically identified fields of the cat auditory cortex. Hear Res, 40:233-246.

Sarko DK, Reep RL. 2005. Differential cytochrome oxidase staining between neonatal and juvenile manatee cerebral cortex reveals uniquely organized somatosensory areas. Soc Neurosci Abstr: 182.16.

Sarko DK, Reep RL. 2007. Somatosensory areas of manatee cerebral cortex: Histochemical characterization and functional implications. Brain Behav Evol 69:20-36.

Scarisbrick IA, Jones EG. 1993. NCAM immunoreactivity during major developmental events in the rat maxillary nerve-whisker system. Brain Res Dev Brain Res 71:121-135.

Schmued LC. 1990. A rapid, sensitive histochemical stain for myelin in frozen brain sections. J Histochem Cytochem 38:717-720.

Schnupp JW, King AJ. 1997. Coding for auditory space in the nucleus of the brachium of the inferior colliculus in the ferret. J Neurophysiol 78:2717-2731.

Schroeder CE, Lindsley RW, Specht C, Marcovici A, Smiley JF, Javitt DC. 2001. Somatosensory input to auditory association cortex in the macaque monkey. J Neurophysiol 85:1322-1327.

Shore SE. 2005. Multisensory integration in the dorsal cochlear nucleus: Unit responses to acoustic and trigeminal ganglion stimulation. Eur J Neurosci, 21:3334-3348.

Sick S, Reinker S, Timmer J, Schlake T. 2006. WNT and DKK determine hair follicle spacing through a reaction-diffusion mechanism. Science.

Simons DJ. 1978. Response properties of vibrissa units in the rat SI somatosensory neocortex. J Neurophysiol 41:798-820.

Simons DJ, Woolsey TA. 1979. Functional organization in the mouse barrel cortex. Brain Res 165:327-332.

Stephens RJ, Beebe IJ, Poulter TC. 1973. Innervation of the vibrissae of the California sea lion, *Zalophus californianus*. Anat Rec 176:421-441.

Strata F, Coq JO, Kaas JH. 2003. The chemo- and somatotopic architecture of the Galago cuneate and gracile nuclei. Neurosci 116:831-850.

Suga N, Ma X. 2003. Multiparametric corticofugal modulation and plasticity in the auditory system. Nat Rev Neurosci, 4:783-794.

Tuckett RP. 1978. Response of cutaneous hair and field mechanoreceptors in rat to paired mechanical stimuli. J Neurophysiol 41:150-156.

Tuckett RP, Horsch KW, Burgess PR. 1978. Response of cutaneous fair and field mechanoreceptors in cat to threshold stimuli. J Neurophysiol 41:138-149.

Ulinski PS. 1984. Thalamic projections to the somatosensory cortex of the echidna (*Tachyglossus aculeatus*). J Comp Neurol 229:153-170.

Van der Loos H. 1976. Barreloids in the mouse somatosensory thalamus. Neurosci Lett 2:1-6.

Welker E, Van der Loos H. 1986. Quantitative correlation between barrel-field size and the sensory innervation of the whiskerpad: A comparative study in six strains of mice bred for different patterns of mystacial vibrissae. J Neurosci 6:3355-3373.

Welker WI. 1973. Principles of organization of the ventrobasal complex in mammals. Brain Behav Evol 7:253-336.

Welker WI, Johnson J. 1965. Correlation between nuclear morphology and somatotopic organization in ventrobasal complex of the raccoon's thalamus. J Anat 99:761-790.

Welker WI. 1974. Principles of organization of the ventrobasal complex in mammals. Brain Behav Evol 7:253-336.

Welker WI, Adrian HO, Lifschitz W, Kaulen R, Caviedes E, Gutman W. 1976. Somatic sensory cortex of llama (*Lama glama*). Brain Behav Evol 13:284-293.

Welker WI., Johnson JI, Reep RL. 1986. Morphology and cytoarchitecture of the brain of Florida Manatees (*Trichechus manatus*). Soc Neurosci Abstr 12:110.

Werner-Reiss U, Kelly KA, Trause AS, Underhill AM, Groh JM. 2003. Eye position affects activity in primary auditory cortex of primates. Curr Biol, 13:554-562.

Wong-Riley M. 1979. Changes in the visual system of monocularly sutured or enucleated cats demonstrable with cytochrome oxidase histochemistry. Brain Res 171:11-28.

Wong-Riley M.T.T, Welt C. 1980. Histochemical changes in cytochrome-oxidase of cortical barrels after vibrissal removal in neonatal and adult mice. PNAS 77:2333-2337.

Woolsey TA, Van der Loos H. 1970. The structural organization of layer IV in the somatosensory region, SI, of mouse cerebral cortex. Brain Res 17:205-242.

Woolsey TA, Welker C, Schwartz RH. 1975. Comparative anatomical studies of the SmI face cortex with special references to the occurrence of "barrels" in layer IV. J Comp Neurol 164:79-94.

Woolsey TA, Welker C, Schwartz RH. 1975. Comparative anatomical studies of the SmI face cortex with special reference to the occurrence of "barrels" in layer IV. J Comp Neurol 184:363-380.

Woudenberg RA. 1970. Projections of mechanreceptive fields to cuneate-gracile and spinal trigeminal nuclear regions in sheep. Brain Res, 17:417-437.

Yan J, Zhang Y, Ehret G. 2005. Corticofugal shaping of frequency tuning curves in the central nucleus of the inferior colliculus of mice. J Neurophysiol, 93: 71-83.

Yohro T. 1977. Structure of the sinus hair follicle in the big-clawed shrew, *Sorex unguiculatus*. J Morph 153:333-354.

Yu YQ, Xiong Y, Chan YS, He J. 2004. Corticofugal gating of auditory information in the thalamus: an in vivo intracellular recording study. J Neurosci, 24:3060-3069.

Zelena J. 1994. Mechanoreceptor complexes associated with hair. In: Nerves and Mechanoreceptors: the role of innervation in the development and maintenance of mammalian mechanoreceptors, London: Chapman & Hall. p 243-260.

Zhou J, Shore SE. (in press). Convergence of spinal trigeminal and cochlear nucleus projections in the inferior colliculus of the guinea pig. J Comp Neurol.

Zhou YD, Fuster JM. 2004. Somatosensory cell response to an auditory cue in a haptic memory task. Behav Brain Res, 153:573-578.

Zook JM. (in press). Somatosensory adaptations of flying mammals. In: Evolution of Nervous Systems (Kaas JH, Krubitzer L, eds), NY: Elsevier Press. chpt. 8.03.

Zook JM. 2005. The neuroethology of touch in bats: cutaneous receptors of the wing. Soc Neurosci Abstr 78.21.

Zook JM, Fowler BC. 1986. A specialized mechanoreceptor array of the bat wing. Myotis 23-24.

BIOGRAPHICAL SKETCH

Diana Kay Sarko was born April 28, 1981 in West Palm Beach, Florida. She graduated from the Math, Science and Engineering (MSE) program at Suncoast Community High School in 1999. Earning enough advanced placement credits in high school to satisfy a year of college, she graduated magna cum laude from Emory University three years later with a B.S. in neuroscience and behavioral biology. Her honors thesis involved creating an ethogram for bottlenose dolphin mirror self-recognition behavior.

Diana's enrollment in the interdisciplinary (IDP) graduate program of the College of Medicine at the University of Florida began in the fall of 2002. From there, she entered the Department of Neuroscience to earn her Ph.D. and joined the lab of Dr. Roger Reep analyzing the somatosensory system of the Florida manatee. Through this lab, she became co-affiliated with the College of Veterinary Medicine and the Marine Mammal Program, which allowed her to participate in necropsies at Sea World, FL, and the Department of Environmental Protection Florida Marine Research Institute (DEP-FMRI) in St. Petersburg, FL. She also served as a student board member of the Save the Manatee Club in order to facilitate education outreach and manatee awareness.

Diana has accepted a postdoctoral position in the labs of Dr. Kenneth Catania and Dr. Jon Kaas at Vanderbilt University in Nashville, Tennessee. She will move there with her fiancé, Jeremy (JJ) Kennard, who works at a hospital as a nuclear medicine technologist.